1997

A model of the complex hydrocarbon component of the interstellar medium: Observational and experimental considerations.

Luther W. Beegle
University of Alabama at Birmingham

INFORMATION TO USERS

This manuscript has been reproduced from the microfilm master. UMI films the text directly from the original or copy submitted. Thus, some thesis and dissertation copies are in typewriter face, while others may be from any type of computer printer.

The quality of this reproduction is dependent upon the quality of the copy submitted. Broken or indistinct print, colored or poor quality illustrations and photographs, print bleedthrough, substandard margins, and improper alignment can adversely affect reproduction.

In the unlikely event that the author did not send UMI a complete manuscript and there are missing pages, these will be noted. Also, if unauthorized copyright material had to be removed, a note will indicate the deletion.

Oversize materials (e.g., maps, drawings, charts) are reproduced by sectioning the original, beginning at the upper left-hand corner and continuing from left to right in equal sections with small overlaps. Each original is also photographed in one exposure and is included in reduced form at the back of the book.

Photographs included in the original manuscript have been reproduced xerographically in this copy. Higher quality 6" x 9" black and white photographic prints are available for any photographs or illustrations appearing in this copy for an additional charge. Contact UMI directly to order.

UMI

A Bell & Howell Information Company
300 North Zeeb Road, Ann Arbor MI 48106-1346 USA
313/761-4700 800/521-0600

A MODEL OF THE COMPLEX HYDROCARBON COMPONENT OF THE INTERSTELLAR MEDIUM: OBSERVATIONAL AND EXPERIMENTAL CONSIDERATIONS

by

LUTHER W. BEEGLE

A DISSERTATION

Submitted to the graduate faculty of The University of Alabama at Birmingham
in partial fulfillment of the requirements for the degree of
Doctor of Philosophy

BIRMINGHAM, ALABAMA

1997

ABSTRACT OF DISSERTATION
GRADUATE SCHOOL, UNIVERSITY OF ALABAMA AT BIRMINGHAM

Degree Ph.D. Program Physics

Name of Candidate Luther W. Beegle

Committee Chair Prof. Thomas J. Wdowiak

Title A Model of the Complex Hydrocarbon Component of the Interstellar Medium: Observational and Experimental Considerations

Experiments in which the simple polycyclic aromatic hydrocarbon (PAH) naphthalene ($C_{10}H_8$) is subjected to the energetic environment of a plasma have resulted in the synthesis of a material having ultraviolet spectral characteristics, suggesting that it is reasonable to consider it as a laboratory analog for the carrier of the 2175 Å interstellar extinction feature. Ultraviolet, visible, infrared, and mass spectroscopy along with gas chromatography, indicate it to be a molecular aggregate in which an aromatic double-ring structure serves as a significant base for the electron "box" chromophore that gives rise to the envelope of the 2175 Å feature. It can also provide the peak of the feature or function in concert with another peak provider such as graphite. This base manifests itself both as a component of an alkyl-aromatic polymer and as a substructure of hydrogenated PAH species. Its spectral and molecular characteristics are consistent with what is expected for a material that has a role as an interstellar constituent. Other results of the research are the synthesis of a material having a spectral signature that correlates with the infrared emission of the proto-planetary nebula IRAS 05341 + 0852, and infrared spectroscopy and molecular modeling that suggests the observed strength of the interstellar 6.2 micron emission band is the signature of hydrogenated polycyclic aromatic hydrocarbons.

DEDICATION

I would like to dedicate this to three women who helped make me what I am today: my mother, Mary Jo, whom I wish had been here to be able to read it; Frannie, who helped me through some very difficult times; and Katherine, who put up with me while I researched and wrote it.

ACKNOWLEDGMENTS

I wish to thank the following people who have made this work possible: my advisor, Prof. Thomas Wdowiak, for his assistance throughout this research; and Prof. David Agresti, Prof. Steven Beale, Prof. Joseph Harrison, Prof. David Krause, and Prof. Chris Lawson for their time and assistance as members of my committee. Prof. Harrison also facilitated the computations described in this thesis. Prof. Robert Bauman (Emeritus) provided valuable advice which was greatly appreciated. I wish to thank Dr. Michael Robinson and Dr. Bruce Lee for their constructive comments and work they have done with/for me as colleagues. Prof. John Cronin and Michael D. McGehee at Arizona State University, as partners in the overall research effort, contributed important analytical chemistry support. I thank Dr. Simon Clemmett of Stanford University for facilitating mass spectroscopy measurements, Rick Smith at the University of Alabama for crafting the discharge tubes, and Jerry Sewell for helped in making different apparatus over the years. I appreciate Kenneth Maurice Arnoult for his help, after Dr. Robinson left, in the complex task of performing experiments. I also appreciate Drs. Lou Allamandola, Max Bernstein, and Yvonne Pendleton of the NASA Ames Research Center for their expressions of interest in this work.

The research was supported by NASA grants NAGW-749 from the Infrared Astronomy Laboratory Astrophysics Program, NAGW-3092 from the Ultraviolet, Visible, and Gravitational Astronomy Research & Analysis Program, NAGW-4079 from the Exo-

biology Program, and especially NAGW-4158 from the Origins of Solar Systems Program which provided stipend and supplies support.

TABLE OF CONTENTS

TABLE OF CONTENTS (Continued)

CHAPTER Page

LIST OF TABLES

LIST OF FIGURES

LIST OF FIGURES (Continued)

LIST OF FIGURES (Continued)

LIST OF FIGURES (Continued)

LIST OF FIGURES (Continued)

1. INTRODUCTION

1.1 Background

In 1847, Wilhelm Struve published an analysis of star counts in different lines of sight in what is now known as the Milky Way Galaxy. He demonstrated that there was an apparent decline in the number of stars per unit volume the greater the apparent distance from the Sun. This had to be due to some attenuating mechanism that scatters, absorbs and re-radiates the light from stars in the volume of space which makes up the interstellar medium (ISM). However, his idea was not readily accepted until early in the 20th century.

In the 1930's, observations by R.J. Trumpler (1930a, 1930b, and 1930c) at the Lick Observatory confirmed the hypothesis that Struve proposed, that there was interstellar dust that obscured the light from clusters of stars. The standard equation for calculating stellar distance had been

$$V - M_v = 5 \log d' - 5$$

where V is the apparent visual magnitude, M_v is the absolute visual magnitude, and d' is the distance to the object. Trumpler attempted to correlate the linear diameter of star clusters with the geometrically observed angular distances. This correlation showed that the deduced cluster diameter appeared to increase as the cluster's distance from the Sun increased. The obvious deduction was that there was a factor of obstruction in the ISM which caused the apparent brightness of stars to be less than what it would have been if interstellar space was a vacuum, and this obstruction was a systematic error present in all

previous distance measurements. A correction factor was needed, so the distance equation was changed to

$$V - M_v - A_v = 5 \log d - 5$$

where A_v is the extinction due to dust and d is the actual distance to the object. The implications are immense. The interstellar extinction had other effects than just causing error in distance measurements. Because the apparent extinction had to be due to sub-micron particles that existed in the ISM, there would be a reddening of stellar light. The apparent shift in the distribution redward is because small particles are more efficient at scattering shorter wavelength light than light of longer wavelengths. A demonstration of this effect is the observed color of the sun at sunset/sunrise being much redder than when it is overhead. Because there is more atmosphere for the solar radiation to transverse at the horizon, more preferential scattering of the shorter wavelength light away from the line of sight takes place. In this case of stellar reddening, observations of stars in the galactic plane confirmed that there should be more dust present in that region. These stars do have much redder colors than their spectral type would indicate.

Particles having dimensions comparable to the visible light being scattered (<1.0 μm) are responsible for the extinction. It is reasonable to assume that the interstellar dust particles have the same densities typical for terrestrial particles, placing the upper bound of atoms per dust particle is ~ 10^9 per particle. Since a vast amount of material was shown to exist in the ISM, it was quite evident that this material should be producing features that should be common to many stars in different lines of sight. Once the spectra of stars were compared, it was quite obvious that there were several features transversing the electromagnetic spectrum from the ultraviolet through the visible into the infrared, for which the

constituents in the ISM were responsible. The first assignments for spectral absorption bands were simple molecules like CO, SiO, and H_2O, which represent a high percentage abundance of interstellar constituents. Even though over 100 molecules to date have been identified in the ISM, the vast majority of interstellar spectral features have thus far escaped assignment.

The five fundamental spectroscopic mysteries in molecular astrophysics that need to be explained if the constituents of the ISM are to be fully understood are 1. The diffuse interstellar bands (DIBs), 2. Interstellar extinction feature at 2175 Å (4.6 μm^{-1}), 3. Unidentified infrared emission bands (UIR), 4. The galactic 3.4 micron absorption band, 5. The extended red emission (ERE) of dust clouds. These have been known for at least a decade in the case of 4 and 5 with the DIBs 1 going back to the 1930's. A global view of the ISM must take into account each part of the observed spectrum and for a reasonable explanation for any of the above five, there must be consistency with the characteristics observed in other spectral regions.

1.1.1 The Diffuse Interstellar Bands

In 1938, Merrill & Wilson described a discovery of several absorption features in the visible portion of the spectra from several stellar sources, which were certainly due to intervening interstellar material of some sort. What they had in common was that the band profiles had a broader or diffuse nature compared to those of atomic species. The features have since become known as the diffuse interstellar bands (DIBs). These features have grown in number such that today over 200 of them have been shown to exist in the blue of the visible to the near infrared (IR) of reddened stars (Jenniskens 1992). These features are similar in that they all have full widths at half maximum (FWHM) in a range of 2-20 Å (a

typical atomic line has FWHM of about 0.2 Å), and they show no doppler broadening in different lines of sight. The strongest features have wavelengths of 4428, 5780, 6284, and 6177 Å.

The most comprehensive studies of DIBs first started with Herbig (1975) and colleagues (Herbig & Leka 1991) and continued with the observational work of Krelowski and colleagues (Krelowski & Walker 1987; Krelowski 1988; Sneden, Woszczky, & Krelowski 1991; Krelowski et al. 1992) who have categorized the bands. A table of DIB wavelengths and strengths is shown in Table 1.1 along with a composite of DIBs in the visible to near IR in Figure 1.1 (Jenniskens & Desert 1995). These studies have shown that the bands have invariant central wavelengths and band profiles that tend to be constant from source to source. Because the DIBs differ widely in shape, depth, and width, they almost certainly are produced by more than a single carrier. Some studies have proposed that the bands might be broken down into families of molecules, each of which could be responsible for multiple bands.

There have been some proposals for the origin of the DIBs, including linear carbon chain molecules, proposed by Douglas (1977) with attempts to produce them by Krätschmer & Nachtigall (1987) by evaporation of carbon from an electrical arc; carbon-bearing molecules synthesized from CH_4 mixed with argon and subjected to an electrical discharge, an experimental technique also inspired by the Douglas hypothesis (Wdowiak 1980; Wdowiak, Lee, & Beegle 1994; Wdowiak et al. 1995b); PAH cations (Van der Zwet & Allamandola 1985; Crawford, Tielens, & Allamandola 1985; Salama & Allamandola 1992a); C_{60} related species (Kroto et al. 1985); and chlorin and related molecules (Miles & Sarre 1992). Far more experimental and observational work is required in this area.

Table 1.1- The Principal Diffuse Interstellar Bands Listed in Wavelength. (Adapted from Whittet 1992)

λ_0	σ	FWHM
4428	0.5	20.0
4501.8	0.2	3.0
4726	0.5	5.0
4754.9	0.5	5.6
4763.0	0.3	5.3
4882	2	17.0
5362	1	4.4
5404.3	0.2	1.0
5420	1	11.0
5449	2	14.0
5487.31	0.13	4.4
5535	5	23.0
5705.12	0.08	3.5
5778.3	1	17.0
5780.41	0.01	2.6
5797.03	0.02	1.3
5844.1	0.2	4.5
5849.79	0.03	1.0
6010.9	0.2	4.2
6042	2	14.0
6113.0	0.2	0.8
6177.1	1	30.0
6195.96	0.041	0.7
6230.6	0.03	2.3
6269.77	0.02	1.4
6283.91	0.02	3.8
6314	2	19.0
6353.5	0.3	3.1
6376.08	0.04	1.5
6613.58	0.01	2.1
6660.71	0.06	2.0
7562.2	1.0	4.0
8620.7	0.3	5.0

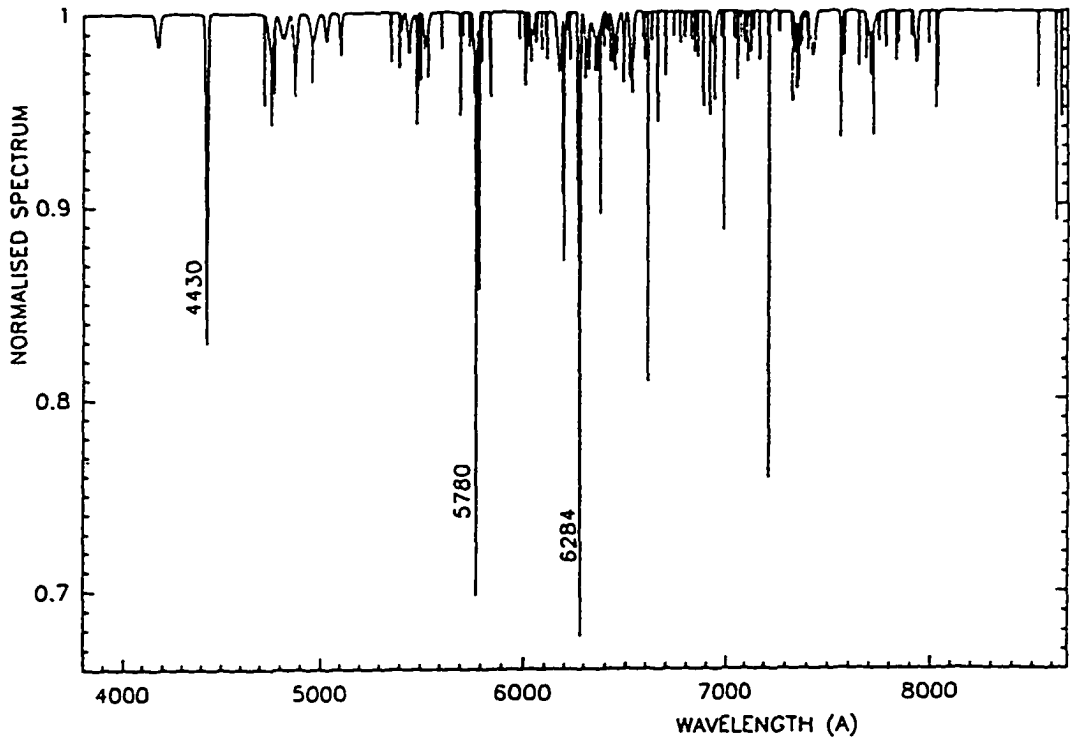

FIG. 1.1— The DIB spectrum, based on the average values of the most certainly detected diffuse interstellar absorption bands of HD 30614, and the three most reddened stars HD 21389, HD 190603, and HD 183143. (Adapted from Jenniskens 1992)

From a historical standpoint, the DIB mystery initiated the efforts of Kroto and colleagues that resulted in the discovery of fullerenes (C_{60} and C_{70}), and the works of Krätschmer, Huffman, and colleagues served as the basis of a process that produced macro amounts of those species.

1.1.2 The λ2175 Extinction Feature

Ted Stecher (1965) launched an ultraviolet spectrometer aboard a rocket to study spectral distributions of several stars at wavelengths between 3000 Å and 1200 Å, a region of the spectrum which is unobservable by ground-based observatories because of the ozone layer. Five pairs of stars that were blue or white were observed. After normalizing for color excess (B - V = 1), the value for the interstellar extinction was plotted. By using data from ground based observations to plot the region above 3000 Å, the general shape of the interstellar extinction curve was plotted down to 1250 Å and is shown in Figs. 1.2 and 1.3. From 1 μm^{-1} to 2 μm^{-1}, the extinction takes on a fairly linear value, before changing slope at around 2.2 μm^{-1}. At about 4.6 μm^{-1}, a distinct feature is evident, and this has become known as the λ2175 "bump."

Since the Stecher rocket flight, several satellites have facilitated observations at wavelengths below the atmospheric limit of 3200 Å, including the Orbiting Astronomical Observatory-2 (Bless & Savage 1972; Savage 1975), TD-1 (Nandy et al. 1975, 1976), Netherlands Astronomical Satellite (Wu, Gilra, & van Duinen 1980; Meyer & Savage 1981), and the International Ultraviolet Explorer (Seab, Snow, & Joseph 1981; Witt, Bohlin, & Stecher 1984; Fitzpatrick & Messa 1986). Almost all of these observations showed the same general character of the extinction curve, including the λ2175 feature. The λ2175 feature was remarkable for several reasons, including its ubiquity, strength,

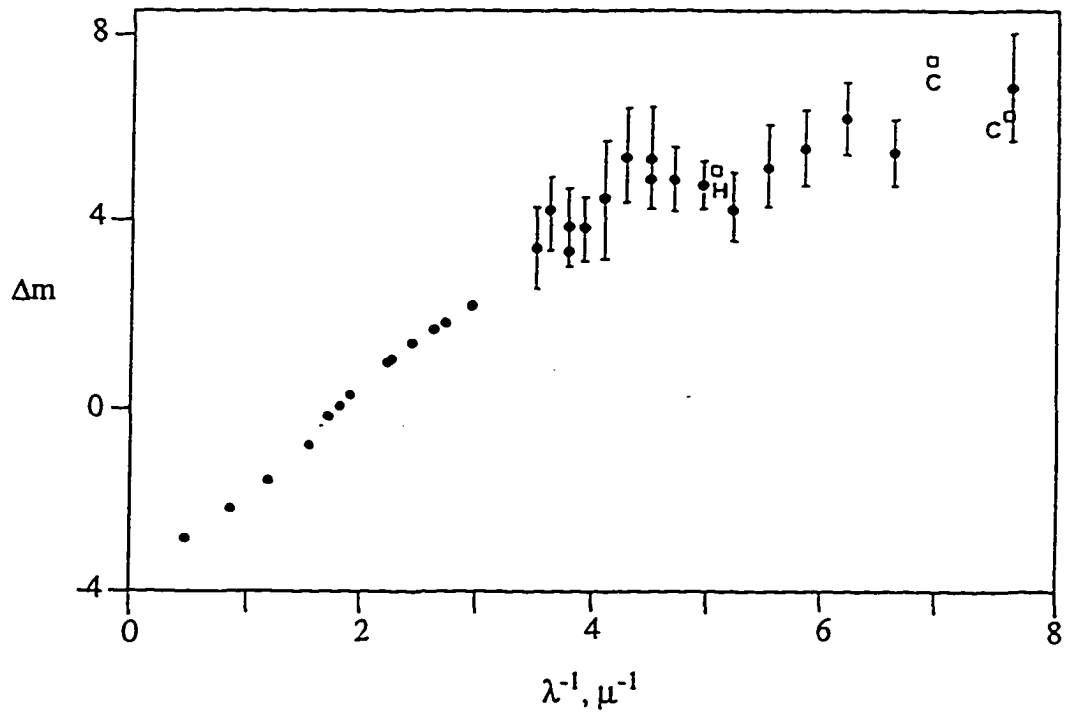

FIG. 1.2— The observed interstellar extinction including measurements at ultraviolet wavelengths showing the discovery of the 2175 Å (4.6 μm^{-1}) feature ("bump"). Solid circles: mean values for interstellar extinction and their mean errors for up to five pairs of stars as a function of inverse wavelength as observed by Stecher; solid circles without error bars: from ground observations; the square marked H and the squares marked C: from previous observations; all values are normalized with respect to B - V = 1 and V = 0 (Adapted from Stecher 1965).

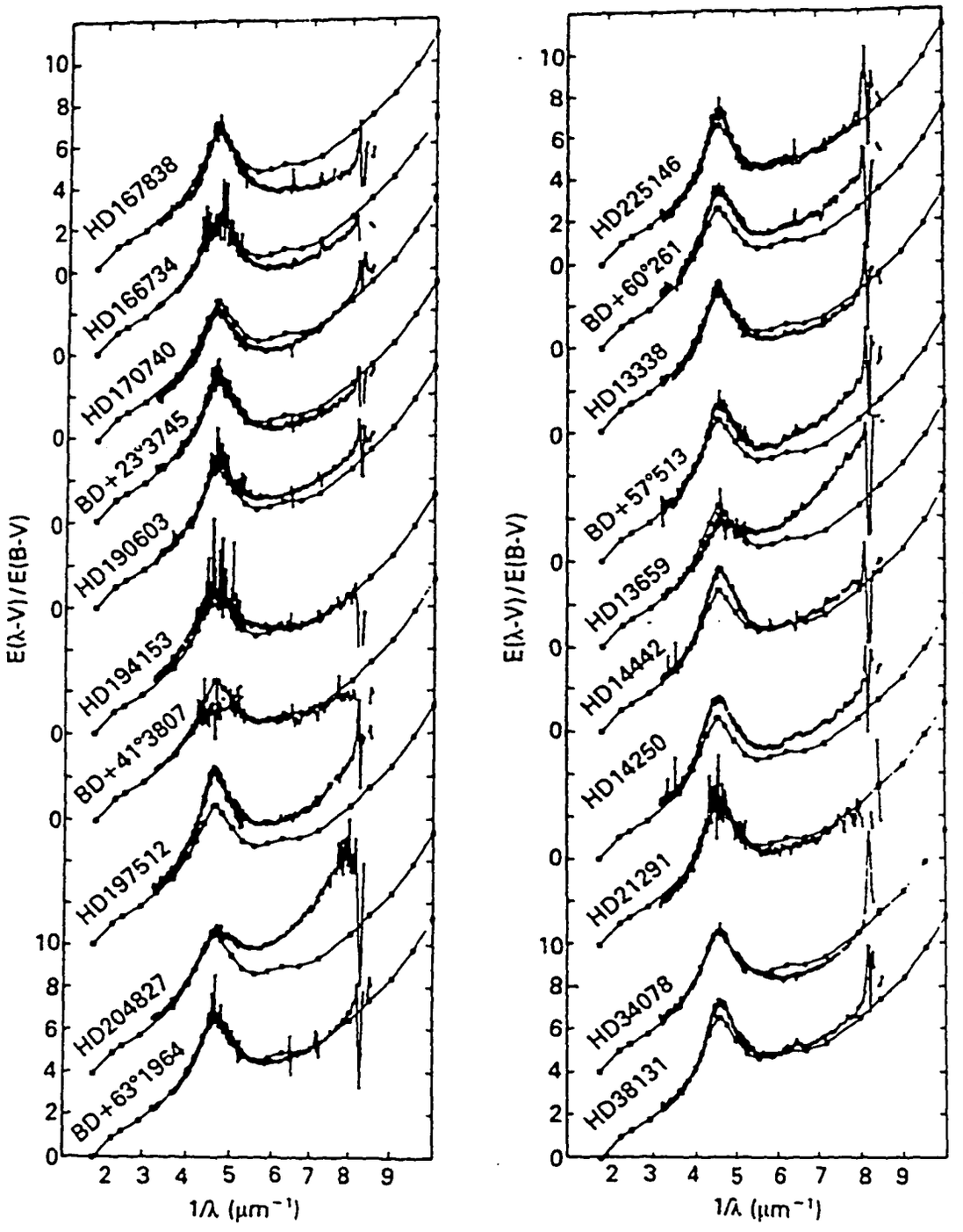

FIG. 1.3— Normalized extinction laws for reddened stars. The mean curve is plotted as solid circles (Adapted from Witt et al. 1984).

symmetry of profile, and the central wavelength, which never varies by more than ~ 10 Å. The average interstellar extinction curve can been seen in Figure 1.3 with observations from different sources plotted along with the average interstellar extinction profile also exhibited in Figure 1.4.

The proposed carrier of the λ2175 feature must satisfy several requirements if it is to satisfactorily explain the observed characteristics of the band. It must be constructed from cosmically abundant elements that match the observed interstellar elemental depletions; it must be robust enough to survive several different interstellar environments; and finally, it must match the observed profile of the λ2175 bump while lacking other features in other spectral regions that are not directly observed in the interstellar medium.

Models that have been proposed can be categorized in terms of the 2175 Å feature being due to the following: 1. a resonance peak in the optical constants; or 2. an independent absorbing component superimposed on the extinction curve. The first proposed carrier of the bump, graphite grains proposed by Stecher & Donn (1965), has gained a measure of acceptance [see reviews by Mathis (1994)] as it satisfies several of the aforementioned conditions. Being a solid form of carbon, graphite easily satisfies the cosmic abundances criterion (Whittet 1992). As a refractory material, graphite is robust enough to survive in the ISM, where substances are subjected to ultraviolet radiation, shock ionization fronts, and cosmic radiation particles. However, several other factors keep graphite from being universally accepted (Huffman 1989). First, observations of circumstellar dust indicate that solid particles in the ISM are predominately non-graphitic, such as silicates. Second, computer models show that there would have to be very tight constraints on the size, shape, and possible surface coatings for graphite that would be difficult to imagine

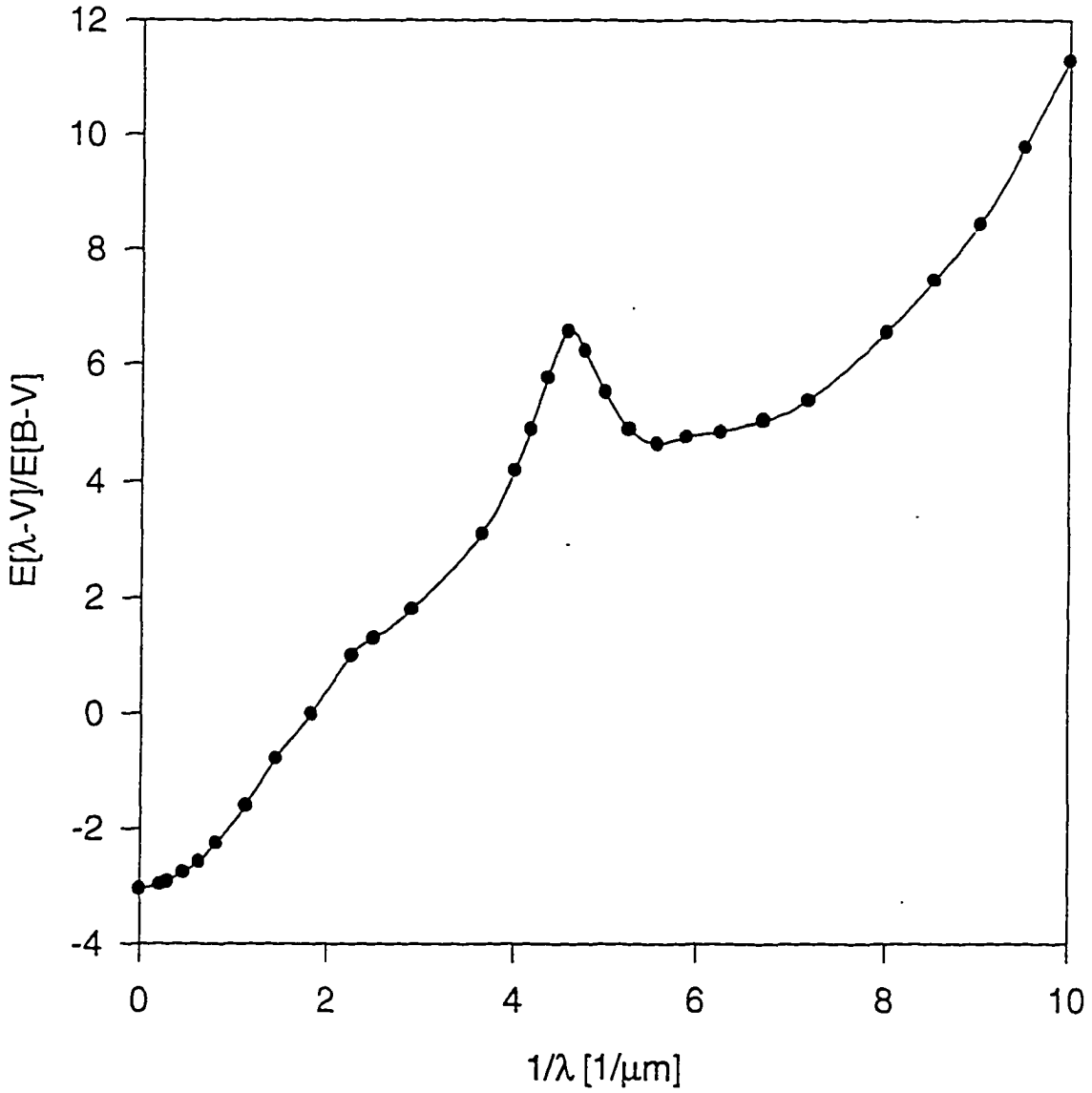

FIG. 1.4— The average interstellar extinction curve plotted over the entire wavelength for which data are available. Taken from data obtained in Whittet 1992.

given the wide range of environmental conditions of the ISM (Draine 1989; Mathis 1990, 1994; Whittet 1992). Finally, and importantly, there has been no successful creation of a graphitic material in the laboratory fitting the above constraints. One would expect, for the λ2175 carrier to be ubiquitous, that it should be easy to create, even for a scientist.

Several other proposed carriers include quenched carbonaceous composites (QCC) (Sakata et al. 1983; Sakata & Wada 1989; Sakata et al.1994); a mixture of PAHs made from coal pitch and a deposit from oil industry catalyzers (Joblin, Léger, & Martin 1992); and hydrogenated amorphous carbon (HAC) produced by a discharge of carbon rods in a hydrogen atmosphere (Blanco et al.1996; Mennella et al. 1996). All of these attempts have several inconsistencies in them, ranging from the multiple absorption peaks (PAH mixture) to band profiles not fitting the λ2175 bump in a satisfactory manner (QCC and HAC).

1.1.3 The Unidentified Infrared Emission Bands

The unidentified infrared emission bands were discovered in 1973 by Gillett, Forrest, & Merrill (1973) while observing the Planetary Nebula NGC 7027 (Fig. 1.5). These features in the infrared at wavelengths of 3.3, 6.2, 7.7, 8.6, and 11.3 μm have been observed in planetary nebula, reflection nebula, HII regions, and starburst galaxies (Cohen et al. 1986; Cohen et al. 1989). Because of the great variety of interstellar conditions in which these bands are observed, they have to be due to interstellar molecules that are easily produced under astrophysical conditions and that are able to withstand the harsh interstellar radiation fields and shock environment. One only has to look at an image of the Orion Nebulae to appreciate the presence of supersonic shock fronts.

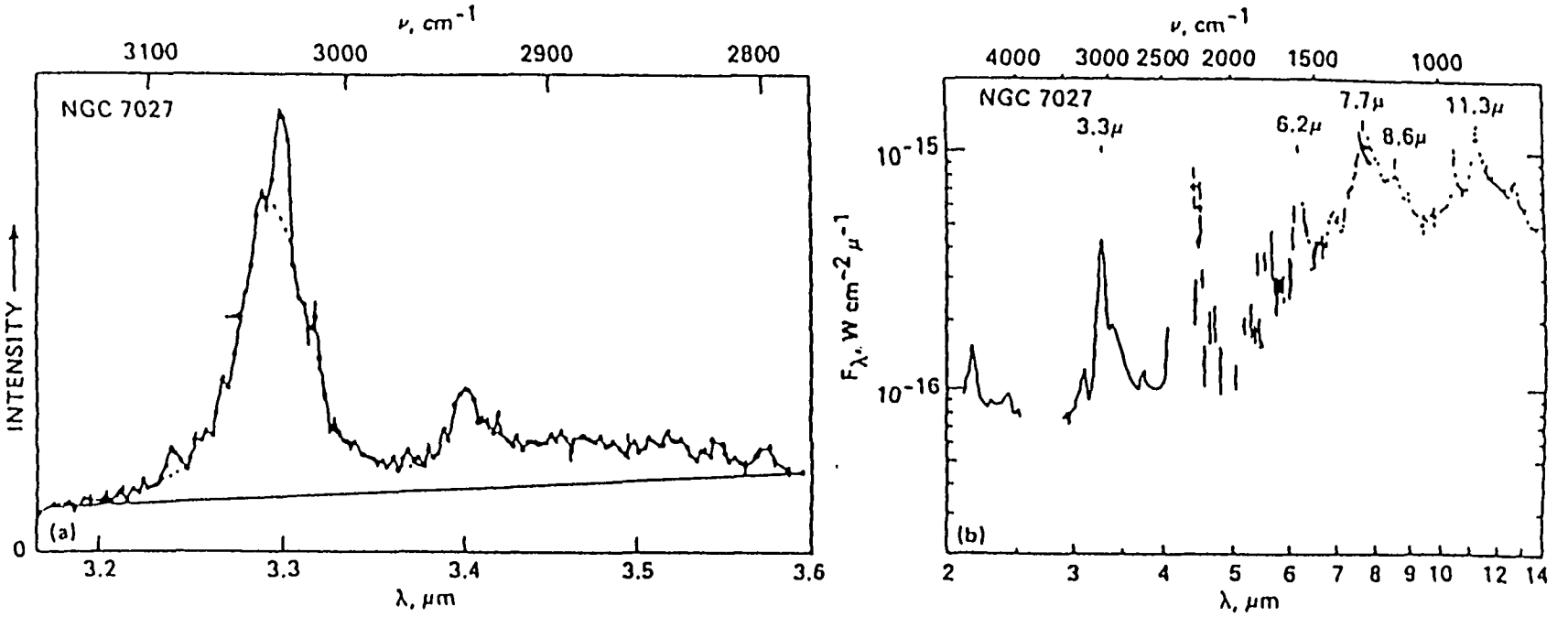

FIG.1.5— The infrared emission spectrum from the planetary nebula NGC 7027. (left adapted from Geballe 1984); (right adapted from Russell, Soifer, & Willner 1977). The principle UIR bands are indicated in μm.

Because of the general spectral match in the infrared, the family of molecules known as the polycyclic aromatic hydrocarbons (PAHs) have gained acceptance as the candidate that is responsible for the UIRs (Fig. 1.6). The assigning of PAHs to the UIR has been proposed by Duley & Williams (1981), Léger & Puget (1984), Allamandola, Tielens & Barker (1985), and Blanco, Bussoletti, & Colangeli (1988). The observed wavelength (λ_{obs}), along with the measured laboratory wavelength (λ_{lab}) and the assignments of modes of oscillation of molecular functional groups, can be found in Table 1.2.

Table 1.2- UIR Band Wavelength (μm) Assignments to the Principal Spectral Features in PAHs (Allamandola et al. 1989)

λ_{obs}	λ_{lab}	Assignments
3.29	3.29	C–H stretch ($v = 1 \rightarrow 0$)
6.2	6.2	C=C in-plane stretch
7.7	7.6-8.0	Blending of several strong C=C stretching bands
8.6	8.6-8.8	C–H in-plane bend
11.3	11.2-12.7	C–H out-of-plane bend for nonadjacent, peripheral H atoms or adjacent H atoms.

The total emission in the infrared of a galaxy having hundreds of billions of stars is dominated by the UIR bands. This energy has been estimated to be 10-30% of the total energy radiated by the galaxy as a whole, which is remarkable when one ponders this fact (Pajot et al. 1986; Ghosh & Drapatz 1987; Puget 1987). The emission is considered to be due to the absorption of UV photons that raise the electronic state of the PAH molecules. Rather than re-emitting the radiation by cascading down through electronic states into the ground state, internal conversion to highly excited vibronic states takes place. Infrared fluorescence from these long-lived states becomes the dominant mechanism for de-excitation

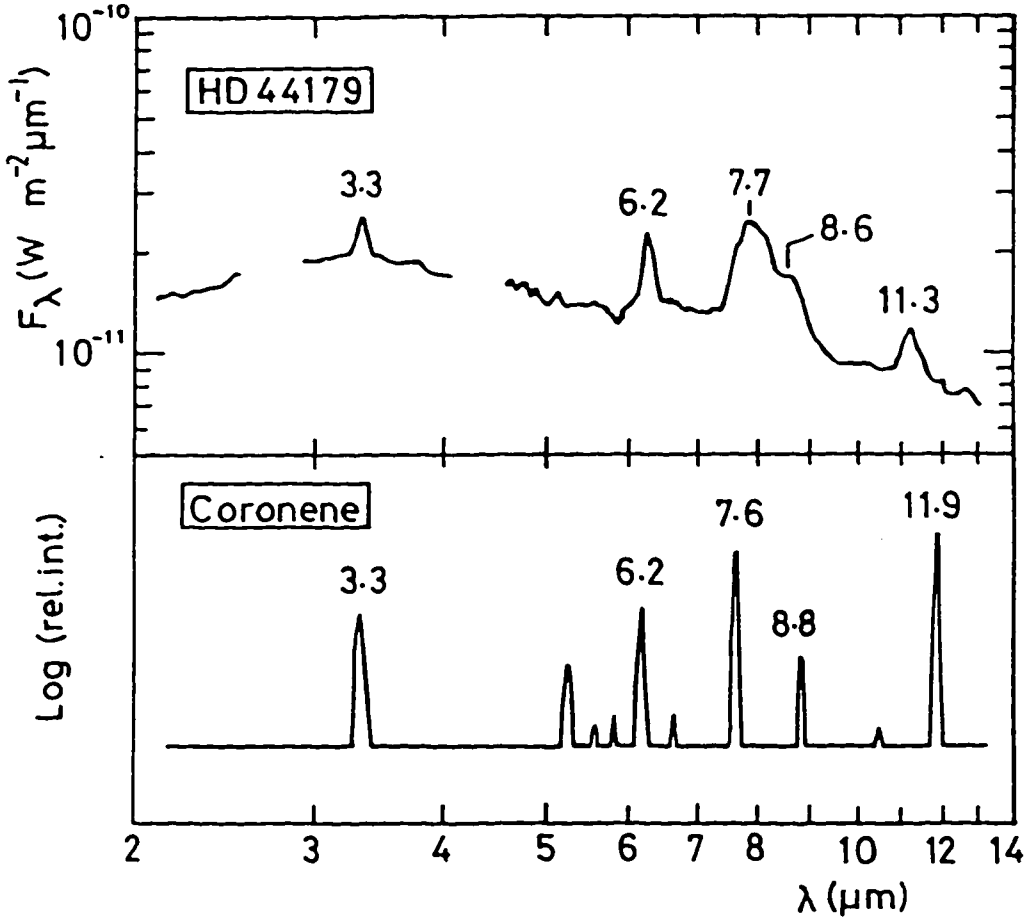

FIG. 1.6— The infrared emission spectrum of HD44179, the "Red Rectangle" (Russell et al. 1978) compared with the absorption spectrum of coronene (Léger & Puget 1984). The principal structural features are labeled by their wavelengths in μm. This diagram played an important role in developing interest in the PAH hypothesis for the UIR Bands.

(Leach 1987, Allamandola, Tielens, & Barker 1989) for both neutral and ionized species (see Figs. 1.7 and 1.8). Since the observed regions that the UIR dominate are heated by UV radiation, theory matches observation very nicely in this case.

Several problems have been voiced over the PAH hypothesis; one of which has been that a precise match to observed spectra has not been obtained through experimental means in the laboratory with known molecules. The situation is best described by the cliche "Close, but no cigar" (i.e., no Nobel prize). The problem is that it has been impossible to realistically recreate conditions of interstellar space in the laboratory. A population of molecules needs to be 10^{16} cm^{-2} for conventional absorption spectroscopy to be successful, and gas phase measurements of large molecular PAHs (30-40 atoms) have not been possible.

There has been success in matching the 3.3 μm band. Recent work (Flickinger & Wdowiak 1990; Flickinger Wdowiak, & Gomez 1991; Joblin et al. 1994; Robinson, Beegle, & Wdowiak 1995) has shown the shape and position of the 3.3 μm band to have a temperature dependence at elevated temperatures of up to 1000 K in the vapor phase. The interstellar absorption band at 3.285 μm has been correlated (Sellgren et al. 1995) with the C-H stretching mode of PAHs measured in the laboratory (Flickinger et al. 1991). More recent work of Bernstein et al. (1996) shows the hydrogenated PAH hexahydropyrene (Fig. 1.9) to have a good match to the spectra obtained of the Orion Bar (Sloan et al. 1997). Since hydrogenated PAHs are less stable than the fully aromatic PAHs the amount of hydrogenated PAH in the ISM should be very low; however, there should be enough to account for some of the weak structure shown in some of the infrared spectrum obtained in the 3.4 region of the infrared spectrum.

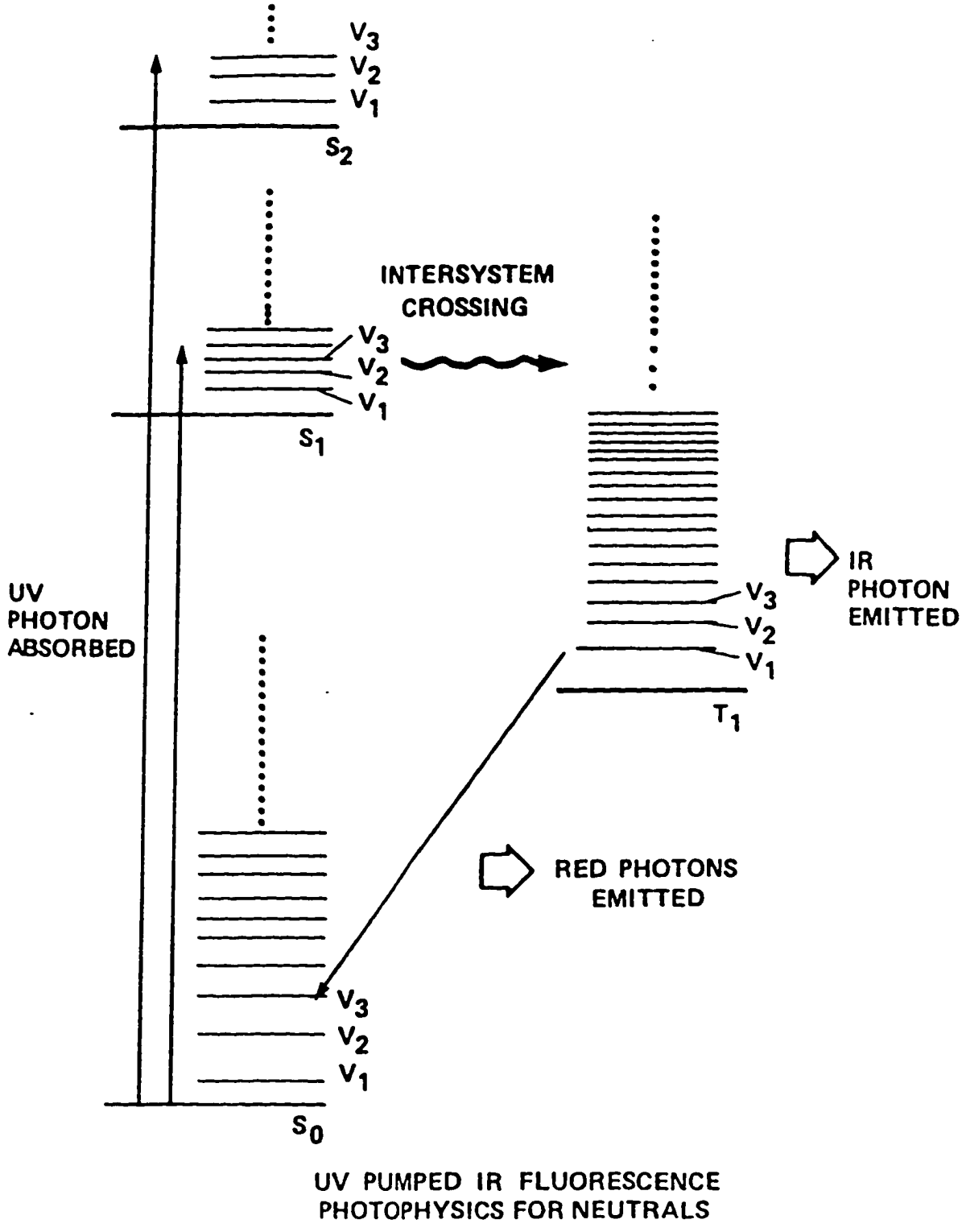

FIG. 1.7— Schematic energy level diagram for neutral PAH showing the various radiative and nonradiative excitation and relaxation channels possible. Note that in the case of a neutral PAH part of the internal energy will be emitted in the IR and part in the visible (Allamandola et al. 1989).

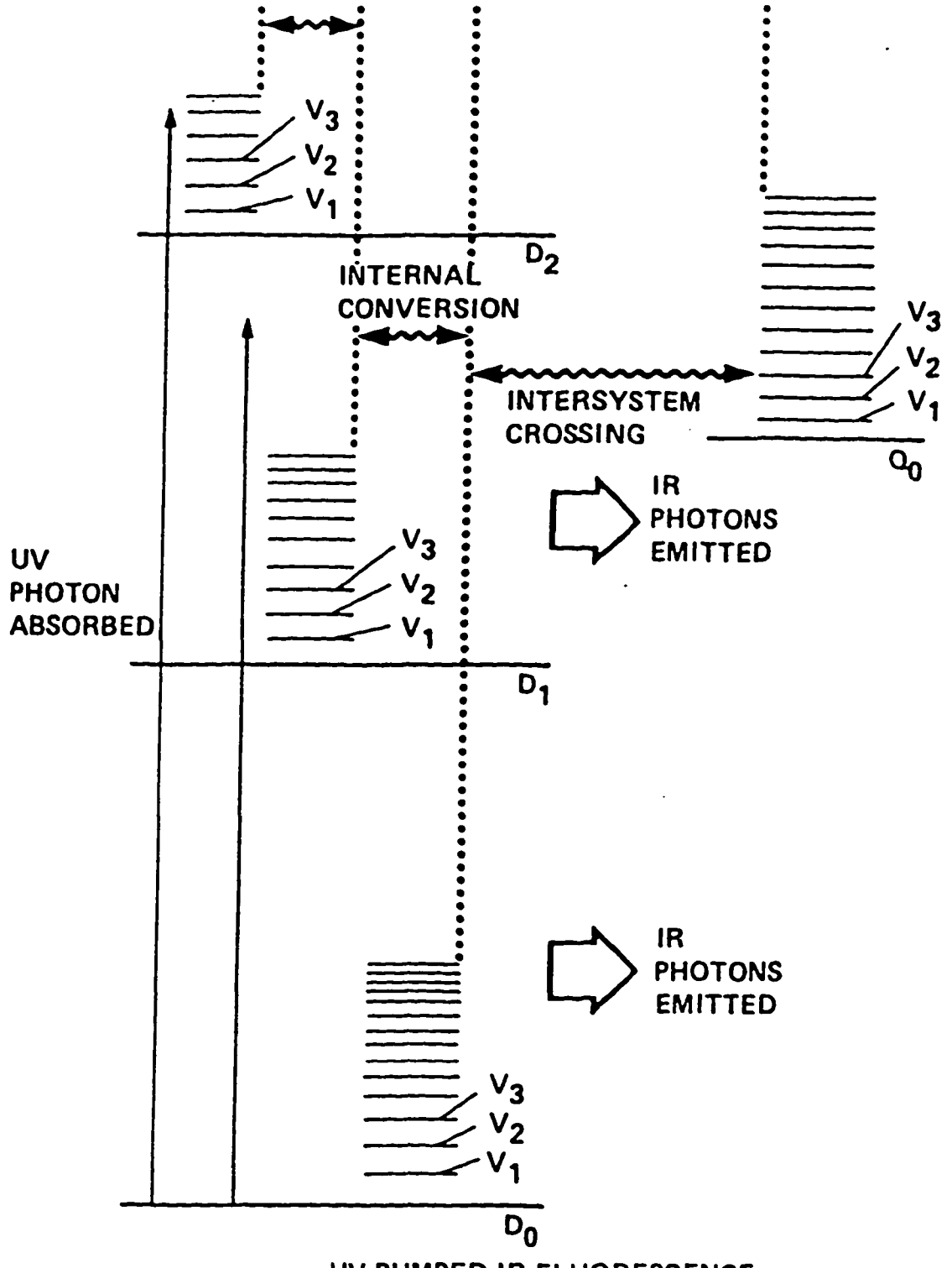

FIG. 1.8— Schematic energy level diagram for an ionized PAH showing the various radiative and nonradiative excitation and relaxation channels possible. Note that in the case of an ionized PAH most of the energy will be emitted in the near- and mid-IR (Allamandola et al. 1989).

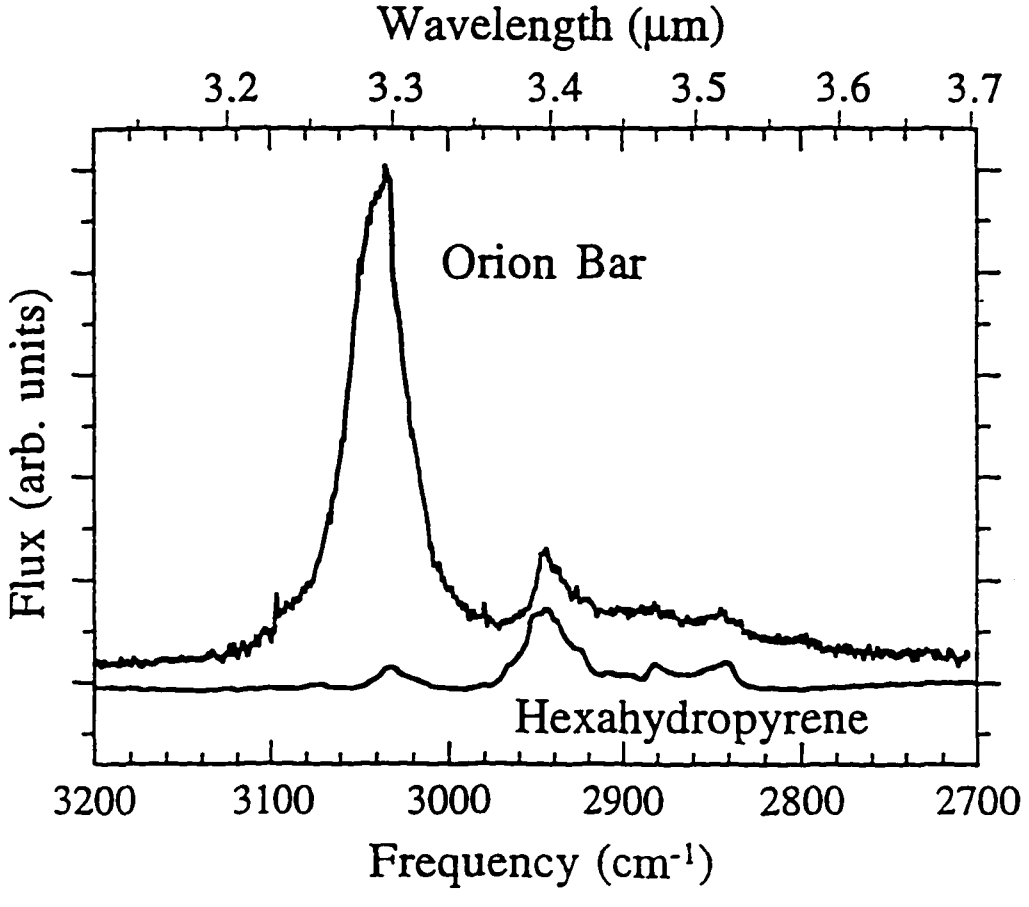

FIG. 1.9— Comparison of the 3200 - 2700 cm^{-1} (3.13 - 3.70 μm) emission spectrum of position 4 in the Orion Bar (from Sloan et al. 1996) with the absorption spectrum of matrix isolated hexahydropyrene. This H_n-PAH provides a reasonable match to the 2940, 2880, and 2850 cm^{-1} (3.40, 3.46, and 3.51 μm) emission features. The dominance of the aliphatic over the aromatic features in H_n-PAH spectra shows that, as a class, they contribute very little to the aromatic C-H stretch near 3040 cm^{-1} (3.29 μm). (Bernstein et al. 1996)

The most important kinds of experiments done are those that induce UIR carrier candidate species to emit radiation. These are difficult to perform for several reasons: 1. fluorescence occurs from long-lived states (see Figs. 1.7 and 1.8 and the discussion by Allamandola et al. 1989) that, at pressures utilized in experiments, are for the most part collisionally de-excited which would not be the situation in the interstellar medium; 2. molecular ions are precluded because of the difficulty of their preparation in the gas phase and their reactive nature, leaving data accessible only from neutral molecules; 3. the availability of samples of large PAH species (larger than hexabenzocoronene) in sufficient abundance is very limited, so experiments are performed only with smaller molecules; and 4. measurements at wavelengths greater than 5 microns (2000 cm^{-1}) require liquid-helium-cooled spectrometers, including infrared photocounting detectors, generally not available to most researchers. The first meaningful attempts at observing the emission of gas phase PAHs in the IR were by Cherchneff and Barker (1989) and Brenner and Barker (1992). Experiments by Williams & Leone (1995) have shown that there is a fairly good match in the 3.3 μm region between the character of laser-induced C-H stretch emission features from small, neutral PAH molecules and that of the UIR bands in that spectral region. Other experiments using laser-induced desorption and excited emission spectroscopy on neutral PAH species (Schlemmer et al. 1994; Cook et al. 1996) have raised significant questions regarding the assignment of the UIR bands to the PAH molecular family. The UIR bands have strong 6.2 and 7.7 μm features compared to the 3.3 μm feature, and the laboratory spectra obtained from small neutral PAH show the opposite strengths for the emissions. These experiments also show that the match between the vibrational modes of small, neutral PAH molecules, including the skeletal and the longer wavelength UIR

features, such as the 6.2 μm, is not clearly indicated. Although the 3.3 μm emission bands of the several neutral PAH species showed a strong invariance in frequency, the same was not true of the 6.2, 7.7, and 11.2 μm features.

Because PAHs are likely to be ionized by the interstellar ultraviolet field, and given objections by Leach (1987) and Donn, Allen, & Khanna (1989) that neutral PAH exhibit bands in the ultraviolet which are not observed, there was a need to look at the spectra of ionized PAH molecules in the visible and ultraviolet regions of the spectrum. In the neutral states, PAHs exhibit a number of strong ultraviolet extinction features that are not seen in the ultraviolet extinction curve. A systematic study of PAH cations in the spectral region 1.22-6.25 μm^{-1} was undertaken by Lee & Wdowiak (1993 and 1994) and Robinson, Beegle, & Wdowiak (1997). In those works, the neutral PAH molecules were dissolved in a boron oxide glass matrix and irradiated by gamma radiation, a technique which converts a portion of the population of neutrals to cations that are isolated. The general spectral characteristics that are exhibited by the neutral molecule disappear, including the UV absorption bands (See Fig. 1.10). These studies also placed the lower energy boundary required for ultraviolet photons that pump the infrared emission from the PAH cations at 7.75 eV, a value higher than previously thought. This has ramifications for the kinds of stellar and nebular conditions that could pump PAH cations into UIR emission.

1.1.4 The Galactic 3.4 Micron Absorption Band

In the infrared spectrum toward the direction of the galactic center, there are absorption features seen against the continuum of IR sources in the center of the Milky Way at 3.0, 3.4, and 18.5 μm, with a very strong feature at 9.7 μm (Fig 1.11). The very strong 9.7 μm and weaker 18.5 μm bands have been attributed to silicate stretching and

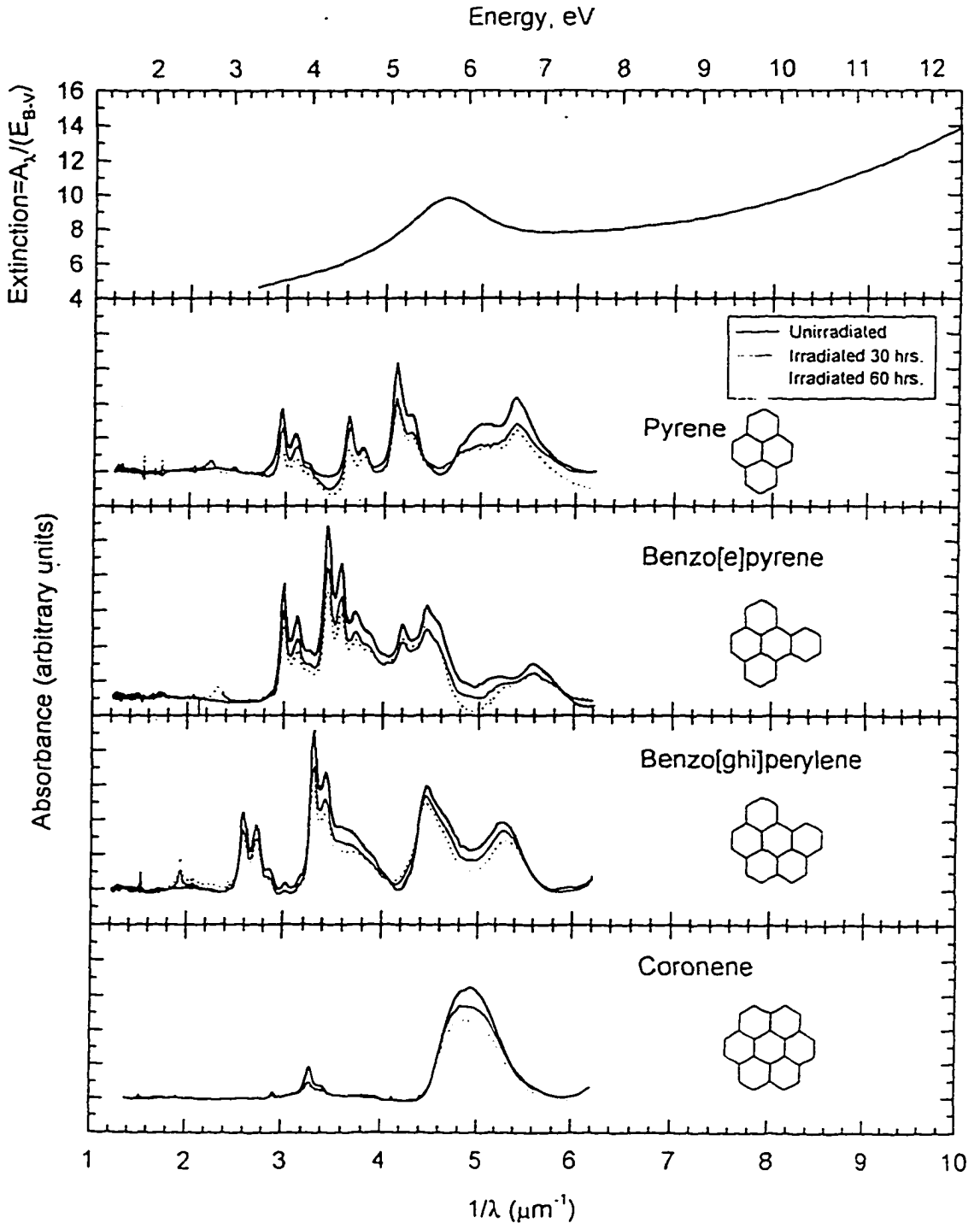

FIG. 1.10— Absorption spectra of neutral (*thick solid line*), 30 hr irradiated (approx. 188 krad, *thin solid line*), and 60 hr irradiated (approx. 377 krad, *dotted line*), sapphire-boron oxide glass PAH samples vs. sapphire-boron oxide glass references under the same conditions. As an increasing number of the PAH molecules become cations the $\pi^* \leftarrow \pi$ features diminish. The average interstellar extinction curve (Seaton 1979) is shown in the top most graph for comparison. (Robinson et al. 1997)

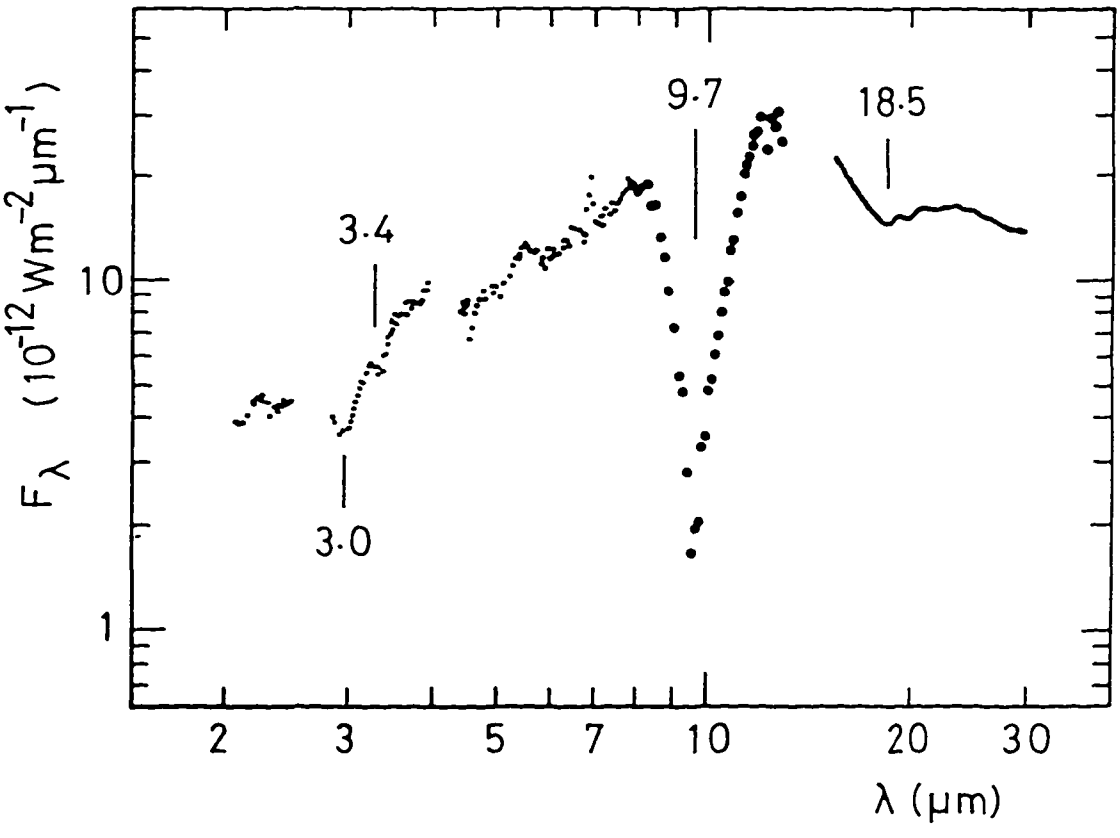

FIG. 1.11— Integrated infrared spectrum of the galactic centre source Sgr A from 2 to 30 μm (adapted from Roche 1988).

bending resonances, with the 3.0 μm band being likely due to water (H_2O) ice (Whittet 1992). The 3.4 μm band, shown in more detail in Figure 1.12, has been attributed to C-H stretching modes of hydrocarbons. Since this band profile is complex, there has been considerable debate and limited success in assigning the exact form of carbon-based species responsible for it (Sanford et al. 1991; Pendelton et al. 1994). One conclusion is that the carrier contains both methylene ($-CH_2-$) and methyl ($-CH_3$) functional groups in the ratio of about 5:2 (Sanford et al. 1991), a result confirmed in the course of this research.

The band has a reasonably good match to the hydrocarbon benzene/methanol extract of the Murchison carbonaceous chondrite CM2 spectra (Fig. 1.13), meaning that the responsible carrier might have made its way unchanged into the primordial meteorite. There have been other attempts to match this feature, with varying degrees of success. These include (see Fig. 1.14) 1. organic interstellar grain mantle analogs consisting of complex molecules formed by irradiation of ices (Greenberg 1978; d'Hendecourt, Allamandola, & Greenberg 1985; Schutte 1988; Sanford et al. 1991; Khare et al. 1993); 2. hydrogenated amorphous carbons (HAC) in various hydrogenation amounts (Jones, Duley, & Williams 1987; Borghesi, Bussoletti, & Colangeli 1987); 3. quenched carbonaceous composite (QCC) material produced by quenching the plasma of methane gas (Sakata & Wada 1989); and 4. others (including E coli bacteria!, Hoyle et al. 1982).

1.1.5 The Extended Red Emission

The extended red emission (ERE) is a broad-band emission feature seen in reflection nebulae around B- and A- type stars, and in its most dramatic observations in certain planetary nebulae such as the Red Rectangle (HD44179), which is also a UIR band emitter. An example of the ERE, the region around the star HD44179, the Red Rectangle, is

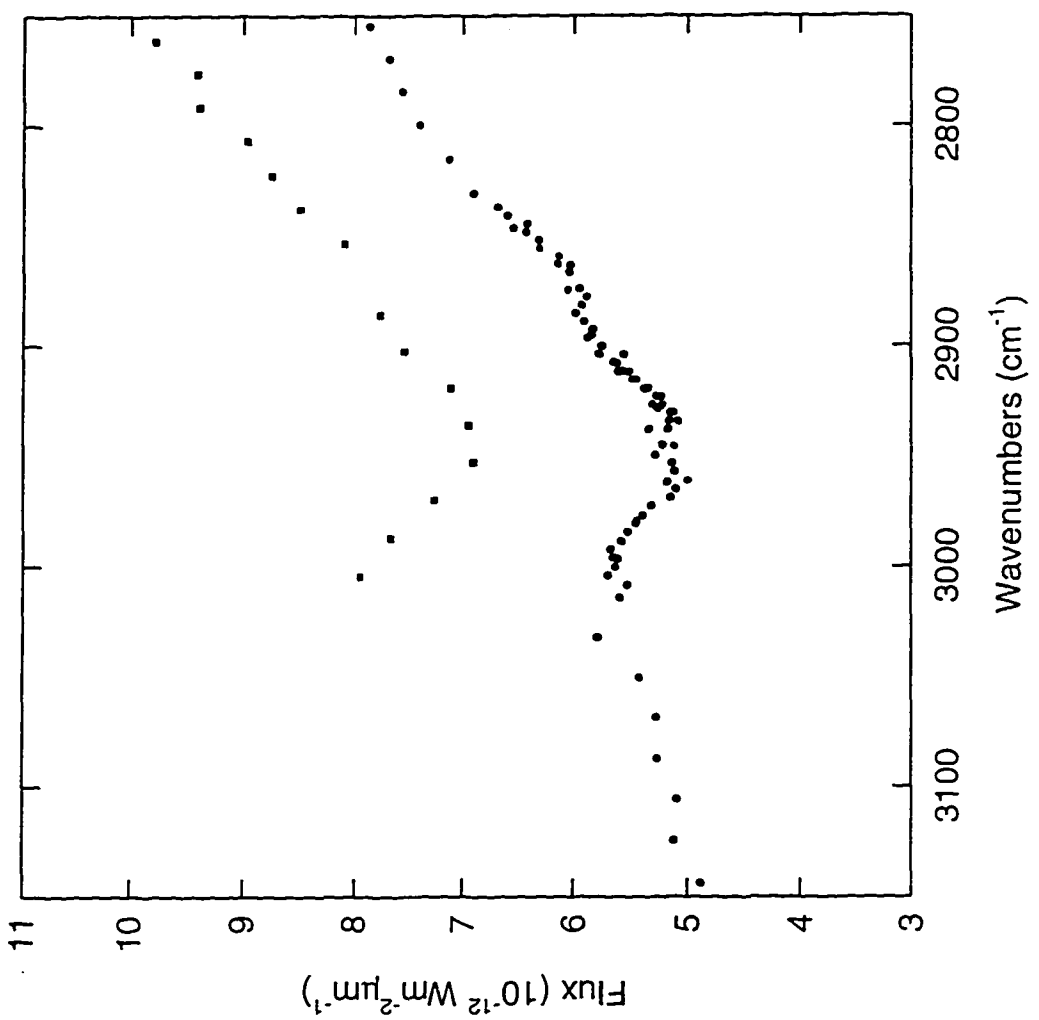

FIG.1.12— Flux spectra of sight lines toward Galactic center sources IRS 7 (*squares*) and IRS 6E (*dots*). (Adapted from Pendleton et al. 1994).

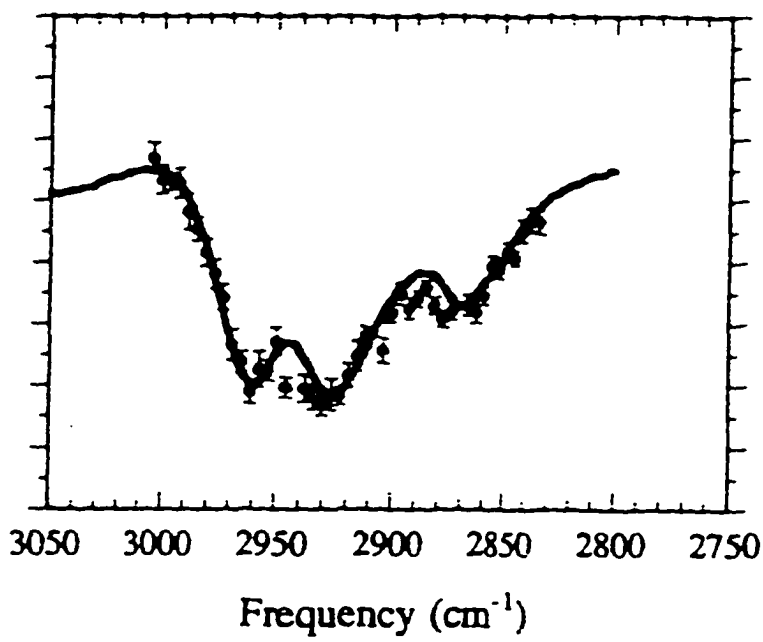

FIG. 1.13— A comparison of the optical depth spectrum of Galactic center source IRS 6E (*solid points with error bars*) to the spectrum of an organic Murchison acid residue (*solid line*) (De Vries et al. 1993; Pendelton et al. 1994)

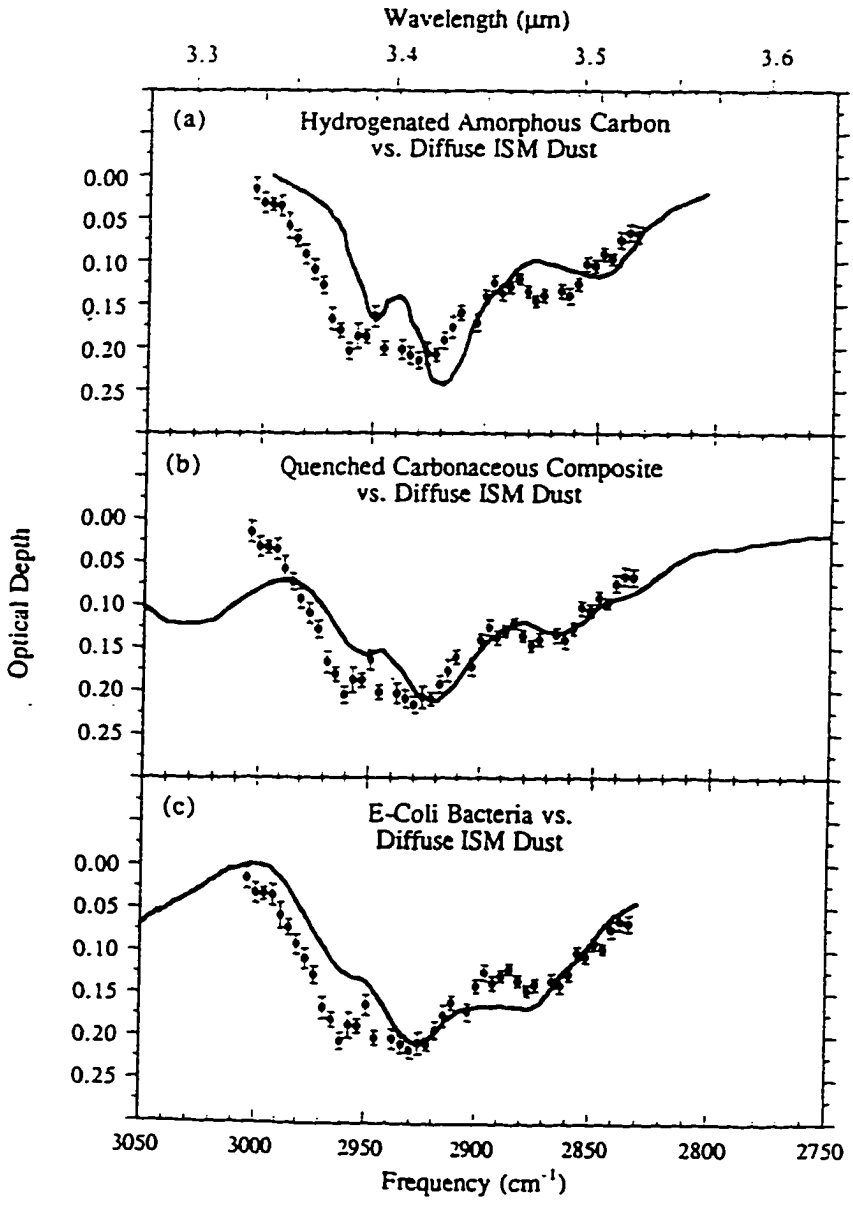

FIG. 1.14— A comparison of the optical depth spectrum of Galactic center source IRS 6E (*solid points*) to (a) the optical depth spectrum of a room temperature hydrogenated amorphous carbon (HAC), (b) the optical depth spectrum of a room temperature filmy quenched carbonaceous composite (QCC), and (c) E-Coli Bacteria (Pendelton et al. 1994).

shown in Figure 1.15 (adapted from Schmidt, Cohen, & Margon 1980). The UIR bands of this nebula indicate the presence of PAH species (Fig. 1.6). The ERE is characterized in the visible wavelengths by a very broad emission feature centered in the region between 5500 and 7500 Å, which can be as much as 30% of the total brightness of the nebula. Since there is a correlation between the ERE and UIR features in the infrared attributed to PAH species, it would seem to indicate that the PAH species are responsible for both the ERE and the UIR. However, it is assumed that the PAH molecules in these regions are likely to be ionized, and there is some debate as to whether they exhibit fluorescence when ionized (Witt & Schild 1988).

Hydrogenated amorphous carbon (HAC) has also been suggested as a species responsible for the ERE. Laboratory measurements of ultraviolet excited HAC films have demonstrated a broad luminescence in the spectral range 5000 to 10,000 Å (Watanabe, Hasegawa, & Kurata 1982). The position of the maxima tends to shift with increasing degrees of hydrogenation, with the highest luminescence quantum yield occurring at ~ 6800 Å. Hydrogenation in amorphous carbon should be dependent on the temperature, with very hot regions pumped by ultraviolet radiation having lower hydrogenation content. As with HAC, several other carbonaceous species have been reported to have a good correlation to the ERE of the Red Rectangle.

Wdowiak et al. (1989) subjected mixtures of CO, Ar, N_2, H_2O, and CH_4 to an electrical discharge. The product was frozen out at 20 K and warmed up to room temperature. When excited by a 337-nm laser, the residue produced a broad band fluorescence in the 5500-6500 Å region (Fig 1.16). Wdowiak et al. (1995b) have also produced a carbonaceous material having broadband luminescence when excited with a 514-nm laser. This

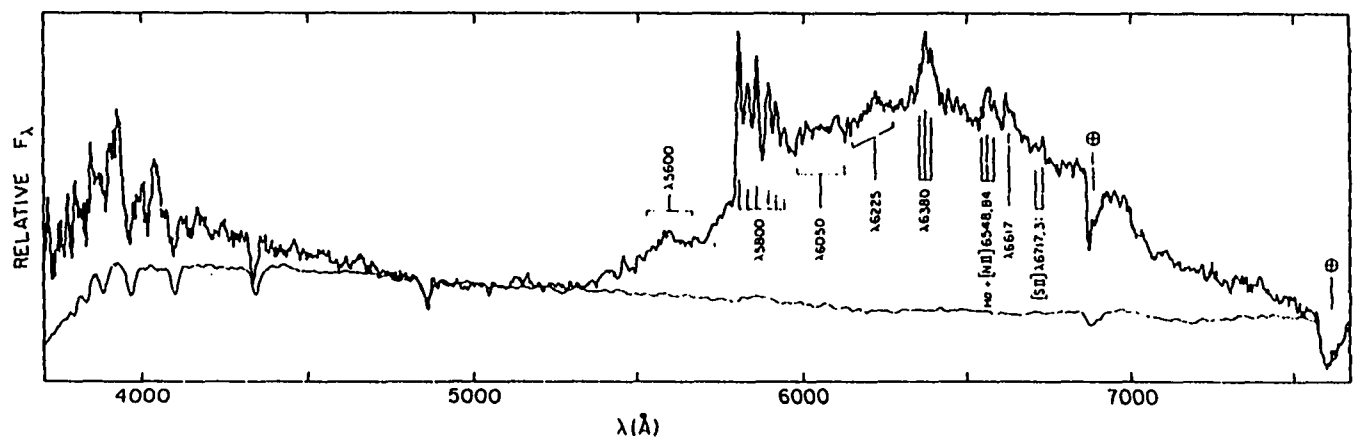

FIG. 1.15— Red Rectangle spectrum exhibiting extended red emission (ERE) in the 5500 Å to 7500 Å range and structured emission features superimposed on the ERE (Adapted from Schmidt et al. 1980).

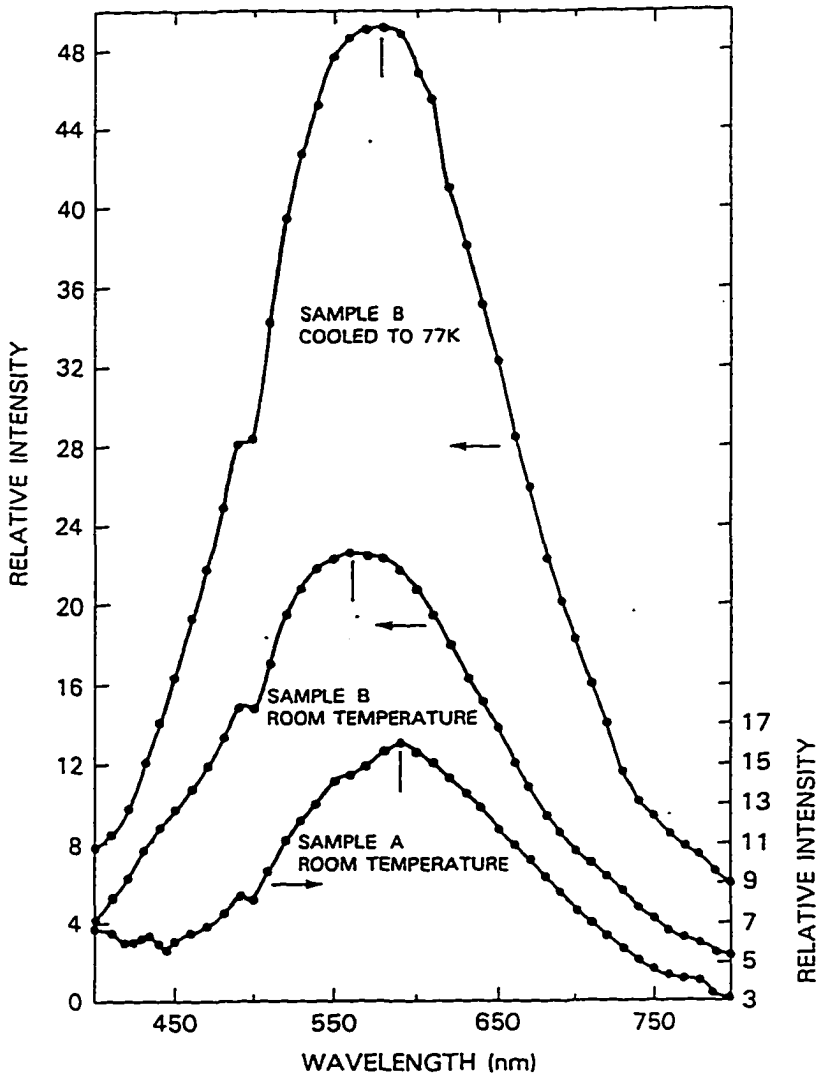

FIG. 1.16— Fluorescence spectra (337 nm excitation) of mixtures of CO, Ar, N_2, H_2O, and CH_4 when they are subjected to an electrical discharge, frozen out at 20K, and warmed to room temperature. Upper spectrum: sample B (high argon content) cooled to liquid nitrogen temperature. Middle spectrum: sample B at room temperature. Lower spectrum: sample A (low argon content) at room temperature. Intensity scale on left applies to upper two spectra. Right scale is for the bottom spectra (Wdowiak et al. 1989).

material was produced when the simplest PAH, naphthalene ($C_{10}H_8$), was subjected to an energetic environment of a plasma, resulting in a product possessing an IR absorption spectrum that was remarkably like that of the hydrocarbon extracted with benzene and methanol from the Murchison carbonaceous chondrite (CM2). The luminescence is exhibited over 2000 Å with a maxima in the 6000-6500 Å region. The laser-excited spectrum is very similar to the broad continuum of the ERE from the Red Rectangle and other dust clouds (Fig. 1.17).

1.2 Energetic Plasma Environments

In 1980, Wdowiak (1980) described an experiment in which a mixture of 0.5% methane in argon was subjected to a plasma discharge and then was frozen at 10 K on a substrate. This produced a band at 4500 Å in absorption that resembled in shape one of the widest and strongest DIBs at 4428 Å. The experiment also resulted in several other bands, including laboratory candidates for the DIBs at 6283 and 6296 Å. This result was not only reproducible, but it was also stable under irradiation of ultraviolet light from a mercury vapor lamp. This was the first of many experiments done on the laboratory candidate for the 4428 Å DIB (Wdowiak et al. 1994, Wdowiak et al. 1995b) and fostered a more general effort in the use of the energetic environments of plasmas for synthesis of materials of astrophysical interest.

In 1993, while attempting to do visible wavelength emission spectroscopy when the PAH naphthalene is subjected to a hydrogen plasma, Lee and Wdowiak (1993) serendipitously synthesized a high molecular weight deposit. This deposit showed the same basic spectral characteristics (Fig. 1.18) of the benzene-methanol extract of the Murchison carbonaceous chondrite in the spectral range 4000-400 cm^{-1} (Cronin and Pizzarello 1990).

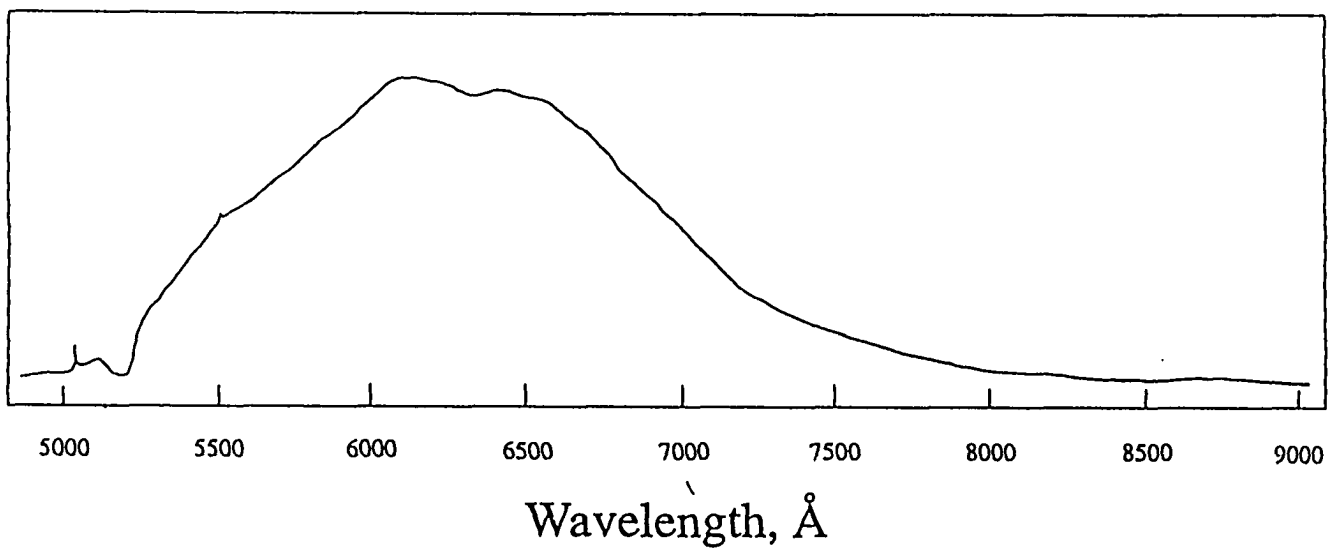

FIG. 1.17— Laser (514 nm) induced luminescence (intensity arbitrary units) from the film whose IR spectrum is displayed in Figure 1.18. The broad band emission is similar to what has been observed for the Red Rectangle (HD 44718).

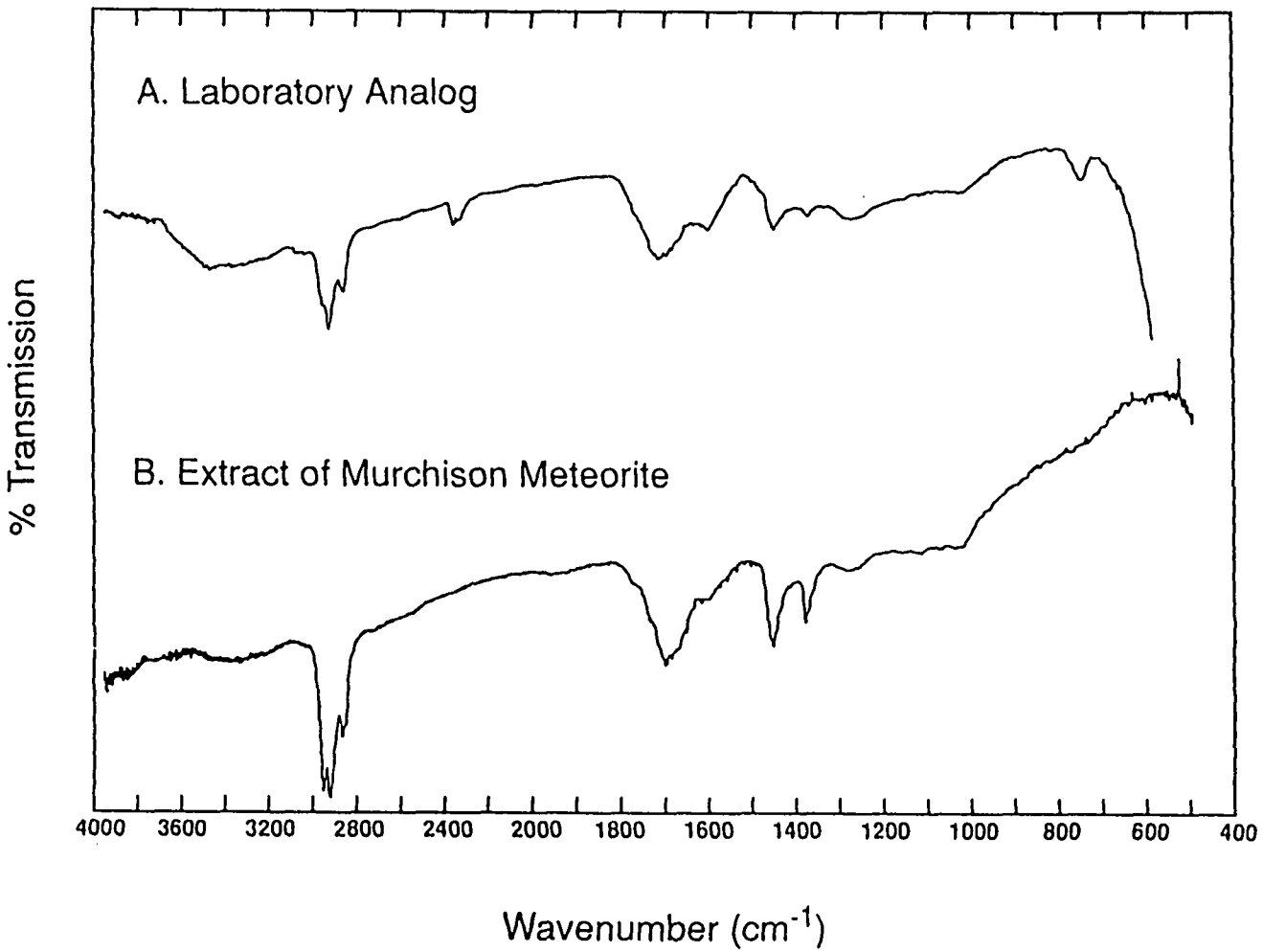

FIG.1.18— Comparison of the infrared spectrum of a laboratory synthesized analog (top) of the hydrocarbon benzene/methanol extract of the Murchison CM2 carbonaceous chondrite (Lee and Wdowiak 1993).

The difference in the spectra was that the ratio of $-CH_2-$ to $-CH_3$ for the synthesized material was much less than the corresponding ratio in the Murchison meteorite extract. Because the discharge tube that was used in these experiments was not designed for easy extraction of the processed material or for the precise control of reagent gas composition, it became apparent that a more sophisticated system was required for better control and monitoring of the gas mixture used to produce the plasma to which the PAH is subjected.

It was this research, more than any other, that initiated the efforts and subsequent results described in the following sections.

2. EXPERIMENTAL INDICATION OF A NAPHTHALENE-BASE MOLECULAR AGGREGATE FOR THE CARRIER OF THE 2175 Å INTERSTELLAR EXTINCTION FEATURE

2.1 Experimental

To study what occurs when the simplest polycyclic aromatic hydrocarbon (PAH) naphthalene ($C_{10}H_8$) is subjected to the energetic environment of a plasma, an advanced plasma reactor system was designed and constructed around a glass plasma tube reactor (Fig. 2.1). The plasma tube reactor was designed for easy extraction of synthesized products and for the ability to visually monitor the emission from various places in the reactor by using fiber optic light guides. The manifold and pumping components of the system permitted greater control over composition of the gases utilized to create the plasma than was possible in earlier experiments carried out in the UAB Astrophysics Laboratory (See Section 1.2)

2.1.1 The Plasma Reactor System

Annular electrodes of 55 mm diameter made from either aluminum or gold-plated brass are installed in the two end chambers of the reactor so that the plasma is funneled through the center of the 12.5 mm interior diameter plasma tube that is a conduit between the end chambers. The electrodes are attached by threaded connections to 1/8 in. threaded steel rods soldered into 1/4 in. brass rods. These, in turn pass, out of the reactor end chambers through 1/4 in. stainless steel Cajon Ultra Torr unions fitted onto glass tube side arms. Solid aluminum blocks (19 mm thick), fitted with an o-ring seal, cap the end chambers.

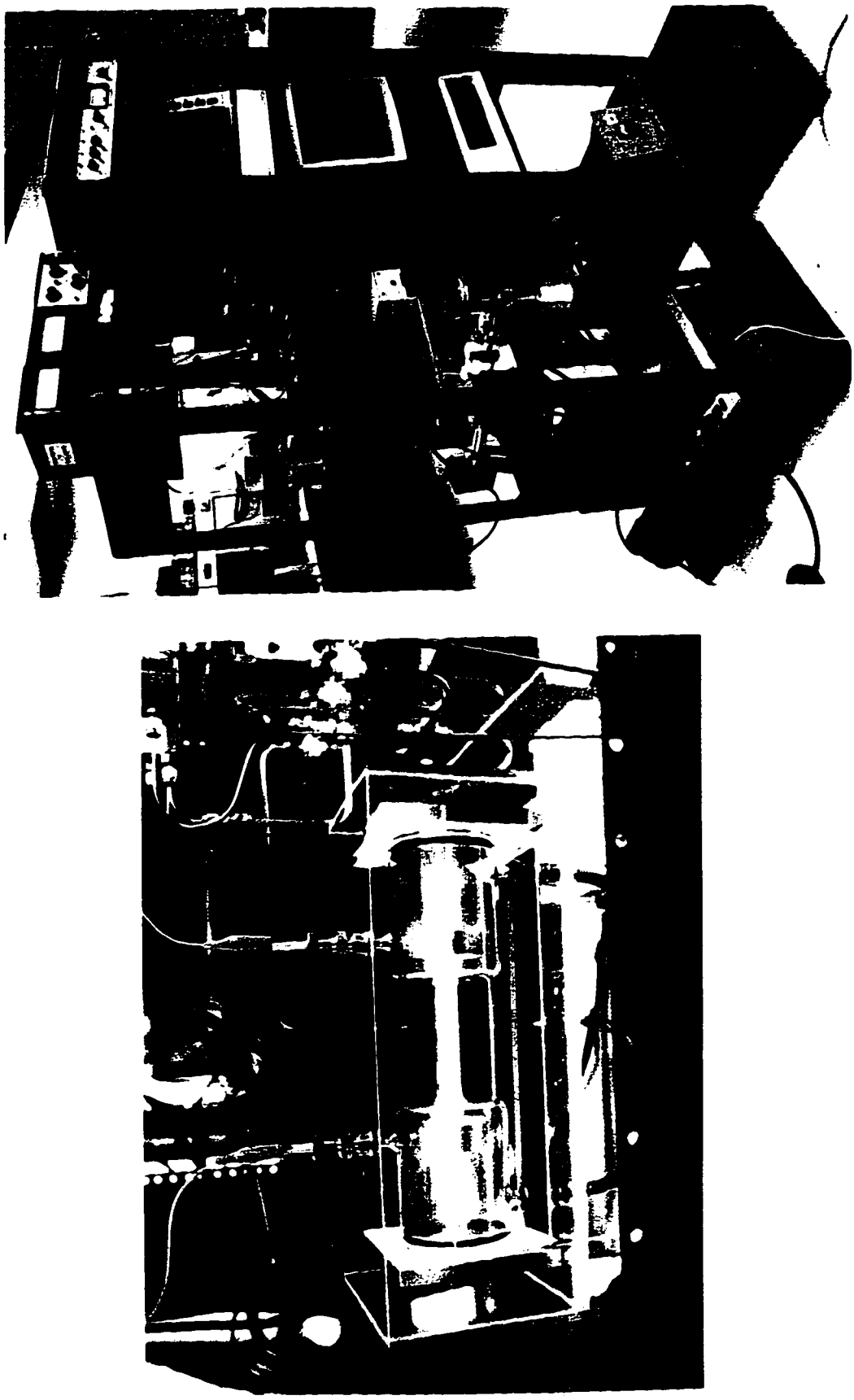

FIG. 2.1— Photographs of the plasma tube reactor during electrical discharge with hydrogen gas (left) and the assembled experimental system (right).

One of these end caps has a port milled through it so that a sapphire disk end window can be sealed into it with an o-ring for visually monitoring the plasma along the axis of the discharge. A sapphire collection disk, inserted in a mounting at the downstream end of the discharge, is used to sample material which had been in the gas phase as it exits the plasma tube. Figure 2.2 shows the plasma tube reactor.

Gas enters and exits the plasma reactor via two glass side arms fitted with two 1/4 in. Cajon stainless steel Ultra Torr fittings connected to lengths of 12 in. Cajon stainless steel flex tube which are attached with Swagelok fittings to the stainless steel manifold. The flex tubing mode of connection was used because it reduced mechanical stress on the glass reactor, reducing the possibility of failure through fracture of the glass.The plasma reactor system, shown in schematic presentation in Figure 2.3, utilizes a liquid nitrogen trapped diffusion pump to reduce pressure prior to introduction of reagents to $\leq 1 \times 10^{-5}$ torr as measured with an ionization gauge. A quadrupole mass spectrometer monitors the composition of gases entering or exiting the reactor, and there is provision for continuous electronic pressure monitoring in the range used during the discharge. Stainless steel was employed in the construction of the manifold to insure minimum contamination in the mixing of gaseous reagents.

In these experiments, approximately 800 mg of naphthalene is coated on the inner wall of a sapphire tube by inserting it into the tube, melting it with a hot plate, and then rotating the tube by hand so there is coverage of the entire interior surface when the naphthalene solidifies. The prepared tube is then inserted in the center section of the plasma tube where the plasma will transit through it. Gases are first introduced into the reactor system at several tens of torr pressure and then pumped down to operational pressure. This

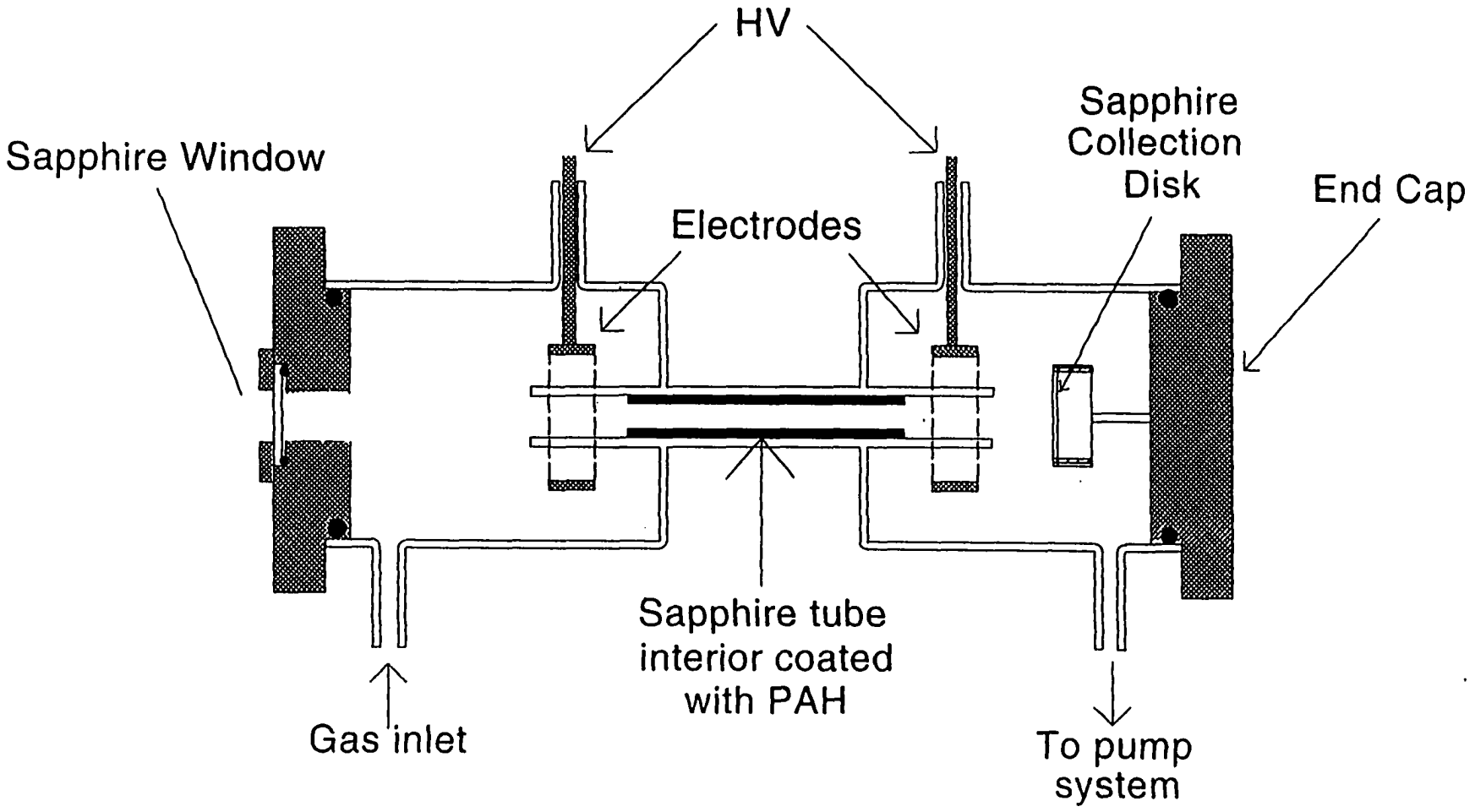

FIG 2.2— Schematic diagram of the plasma tube reactor.

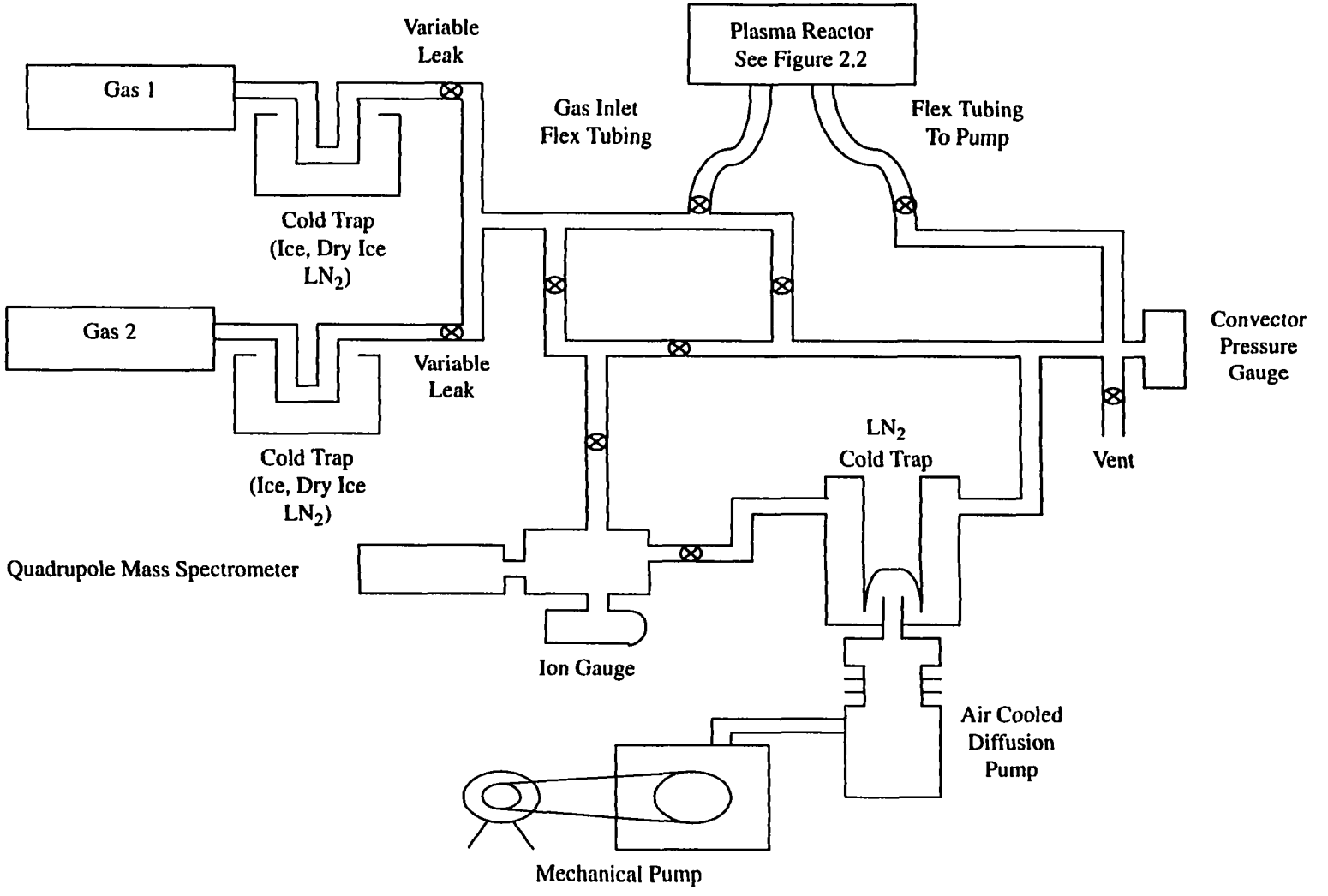

FIG. 2.3— Schematic of the plasma reactor system.

purging is repeated several times to ensure that residual atmospheric contaminants are negligible which is confirmed by mass spectroscopy. The pressure inside the system was monitored with a Varian ConvecTorr pressure gauge. This allowed continuous monitoring of the pressure during a run. However, because most electronic pressure gauges are designed to operate with gases of an atmospheric composition, a McLeod gauge is employed to calibrate the Varian ConvecTorr pressure gauge for use when gases different from atmospheric (i.e. hydrogen) are present. The calibration curve of the Varian Convec-Torr derived from this procedure is shown in Figure 2.4. Gases are introduced through cold traps that can be cooled with liquid nitrogen (LN_2), dry ice (CO_2), or water ice (H_2O). The cryogen selection was determined by the characteristics of the gas being utilized. For hydrogen and helium, the traps were filled with LN_2. The pressure at which most experimental runs took place was 500 millitorr, although some experiments were done at 300 millitorr or 1.2 torr. Once the desired pressure is established, the discharge is initiated with an electrical current from a 9400 VAC transformer. That transformer is in turn controlled with a variable transformer operating from line voltage.

2.1.2 Description of an Experimental Run

Gases and gas mixtures used in the experiments with naphthalene have been hydrogen, hydrogen with a 5% concentration of methane or oxygen, hydrogen with a 10% concentration of methane or propane, helium, and helium with a 10% concentration of oxygen. During an experimental run, the coating of naphthalene in the interior of the sapphire tube undergoes a chemical change which is made evident by a bright luminescence that progresses through a remarkable color sequence of ultraviolet (from the naphthalene precursor), blue, white, yellow, orange, and finally deep red, in a time frame of about 30

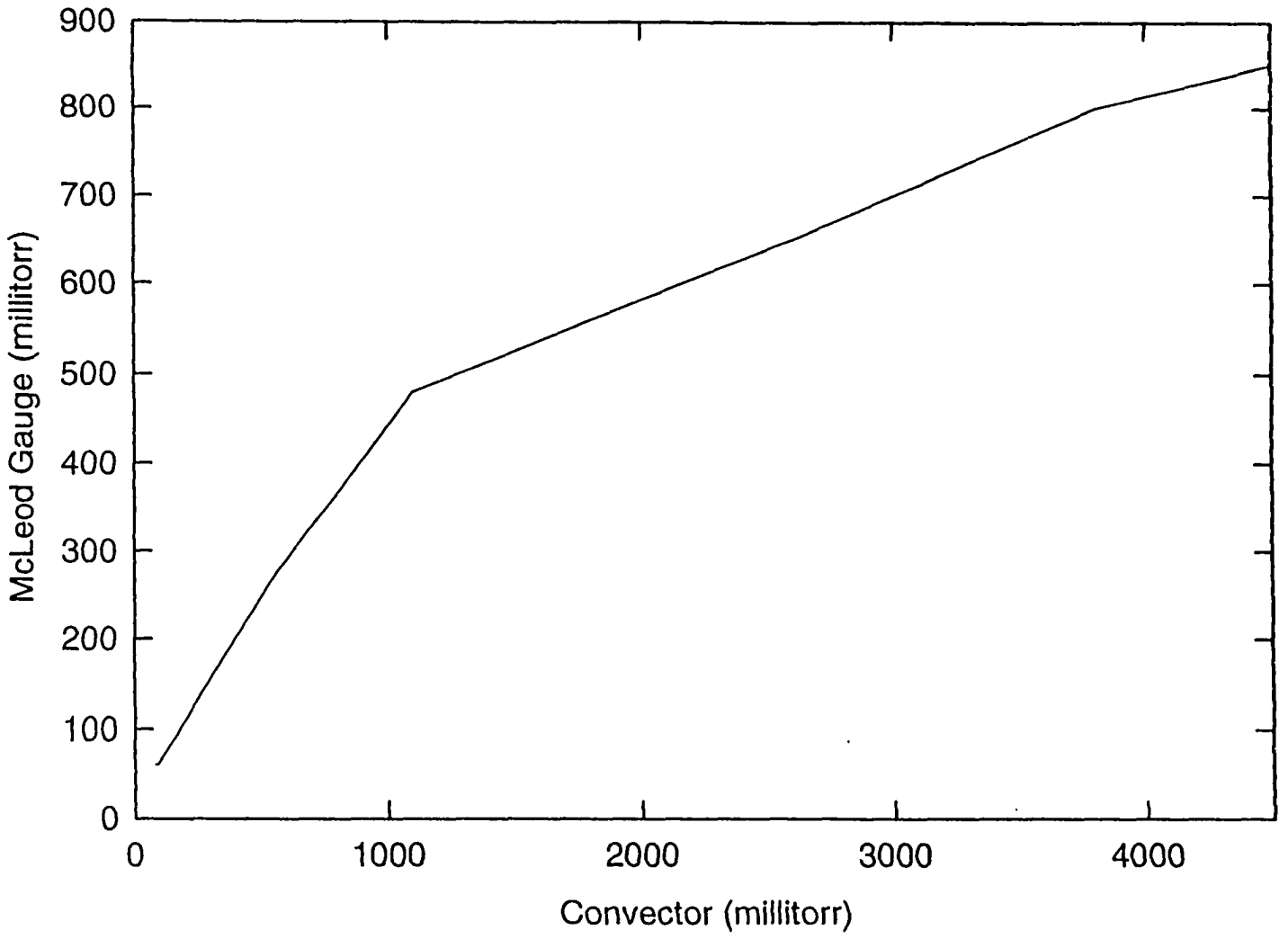

FIG. 2.4— McLeod gauge calibration curve for the Varrian ConvecTorr pressure gauge when hydrogen is the measured gas.

min. Figure 2.5 shows photographs of the vivid sequence. Once the luminescence is deep red, it remains stable in color for discharge times up to the 5 hr. maximum the experiment has been run. This luminescence is excited in the solid product by the radiation emitted from the plasma. The resulting product residing in the sapphire tube has a yellow color in reflected room light and a texture that are both distinctly different from the naphthalene precursor. Material forming in the gas phase and then deposited out on the sapphire collection disk remains in the discharge, where it can undergo further alteration.

2.1.3 Spectroscopic Technique

Upon termination of the discharge, the residue is harvested from within the sapphire tube that held the naphthalene precursor. Material is also scraped from the electrodes, where it appears as a black deposit. The downstream sapphire disk, which also has a deposit on it, is removed from the plasma reactor and placed directly in the sample compartment of a Mattson Polaris FTIR spectrometer for spectral measurements in the 4000 to 2000 cm^{-1} sapphire transparency range at a resolution of 4 cm^{-1}. Samples in the amount of 1 mg, from the residue harvested from the inside of the sapphire tube or the electrode deposits, are pressed with 100 milligrams of spectroscopic grade KBr into a pellet for infrared spectroscopy measurements in the 4000 to 400 cm^{-1} range at the same resolution. An agate ball mill, aluminum pellet collar, and hydraulic press were used for this procedure. Films deposited on KBr by vacuum evaporation onto quartz or KBr were used as well, as described in Section 2.2.4. All spectra were ratioed against a background obtained from blank KBr pellets or disks. For most of the measurements, a liquid nitrogen boiler heated by a ceramic resistor was employed to produce a dry nitrogen purge of the spectrometer.

FIG. 2.5— Photographs showing the luminesce when the solid product progresses through the remarkable color sequence of ultraviolet, blue, white, yellow, and finally a deep red in a time frame of about 30 min. The emission apparent in the top photograph is primarily from the plasma itself as the naphthalene precursor has yet to be altered and hence emits in ultraviolet wavelengths not recorded by the film because of the attenuation of the camera optics. Photographs were taken with Kodak Ektachrome 400 ASA slide film, 0.5 sec exposure time, and a lens setting of 1.8.

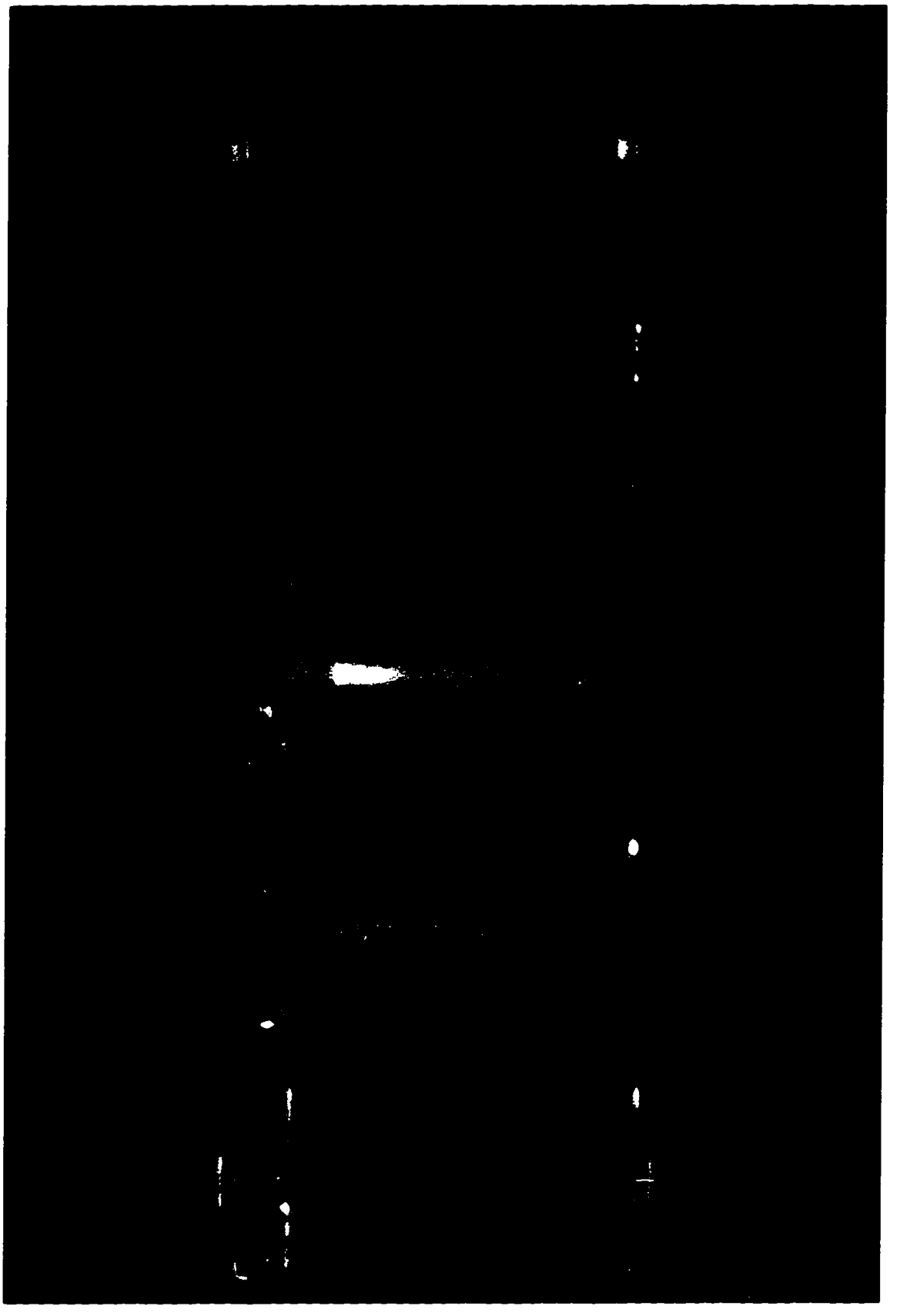

Spectra in the 190 nm to 820 nm ultraviolet/visible (UV/VIS) range were obtained with a Hewlett-Packard 8452 diode array spectrometer at a spectral resolution of 2 nm. Integration times of up to 25 sec can be made with this instrument, and the maximum time was generally used. Satisfactory absorption spectral measurements in the UV/VIS spectral range typically require areal densities on the order on 10^{16} cm^{-2} to produce an absorbance of 1 to 2. This is smaller by one or two orders of magnitude than that required to produce the same abundance for infrared spectroscopy.

Uniform samples suitable for UV/VIS spectroscopy are best prepared by evaporating a small amount of the residue material onto a quartz plate in a vacuum produced by a liquid nitrogen trapped diffusion pump. To do this, residue from the interior of the sapphire tube is placed into a graphite crucible heated by a tungsten filament basket. A clean quartz collection plate, which has been characterized by UV/VIS and FTIR absorption spectroscopy, is then mounted in a holder that is 50 mm above the crucible. Moderate heating of the crucible to temperatures of 200-300°C results in a flash-over of material that is easily observed visually, as a film depositing on the quartz plate. It is desirable to have a film that has the range of 1 to 2 absorbance units when doing UV spectroscopy which, in this case, possess one set of interference fringes when examined with a visible light source such as a fluorescent room lamp or a sodium vapor lamp. Thicker films deposited on KBr disks are generally required when doing infrared spectroscopy. Infrared spectroscopy is possible in the 3150-2750 cm^{-1} range for a sample evaporated on quartz; however, the film necessary for a satisfactory spectra must be thicker than that utilized to obtain UV/VIS spectra in the 1-2 absorption unit range. To determine if the naphthalene precursor contributed to the evaporated films, an amount was placed in the graphite crucible and

heated, however no detectable film was found to form on the quartz substrate.

Measurements at UV/VIS wavelengths were also made on 5 mg of the yellow residue introduced into 500 ml of methyl alcohol. A quartz cuvette was filled with the mixture and UV/VIS absorption spectra obtained relative to a methyl alcohol reference in the same quartz cuvette. It was our experience that a component of the residue exhibited limited solubility in methyl alcohol, which was the principal reason evaporated films were employed. The less soluble black deposits harvested from the reactor electrodes were dispersed in Dow Corning silicone grease for ultraviolet absorption measurements. By circumstance, we discovered this grease has only continuum absorption at wavelengths ≥ 190 nm, as shown in Figure 2.6, allowing it to be used for making mulls in a manner similar to what can be done for infrared measurements using Nujol oil.

2.2 Spectroscopy and Chemical Analysis

2.2.1 Ultraviolet Spectroscopy

The samples utilized for UV/VIS absorption spectroscopy were the yellow-colored residue from the interior of the sapphire tube insert, where the naphthalene had been in intimate exposure to the plasma, and a black deposit formed on the surface of the annular electrodes. It should be noted that neither of these materials exhibited the distinctive odor of naphthalene. Figs. 2.7, 2.8, and 2.9 show spectra that were arbitrarily selected from the 28 experiments on a normalized absorbance scale and in units of μm^{-1} of films prepared from the yellow residues of three separate experiments (15: 96% H_2, 4% O_2, 0.6 torr; 22: 90% H_2, 10% C_3H_8, 0.6 torr; and 23:100% He, 0.6 torr) on quartz ratioed against the quartz spectrum obtained prior to deposition of the film. Comparison of these spectra with the 300 K spectrum shown in Figure 2.14 where 100% H_2 was utilized demonstrates that

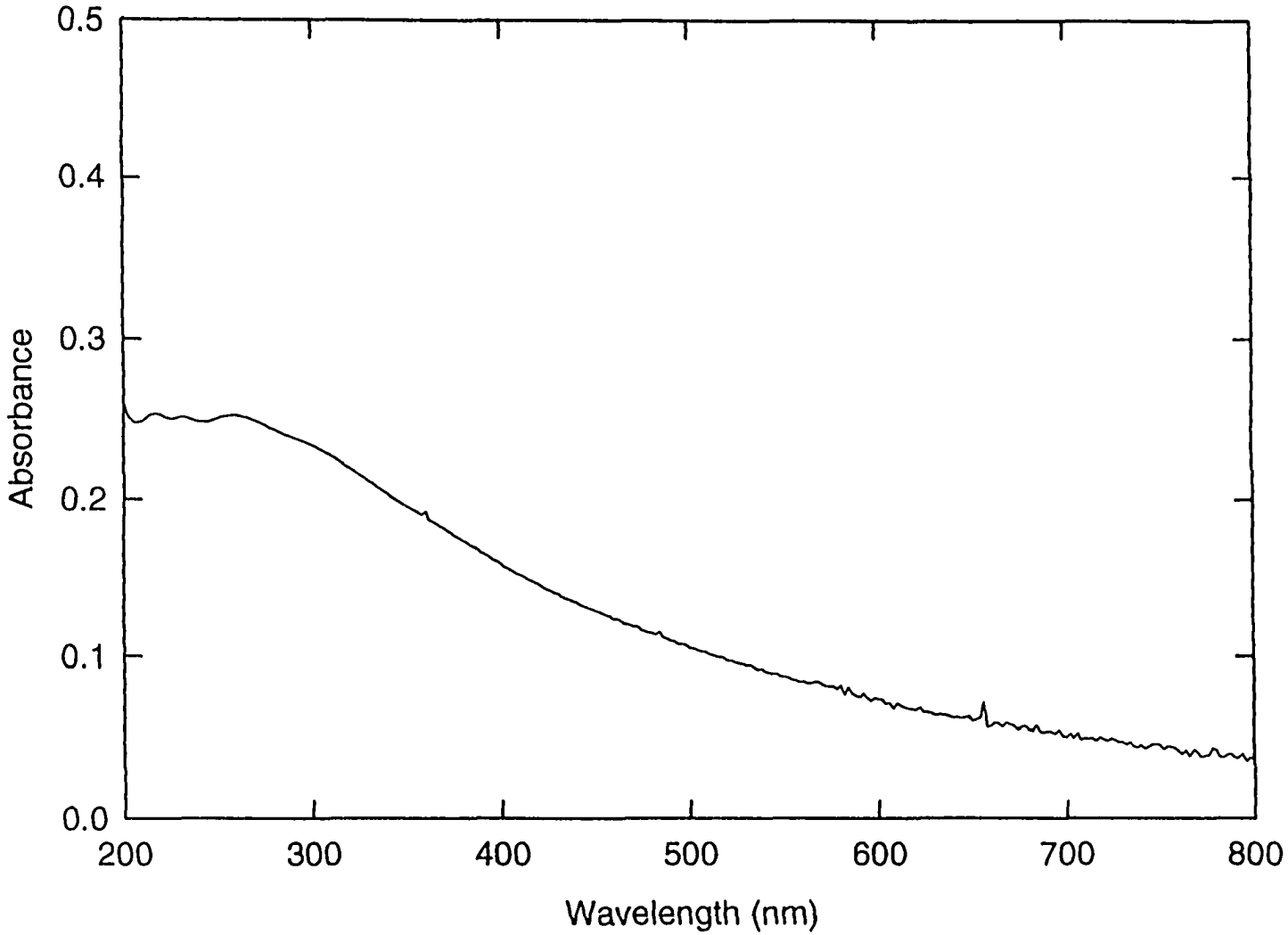

FIG. 2.6— Ultraviolet/Visible spectrum of Dow Corning high vacuum grease between 2 quartz plates ratioed against 2 quartz plates (0.00522 g/cm^2). This indicates it can be used to produce mulls of insoluble materials for UV/VIS absorption spectroscopy.

the character of the product is not a result of gas used to produce the plasma. Figure 2.10 shows the normalized spectrum of the black deposit harvested from an electrode of experiment 15 which peaks at 218 nm; Figure 2.11 shows the co-added result plotted on a scale approximately 2x that of the others. The co-added result is then plotted (line) along with the average interstellar extinction (dots) taken from the table of Whittet (1992) as shown in Figure 2.12. The fit to the interstellar 2175 Å (4.6 μm^{-1}) extinction feature in terms of breadth and peak position is a very good one, strongly supporting the material being a laboratory analog for what is the carrier of the 2175 Å "bump."

An exercise was performed in which the co-added result of the laboratory spectra displayed in Figure 2.11 was added to the curve considered to represent the contribution to extinction by classical size particles (Greenberg 1973) and to a curve representing the contribution to extinction at ultraviolet wavelengths by small particles as discussed by Whittet (1992). These curves were generated using the data contained in the table of Whittet (1992) in which the absolute extinction is normalized at $\lambda^{-1} = 1.82\ \mu m^{-1}$. The curve representing the contribution of classical-sized particles was generated by fitting a sixth order polynomial to the data in the $0\ \mu m^{-1} \leq \lambda^{-1} \leq 3\ \mu m^{-1}$ range and generating a third order polynomial (exponential) anchored at $\lambda^{-1} = 0\ \mu m^{-1}$ and $A(\lambda^{-1}) = 0$, such that the sum of these curves is a representation of the absolute extinction curve *sans* the 2175 Å (4.6 mm-1) feature. The third order polynomial represents the contribution from small particles. Both generated curves along with the co-added laboratory result are displayed independently in the bottom half of Figure 2.13. In the spectral range beyond that of the laboratory data ($\lambda^{-1} \geq 5.26\ \mu m^{-1}$), the generated curves are displayed by dotted and dashed lines.

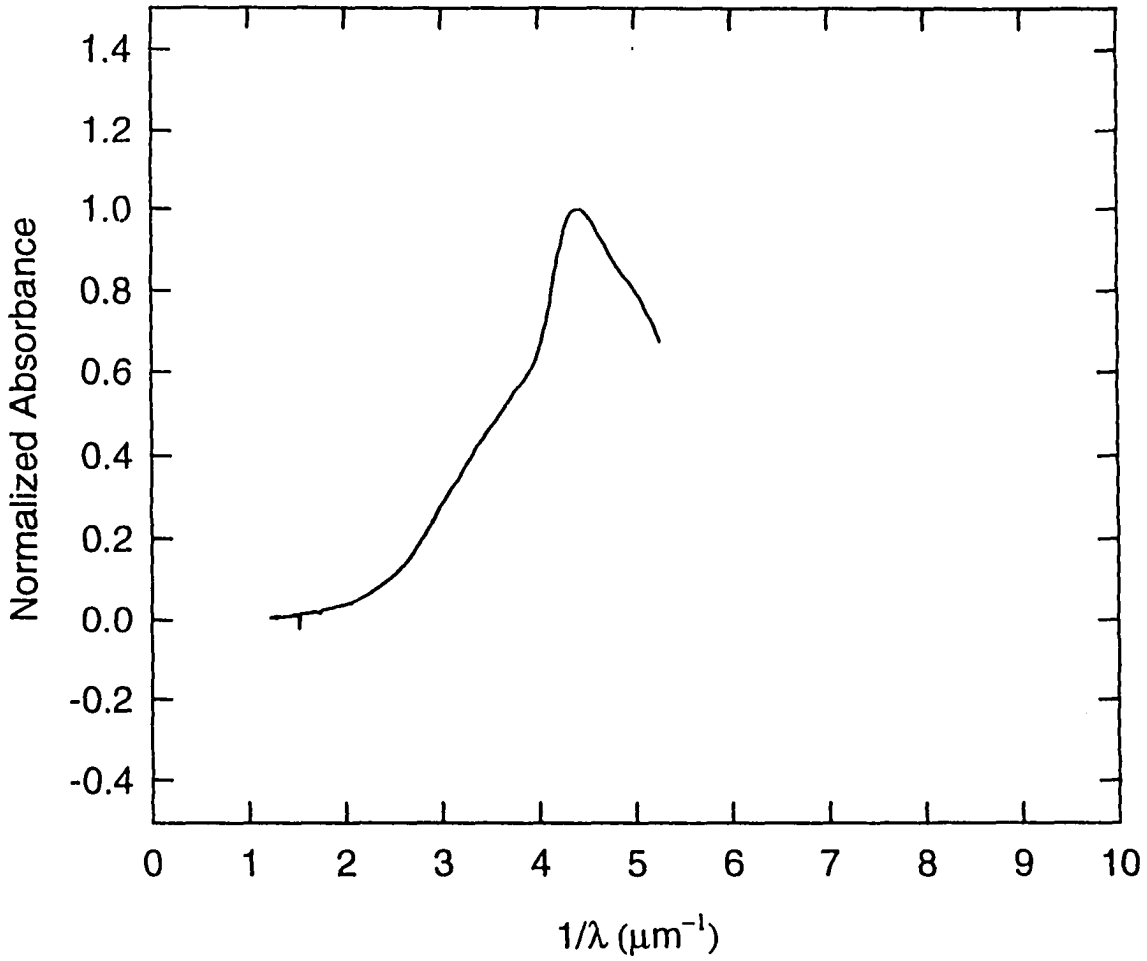

FIG. 2.7— Yellow residue of experiment 15 evaporated onto quartz ratioed against the quartz spectra prior to deposition of the film. The gas mixture in the experiment was 4% O_2 and 96% H_2 at 0.6 torr.

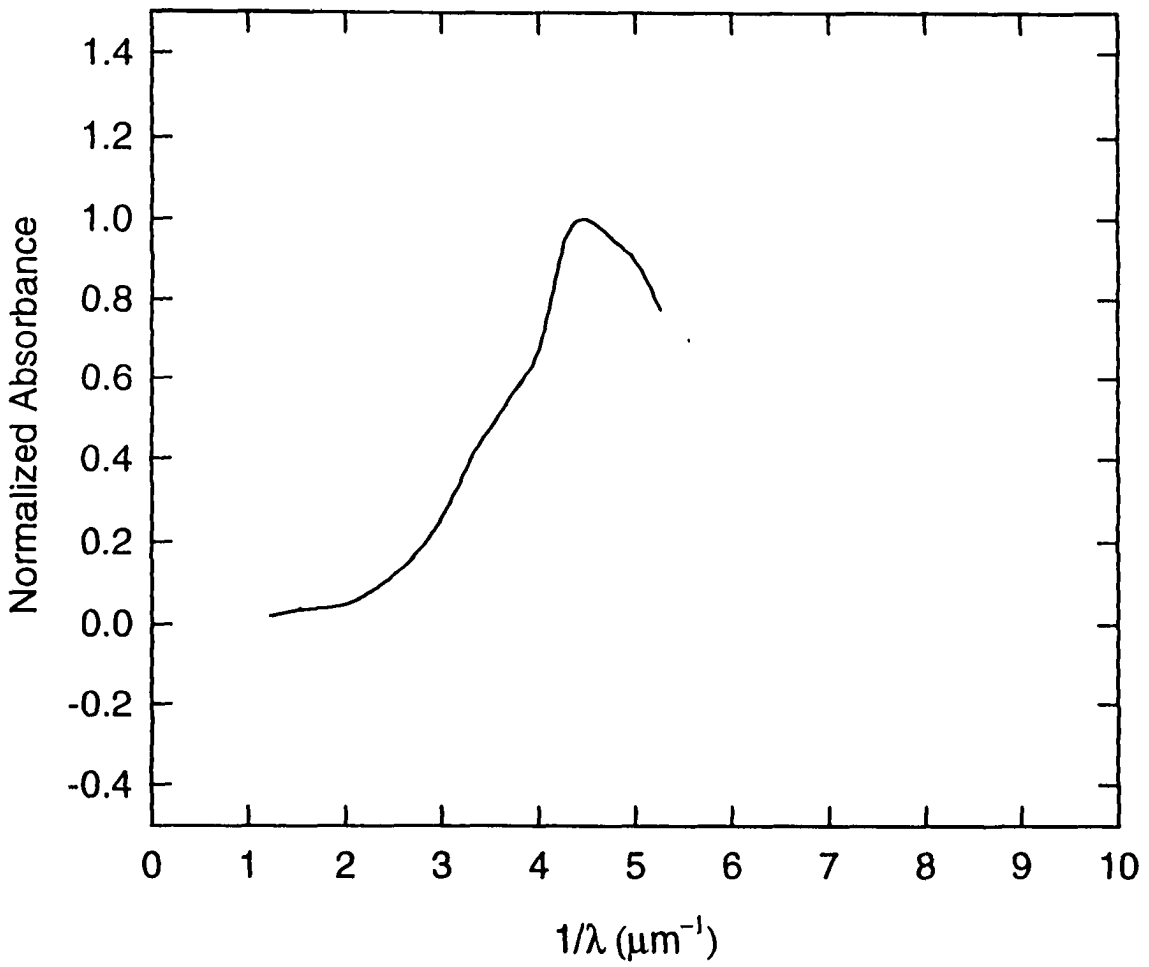

FIG. 2.8— Yellow residue of experiment 22 evaporated onto quartz ratioed against the quartz spectra prior to deposition of the film. The gas mixture in the experiment was 10% C_3H_8 and 90% H_2 at 0.6 torr.

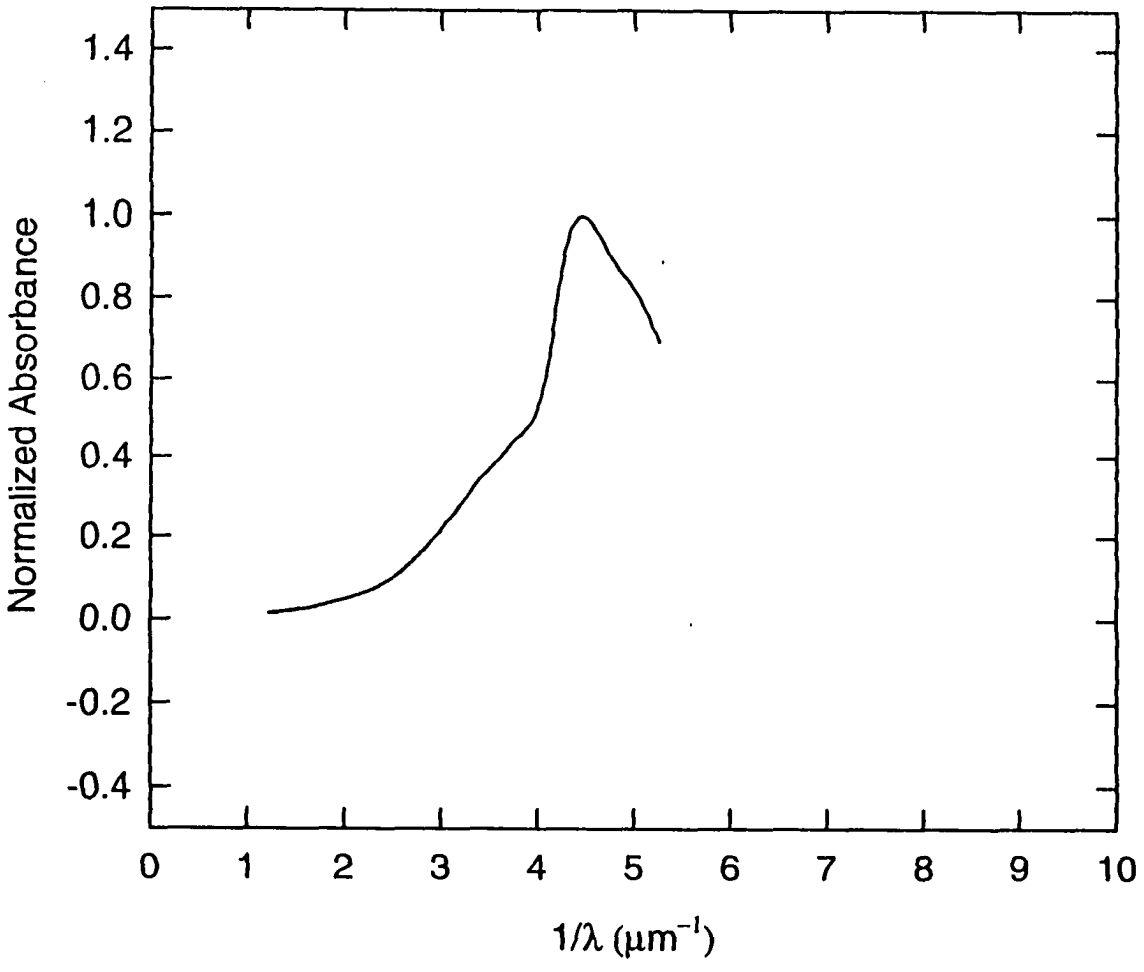

FIG. 2.9— Yellow residue of experiment 23 evaporated onto quartz ratioed against the quartz spectra prior to deposition of the film. The gas mixture in the experiment was 100% He at 0.6 torr.

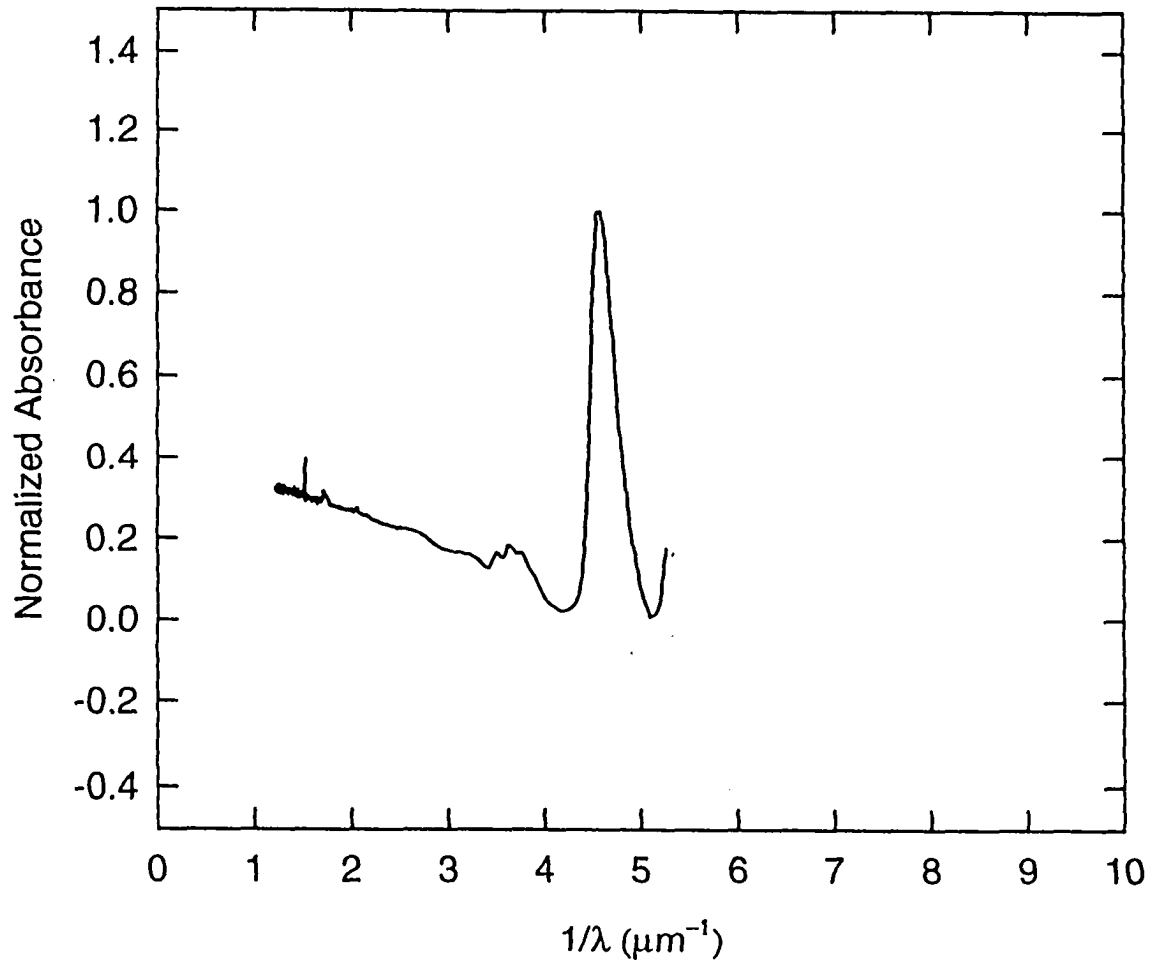

FIG. 2.10— Black deposit of experiment 15 in a silicone grease mull ratioed against pure silicone grease. The gas mixture in the experiment was 4% O_2 and 96% H_2. The declining base line for 1 $\mu m^{-1} \leq \lambda^{-1} \leq 3\ \mu m^{-1}$ is an artifact stemming from a difference in the thickness of the mull and the reference.

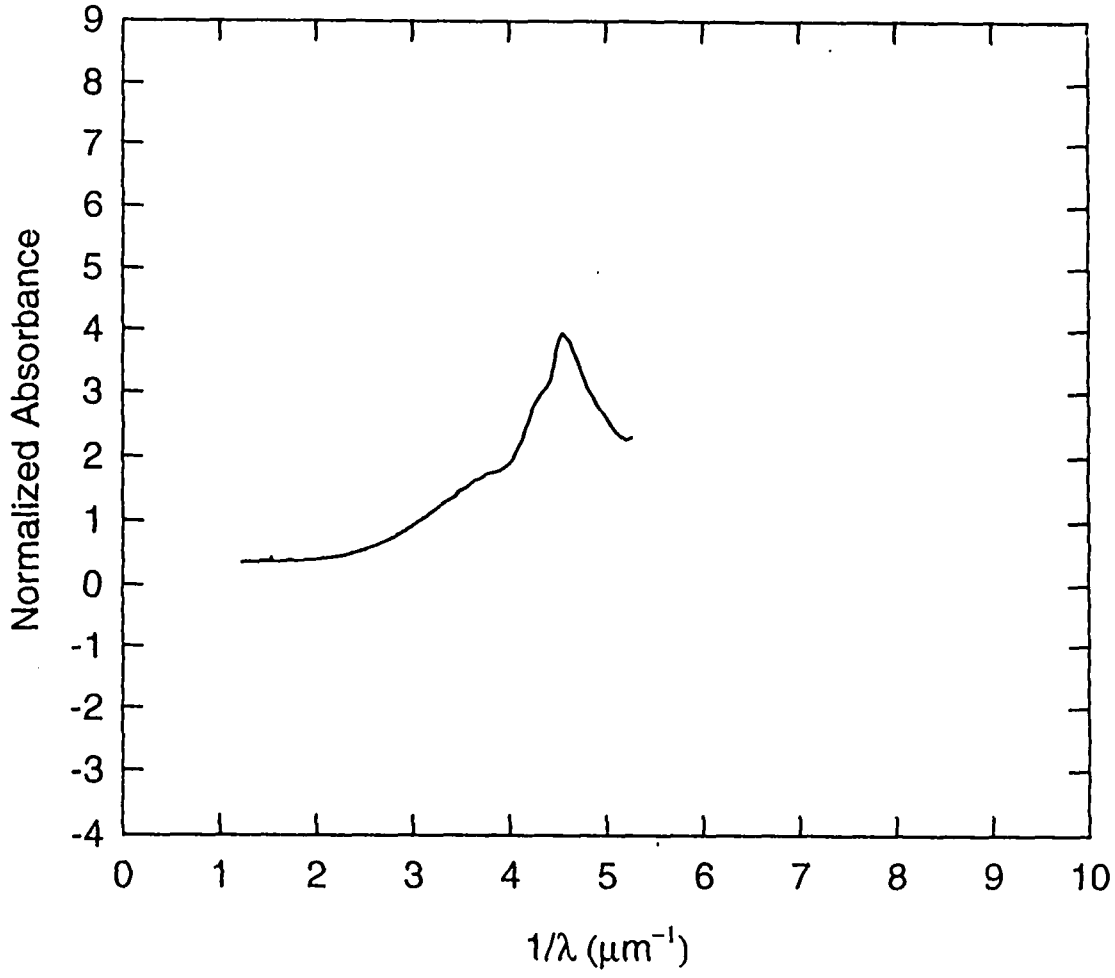

FIG. 2.11— Co-Added spectrum of the black deposit from experiment 15 (see Fig. 2.10) and the evaporated yellow films onto quartz using residues from experiments 15, 22, and 23 (see Figs. 2.7, 2.8, and 2.9)

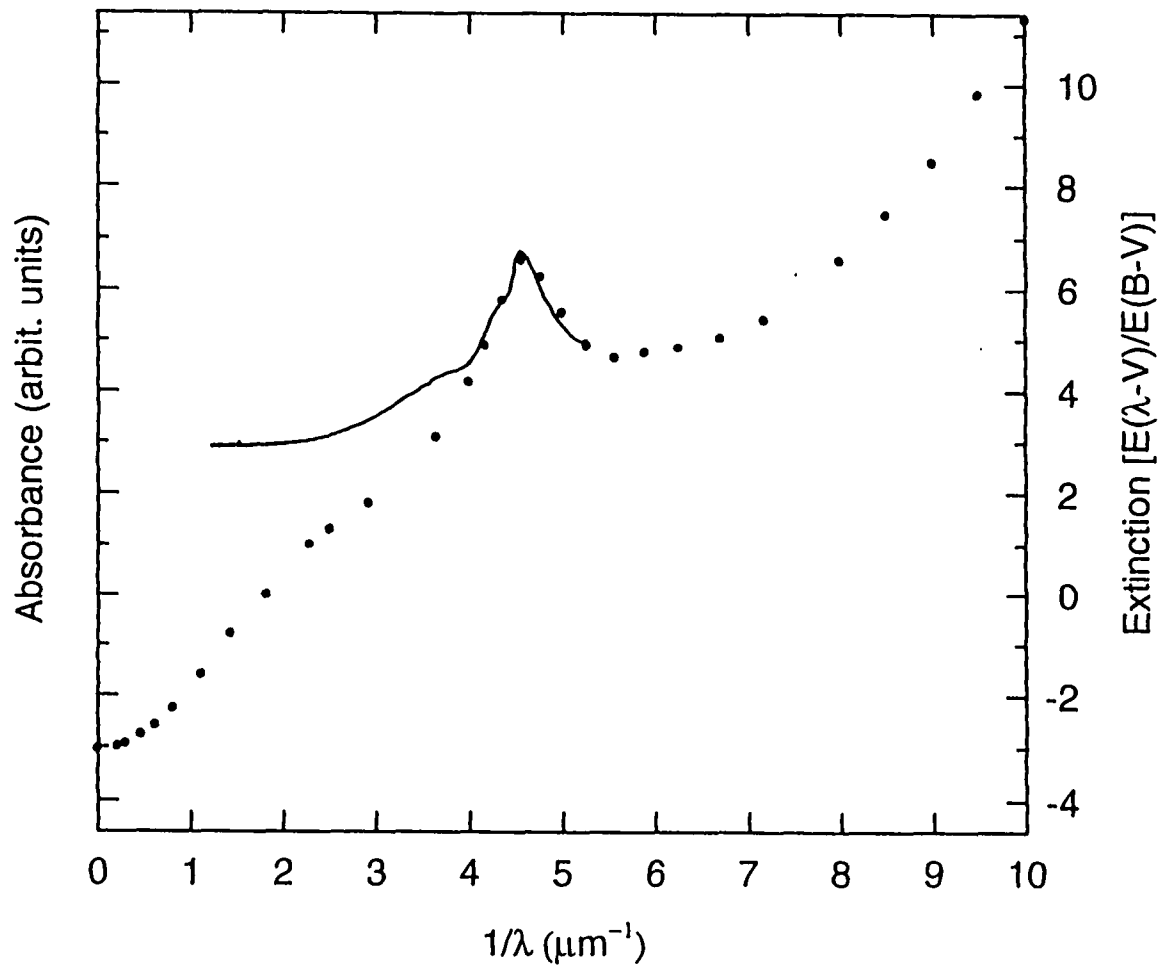

FIG. 2.12— Co-Added spectrum of Figure 2.10 along with the average interstellar extinction curve from the table in Whittet (1992). This suggests that the 2175 Å (4.6 μm^{-1}) extinction feature can be due to a chromophore that is present in the materials synthesized from naphthalene using a plasma.

The top half of Figure 2.13 shows the result of co-adding the three curves over the spectral range of the laboratory data ($1.22\ \mu m^{-1} \leq \lambda^{-1} \leq 5.26\ \mu m^{-1}$), superimposed against the absolute extinction data points (*bold dots*) from Whittet's table. This exercise illustrates how the absorption from the laboratory synthesized material, when added to other possible components, can provide the general aspects of the observed interstellar extinction and thereby represent an independent absorber for the 2175 Å interstellar extinction feature.

The exercise does show that in the $2.5\ \mu m^{-1} < \lambda^{-1} < 4\ \mu m^{-1}$ range there is some excess contribution from the laboratory derived component. The spectra exhibited in Figs. 2.7 to 2.10 have, in profile, a low level of absorption at $\lambda^{-1} < 4\ \mu m^{-1}$. This is in excess when considering the interstellar extinction in the range of $3\ \mu m^{-1} < \lambda^{-1} < 4\ \mu m^{-1}$, and consideration must be given to its presence in the laboratory-synthesized material. The TOF and GCMS data (Table 2.1 and Fig. 2.19) show anthracene (MW 178) and pyrene (202) to be a fraction of the yellow residue along with the species we now consider to be of interest in the issue of the 2175 Å ($4.6\ \mu m^{-1}$) extinction feature. These molecules, although a fraction, by virtue of strong bands (Murrell 1963; Lee & Wdowiak 1993) would account for the absorption at $\lambda^{-1} < 4\ \mu m^{-1}$. The experiment is a means of synthesis, and while it produces in abundance the kinds of PAH species discussed regarding the chromophore for the 2175 Å ($4.6\ \mu m^{-1}$) extinction feature, it also produces to a limited extent PAH species such as anthracene and pyrene which do not have the required properties of a carrier. A mixture having a reduced amount of PAH species such as anthracene and pyrene, relative to what has been synthesized, would also not exhibit the spectral excess.

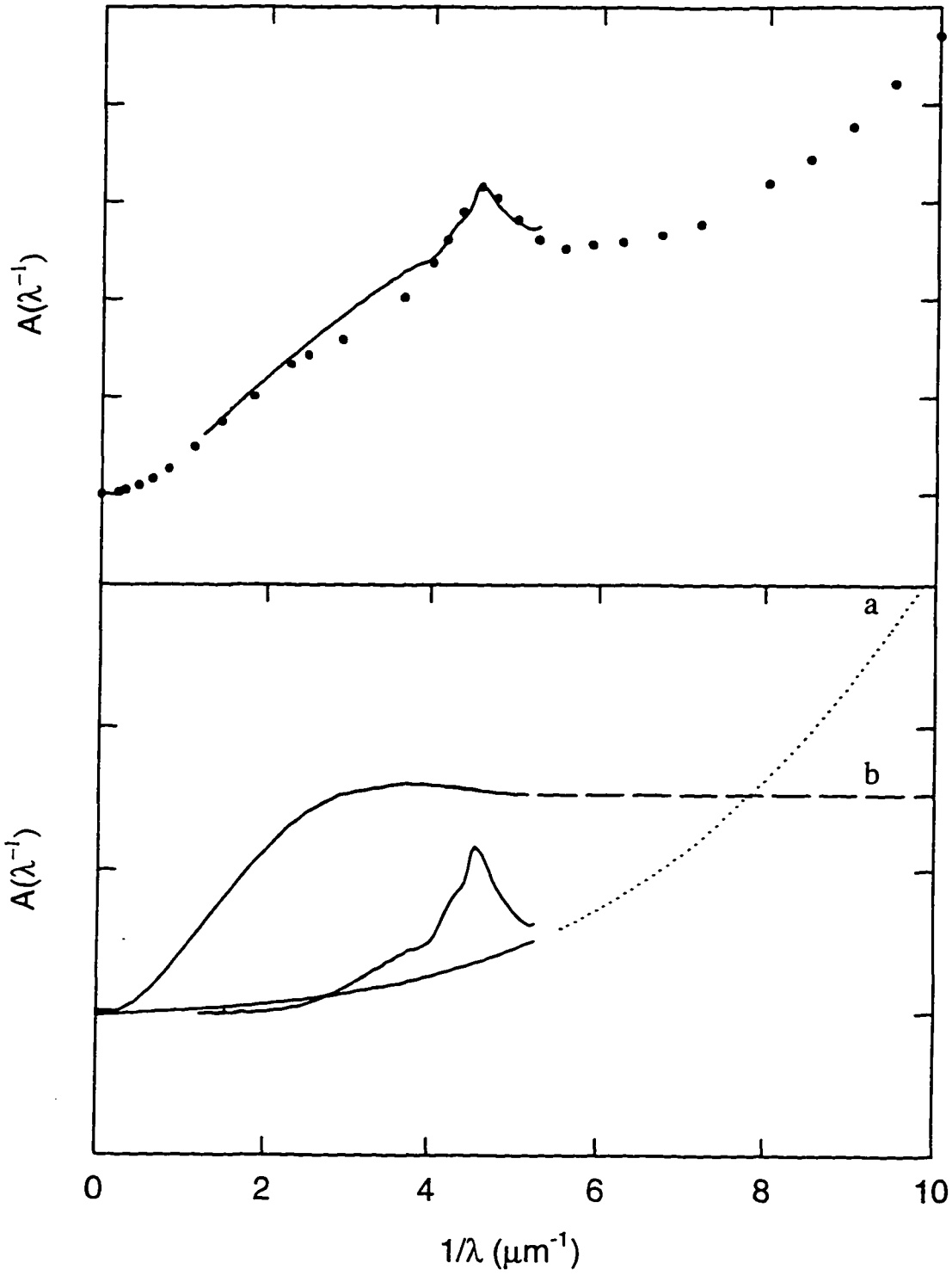

FIG. 2.13— Bottom: the profile shown in Figure 2.11 along with two curves that represent the exponential extinction component (a) and the extinction component presumably due to classical sized particles (b). Top: Co-added result in the range of laboratory profile superimposed against the absolute extinction (*bold dots*) adapted from Whittet 1992.

It should also be noted that this excess contribution is relatively unstructured and less than what occurs when the spectra of individual PAHs have been co-added or when spectra are taken of other laboratory formulations such as coal tar (Joblin et al. 1992). The effect of this contribution on the co-added result also depends on the shape of the curve depicting the contribution of the classical-sized particles, which could exhibit more of a down-turn in this spectral range than what has been utilized in the exercise. Having expressed the preceding, it is important to keep in mind that the laboratory-synthesized material, by virtue of a good match in the 4 $\mu m^{-1} \leq \lambda^{-1} \leq 5.25\ \mu m^{-1}$ spectral region and available chemical analysis, serves to provide insight to the nature of the chromophore that can give rise to the 2175 Å (4.6 μm^{-1}) extinction feature. The basic molecular structure of the hypothesized chromophore is also incorporated in species to which spectral characteristics in other spectral regions, most notably the infrared, can be attributed.

From experiment 22, a small amount of yellow residue prepared using 100% H_2 was evaporated as a film onto a sapphire disk and placed in the sample holder of an Air Products Inc., Model 202 Displex expansion engine refrigerator (water cooled system). UV/VIS spectra taken as the sample was cooled to various temperatures over a temperature range from 300 K to 15 K (Fig. 2.14) demonstrated invariance with temperature. The temperature range more than reflects what exists in the general interstellar medium.

2.2.2 Infrared Spectroscopy

Infrared absorption spectroscopy in the C-H stretch region (~ 3000 cm^{-1}) of the residue in a KBr pellet or evaporated onto a KBr disk is indicative of both aromatic and aliphatic components being present. The spectra of the yellow residue harvested from the sapphire tube are shown, along with naphthalene, in Figure 2.15. The spectrum of the yel-

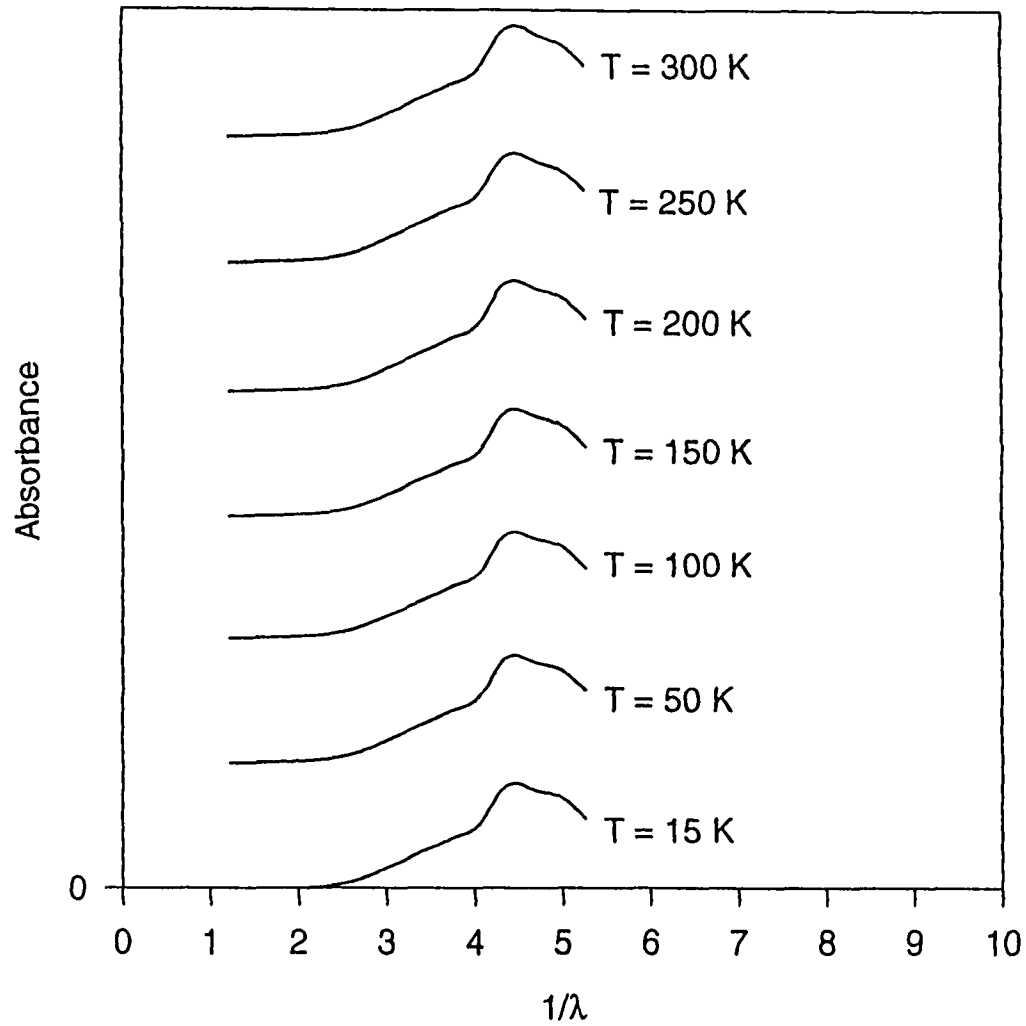

FIG. 2.14— UV/VIS spectra at various temperatures of the yellow residue prepared using 100% H_2 at 0.6 torr in experiment 25 as a film evaporated onto a sapphire disk. These spectra demonstrate spectral invariance with temperature.

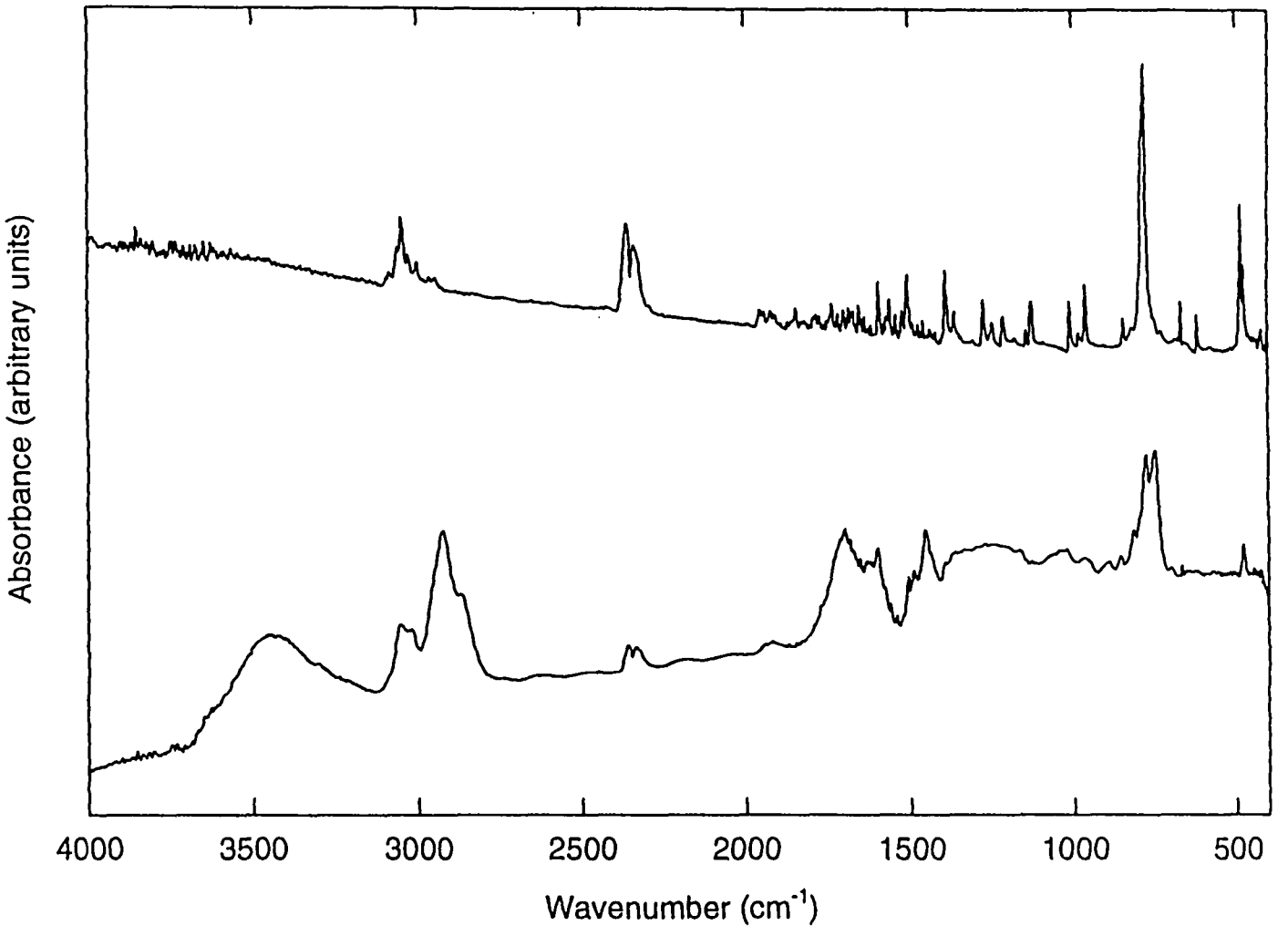

FIG. 2.15— The infrared spectrum of the naphthalene precursor (top) and the residue harvested from the sapphire tube of experiment 1 (bottom) in the range 4000 to 400 cm^{-1}.

low residue is clearly not the spectrum exhibited by naphthalene. The sapphire collection disk in the wavenumber range 3150-2750 cm^{-1} of experiment 1 is shown in Figure 2.16 along with that of naphthalene. The sapphire disk is transparent in the 4000-2000 cm^{-1} range. The aliphatic component is very interesting in that it is dominated by the C-H stretch features (2925 and 2860 cm^{-1}) attributable to the methylene or $-CH_2-$ functional group, relative to contribution of the methyl or $-CH_3$ functional group (2960 cm^{-1}). The significance of the dominant $-CH_2-$ signature will be discussed later. It is also worth pointing out that the spectrum in this wavelength region of a film prepared from the yellow residue from experiment 17 (Fig. 2.17) is similar to that of the UIR emission from the protoplanetary nebula IRAS 05341+0852 (Geballe & van der Veen 1990; Joblin et al. 1996).

During experiment 24, a series of IR spectra was obtained of the deposit formed on the sapphire collection disk at selected intervals when the luminescence was blue, white, orange, red, and red + 2 hours (Fig. 2.18). The progression clearly shows that the naphthalene migrates in the vapor phase, deposits onto the sapphire collection disk, and is transformed through a sequence into the final product over the duration of the experimental run.

Our experience in the 28 experiments performed on the naphthalene precursor is that on the basis of infrared and ultraviolet spectroscopy there is little variation in the nature of the reaction product.

2.2.3 Gas Chromatography/Mass Spectroscopy and Laser Desorption Time-of-Flight Mass Spectroscopy

Gas chromatography/mass spectroscopy (GCMS) analysis of yellow residues and black deposits, which was done at Arizona State University, and laser desorption (10.6 μm) multi-photon (266 nm) ionization time-of-flight (TOF) mass spectroscopy of a film

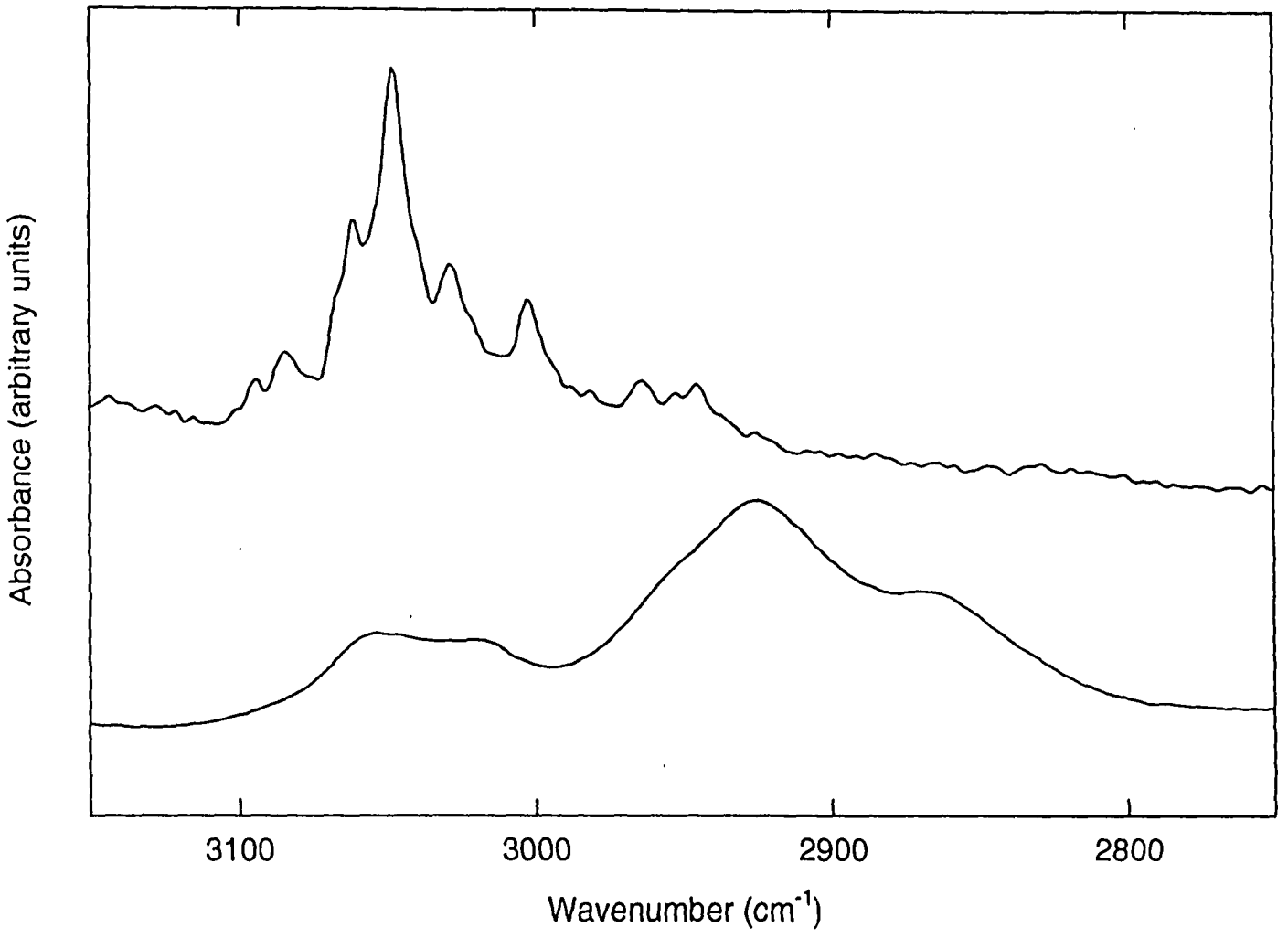

FIG. 2.16— The infrared spectrum of the naphthalene precursor (top) and the residue harvested from the sapphire tube of experiment 1 (bottom) in the range 3150 to 2750 cm^{-1}.

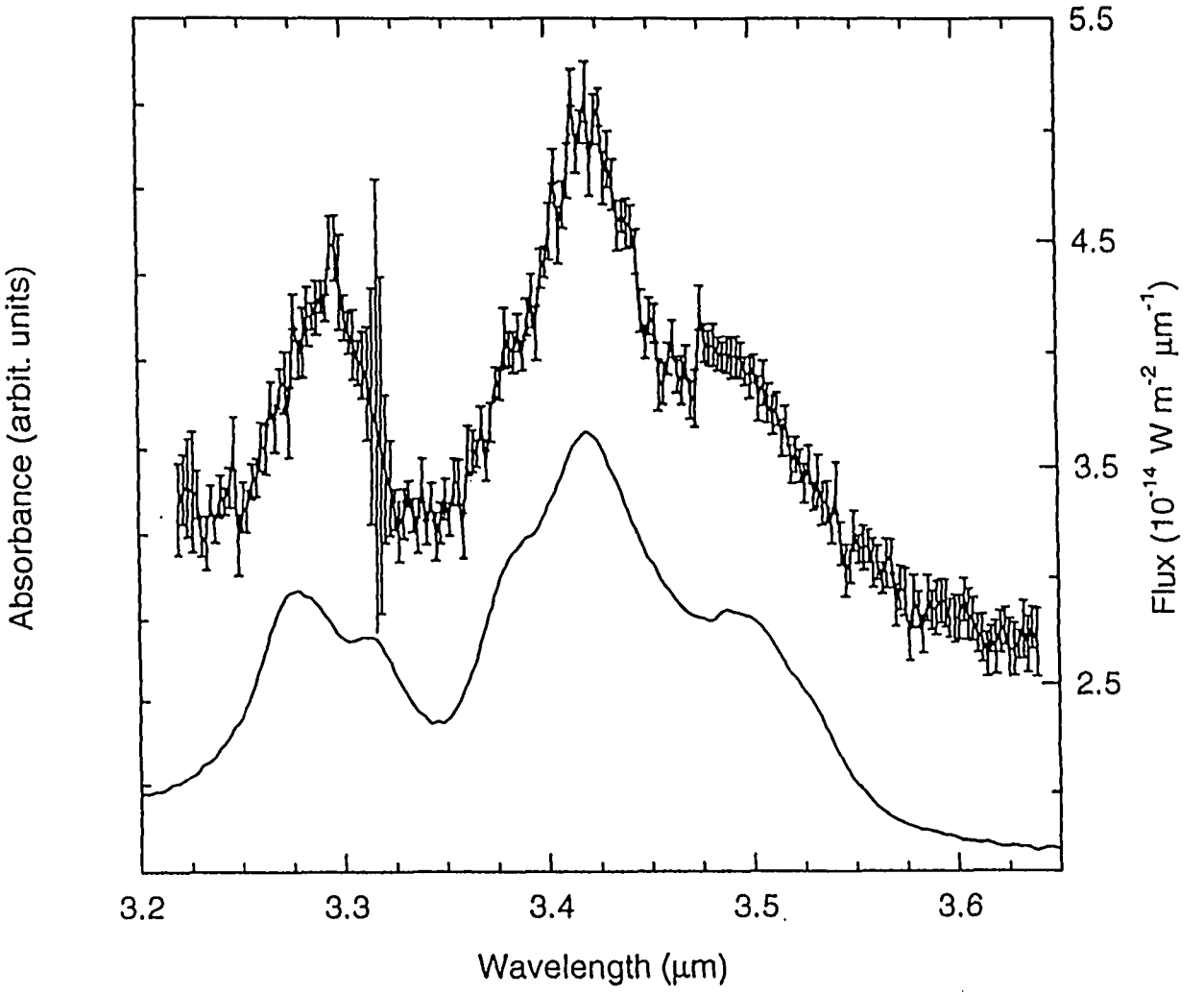

FIG. 2.17— Infrared spectra of the CH stretch region of a film on KBr prepared from yellow residue (experiment 17, 5% CH_4/95% H_2) harvested from the sapphire tube (lower) and the emission of proto-planetary nebula IRAS 05341+0852 (upper) taken from Geballe & van der Veen 1990, as presented in Joblin et al. 1996.

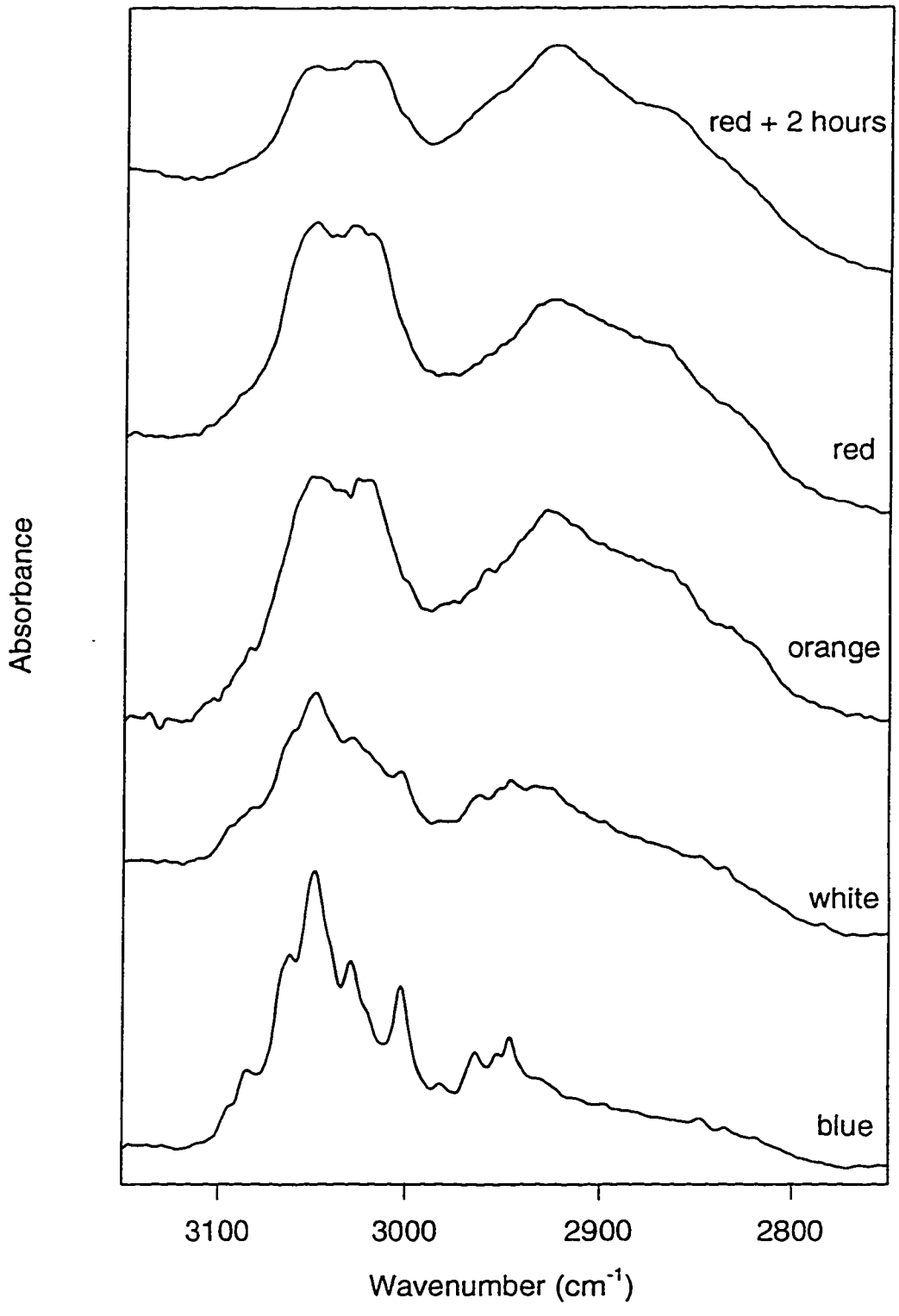

FIG. 2.18— Infrared spectra of the sapphire collection disk sampled when the luminescence is blue, white, orange, red, and red + 2 hours. Refer to Figure 2.5 which includes the blue through red sequence in photographs.

prepared by evaporating yellow residue onto a quartz plate, carried out at Stanford University, reveal that the naphthalene precursor having the molecular weight (MW) 128 is converted into rich variety of more complex PAH species with molecular weights as high as 574. Some specific molecular weight assignments are included in Table 2.1. The GCMS analysis confirms the interpretation of the infrared and ultraviolet spectroscopy that the composition of the product of the experiments is qualitatively and quantitatively similar, despite the use of different gases and gas mixtures. The most significant deviation from a common product occurred when hydrogen or helium with oxygen was used, resulting in oxygenated derivatives, in some cases, being produced.

Of particular significance from both GCMS and the TOF analysis mass distribution (Fig. 2.19) is the presence in abundance of binaphthyl and associated species. Binaphthyl, at a MW of 254, is a structure where two double-ringed (naphthalene) components are linked together. It was present in both the yellow residue film analyzed by TOF and in the black deposit for which three isomers were resolved by GCMS (Fig. 2.20). The combined peak strengths for the three binaphthyl isomers is 3.3x that of naphthalene. Other binaphthyl related species that appear to be in abundance in the yellow residue are dinaphthylmethane (MW 268) and dinaphthylethane (MW 282) where the two double-ringed-(naphthalene) components are linked with methylene- (-CH_2-) and ethane- (-CH_2-CH_2-) functional groups. The overall pattern associated with molecular weights 254, 268, 282, and a peak at 296 in the TOF mass distribution is also suggestive of the presence of a polymer based upon a naphthalene mer. Dihydrobinaphthyl can be the assignment for the TOF peak at MW 256 and the three isomers indicated by GCMS also at MW 256. An even more hydrogenated form of binaphthyl, namely tetrahydrobinaphthyl, is the likely assign-

Table 2.1. Predominant Assignments Through GC/MS and Laser Desorption TOF MS of Products from the Naphthalene Precursor. Alkyl-substituents on 178, 202, 228, and 252 Were Also Formed.

Mass	Formula	Assignment
128	$C_{10}H_8$	naphthalene (aromatic double-ring)
142	$C_{11}H_{10}$	methylnaphthalene (aromatic double-ring)
152	$C_{12}H_8$	acenaphthylene
154	$C_{12}H_{10}$	acenaphthene (hydrogenated PAH with aromatic double-ring)
156	$C_{12}H_{12}$	dimethylnaphthalene, ethylnaphthalene (aromatic double-ring)
168	$C_{13}H_{12}$	phenalan (hydrogenated PAH with aromatic double-ring)
178	$C_{14}H_{10}$	phenanthrene, anthracene
202	$C_{16}H_{10}$	pyrene, fluoranthene
204	$C_{16}H_{12}$	phenylnaphthalene (aromatic double-ring)
208	$C_{16}H_{16}$	hexahydropyrene (hydrogenated PAH with aromatic double ring)
218	$C_{17}H_{14}$	phenyl, methylnaphthalene (aromatic double-ring)
228	$C_{18}H_{12}$	chrysene, naphthacene, triphenylene
252	$C_{20}H_{12}$	perylene, benzopyrene, benzofluoranthene
254	$C_{20}H_{14}$	binaphthyl (multi aromatic double-ring, GC/MS indicates 3 isomers present)
256	$C_{20}H_{16}$	dihydrobinaphthyl (hydrogenated PAH with aromatic double-ring, GC/MS indicates 3 isomers present)
258	$C_{20}H_{18}$	tetrahydrobinaphthyl (hydrogenated PAH with aromatic double-ring)
268	$C_{21}H_{16}$	methylbinaphthyl, dinaphthylmethane (multi aromatic double-ring)
278	$C_{22}H_{14}$	dibenzo(a,h) anthracene, benzoperylene
282	$C_{22}H_{18}$	dimethylbinaphthyl, dinaphthylethane (multi aromatic double-ring)
378	$C_{30}H_{18}$	naphthyl substituents on 252 (multi aromatic double-ring)
380	$C_{30}H_{20}$	trinaphthyl (multi aromatic double-ring)
434	$C_{34}H_{26}$	alkyl naphthyl-substituents on 252

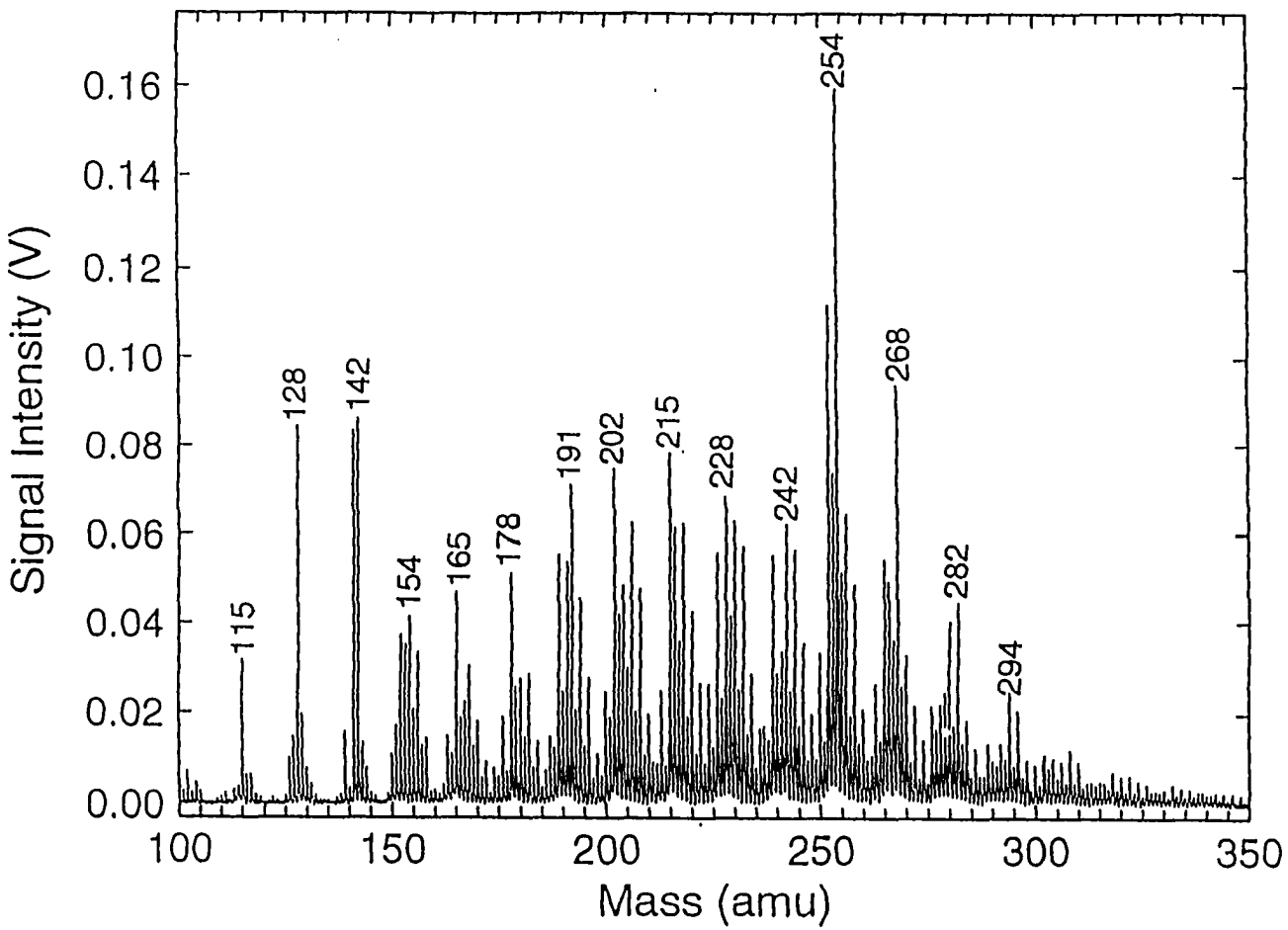

FIG. 2.19— The mass distribution of a film evaporated onto quartz prepared from the yellow residue harvested from the sapphire tube in experiment 24 in which hydrogen was used to create the plasma. This distribution was obtained by laser desorption multi-photon ionization time-of-flight mass spectroscopy. The distribution with the spectroscopy and gas chromatography is strongly suggestive of a molecular aggregate where an aromatic double-ring base (naphthalene-like) is a dominant structure.

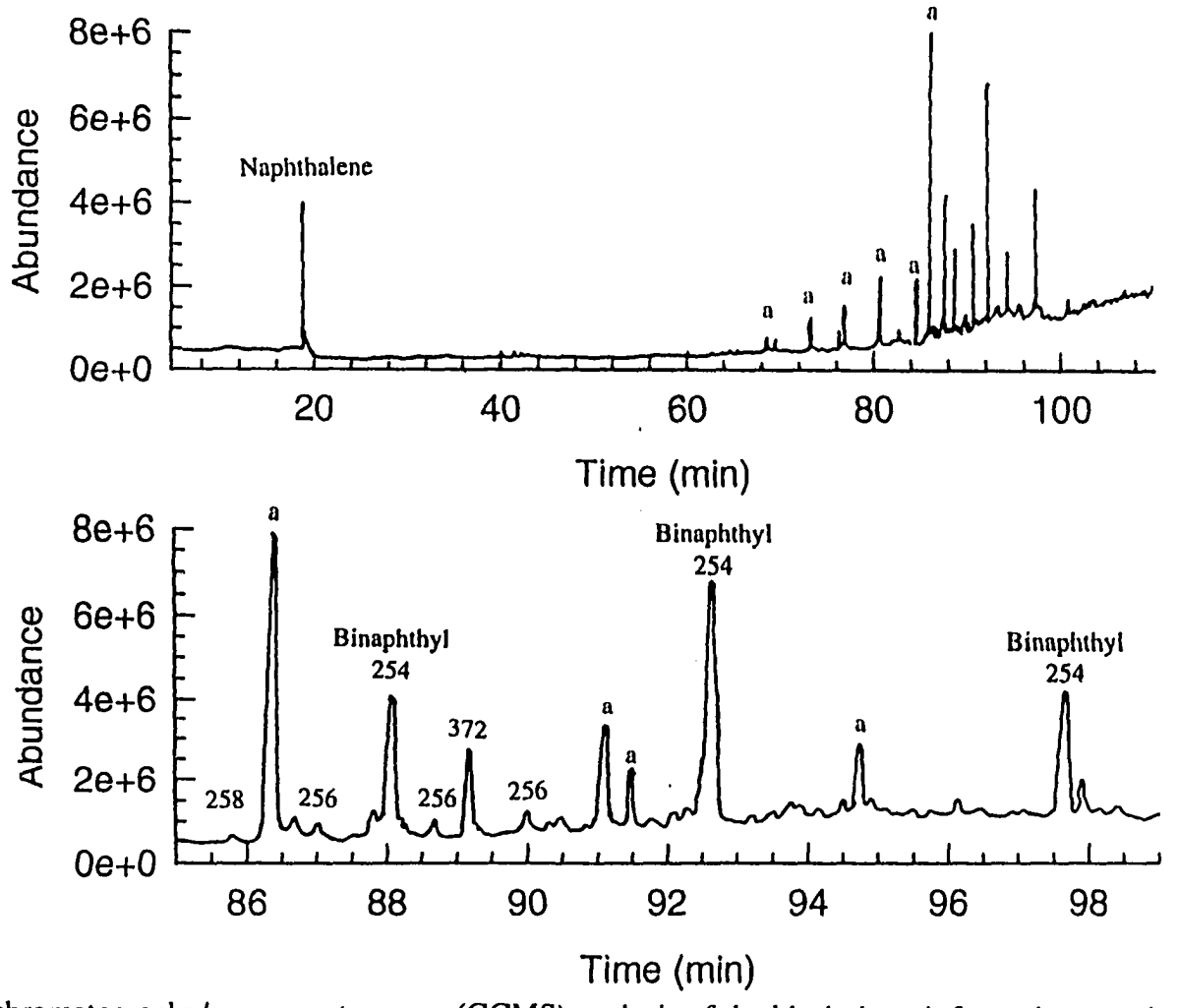

FIG. 2.20— Gas chromatography/mass spectroscopy (GCMS) analysis of the black deposit formed on an electrode of experiment 15 which had a gas content of 4% O_2 and 96% H_2, which was done at Arizona State University. The peaks represented by "a" are from column bleed and hence are artifacts. The main component consists of the 3 isomers of Binaphthyl. Also present are the hydrogenated forms of Binaphthyl, dihydrobinaphthyl (3 isomers present at MW 256) and tetrahydrobinaphthyl (MW 258).

ment for the TOF and GCMS peaks at MW 258. Both incorporate the methylene (-CH_2-) functional group into a ring, resulting in less of an aromatic nature than binaphthyl. The strengths of the TOF peaks at molecular weights 256 and 258 are comparable to or greater than the peaks which can be assigned to hexahydropyrene (MW 208) and acenaphthene (MW 154).

The -CH_2- structure is also present as a group in semicyclic rings incorporated in acenaphthene (MW 154) and hexahydropyrene, which is the probable assignment for MW 208, both observed in apparent comparable abundance in the TOF mass distribution. Also, MW 168 can be given the assignment of phenalan, which has -CH_2- groups in a semicyclic ring. Those species in which -CH_2- is incorporated in a link between aromatic double rings, such as dinaphthylmethane and dinaphthylethane, or a semicyclic component of a structure also incorporating the aromatic double ring as in acenaphthene, phenalan, and hexahydropyrene, would be responsible for ultraviolet absorption in the 2200 Å region and infrared bands dominated by methylene C-H stretch vibrations. The abundance pattern in the TOF mass distribution of molecular weights 254, 268, 282, and 296 strongly suggests that the yellow residue is an aggregate of individual molecules and polymer.

2.2.4 Summary of Spectroscopy and Chemical Analysis

Our experience in all of some 28 experiments when naphthalene is the precursor material is that on the basis of infrared and ultraviolet spectroscopy, and gas chromatography, there is little variation in the nature of the reaction product. Since this result even occurred when using helium gas alone, it must be concluded that the product is more the result of the choice of the naphthalene precursor rather than a result of the specific gases used to produce the plasma environment.

It is instructive to examine the UV/VIS spectra of some of the individual molecules identified by GCMS and TOF analysis to be present in the yellow residue and black deposit. They were selected because all incorporate the aromatic double-ring structure that can function as the naphthalene-base chromophore, which can be the most general aspect of the carrier of the 2175 Å extinction feature. UV/VIS spectra were obtained by dissolving amounts of naphthalene, acenaphthene, hexahydropyrene, and 1,1′ binaphthyl in methyl alcohol to achieve a concentration of molecules in the solvent of 2×10^{16} cm^{-3}. A montage of the obtained UV/VIS spectra, along with structure diagrams illustrating the common aromatic resonance, is exhibited in Figure 2.21.

This montage is a graphic demonstration of how these specific molecules, which are identifiable constituents of both the laboratory analog and the yellow residues and black deposits, can be components of the profile of the 2175 Å (4.6 μm^{-1}) interstellar extinction feature. A search of the literature yielded spectra of isomers of hydrogenated binaphthyl which, on the basis of GCMS and TOF analysis as discussed in section 2.2.4, are also constituents of the yellow residues and black deposits and of the base chromophore incorporated into the structure. Figure 2.22 shows the UV spectra along with structure diagrams of 3,4-dihydro-1,1′-binaphthyl and 1,2,3,4-tetrahydro-1,1′-binaphthyl, as presented on a scales of absorbance (log ε) and wavelength (Miller & Mann 1951). Again, it is clear that the peak absorption for these two species lies within the profile of the 2175 Å (217.5 nm) interstellar extinction feature. Surely, there are other members of the chromophore family lurking in the laboratory-derived material that makes it so attractive when considering the nature of the carrier of the 2175 Å "bump" in the cosmic night.

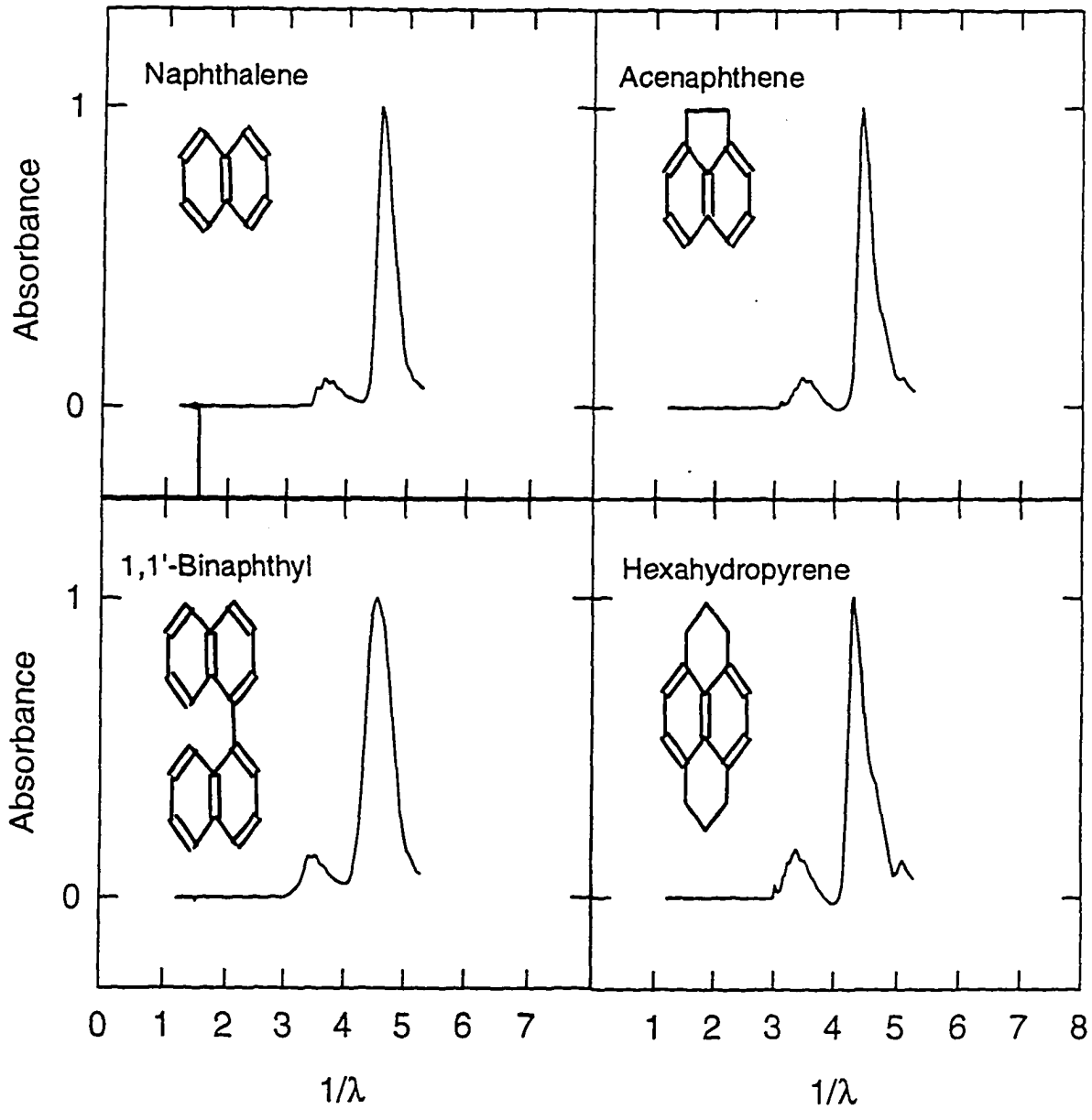

FIG. 2.21— UV/VIS spectra and structure diagrams of individual molecules identified by GCMS and TOF to be present in the yellow residue and black deposit. UV/VIS spectra were obtained from naphthalene, acenaphthene, hexahydropyrene, and 1,1′ binaphthyl in methyl alcohol. These spectra demonstrate how the aromatic double-ring chromophore results in absorption in the spectral region of the profile of the 2175 Å (4.6 μm^{-1}) extinction feature.

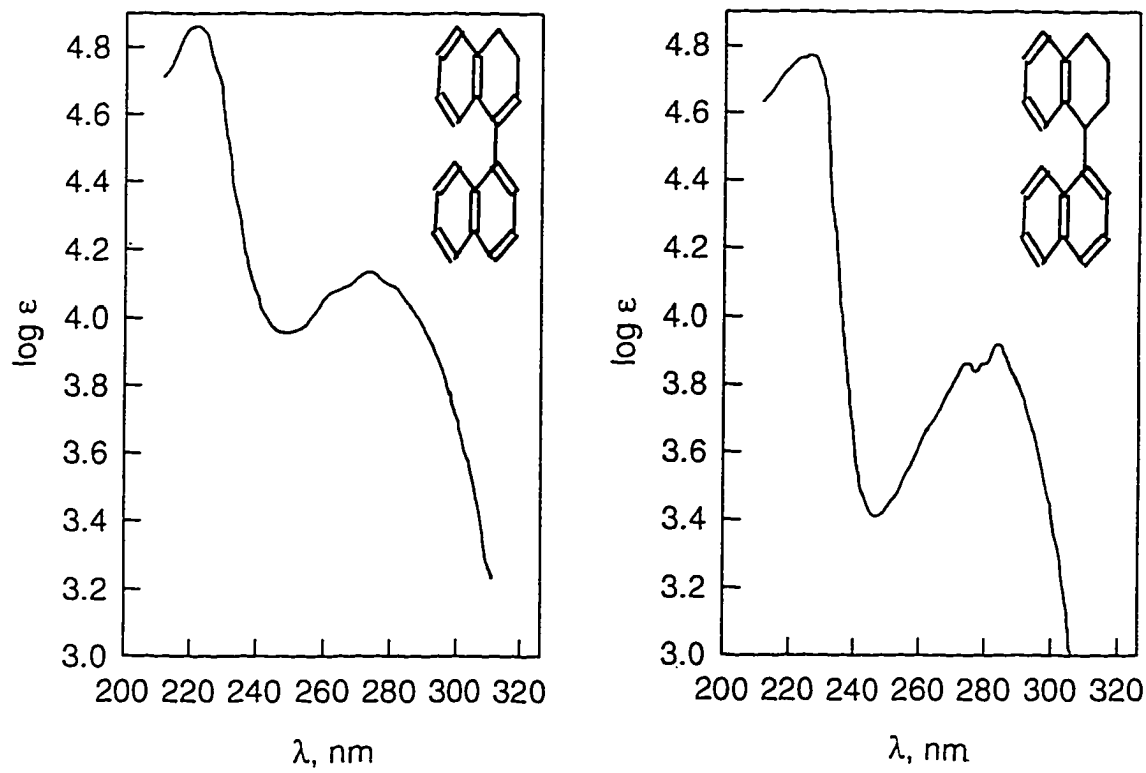

FIG. 2.22— Ultraviolet spectra and structure diagrams of 3,4-dihydro-1,1′-binaphthyl (left) and 1,2,3,4-tetrahydro-1,1′-binaphthyl (right) (Adapted from Miller and Mann 1951). These spectra along with those of Figure 2.21 demonstrate how the aromatic double-ring chromophore results in absorption in the spectral region of the profile of the 2175 Å (4.6 μm^{-1}) extinction feature.

2.3 Implications

The experiments indicate that the 2175 Å interstellar extinction feature can be due to a carrier that is a molecular aggregate in which an aromatic double-ring structure serves both as a significant base and the electron "box" chromophore. The spectral characteristics of this aggregate produce the envelope of the feature while not contributing structure at other wavelengths, an aspect of particular importance. The aggregate can incorporate a component, as demonstrated, that will match the remarkably consistent wavelength peak at 2175 Å which does not vary by more than 10 Å when the direction of the line sight is different. It may be that another peak-provider such as graphite is present in the interstellar medium, but even in such a situation, the material described here would serve well as a coating or mantle that establishes the envelope of the 2175 Å feature. Observed variations, in that regard, can be attributed to a varied distribution in the composition of the aggregate, keeping in mind that the more general aspects of its character, which are established by the double-ring chromophore, would persist. A surprising result of the almost thirty experiments to date is that the resulting product does not vary in a significant manner in its characteristics when different gases nor over a wide range of temperatures. The ubiquity of the 2175 Å interstellar feature, it would appear, demands such consistency in the production of its carrier.

The spectral and molecular characteristics of the laboratory synthesized material are consistent with what is expected for a material that has a role as an interstellar constituent. Keller (1987), in a study of condensation of carbon in stellar winds, has shown that naphthalene is the likely first PAH from which other polycyclics (acenaphthylene being the next) are formed (see section 3.4). As pointed, out the infrared spectrum in the ~ 3000

cm^{-1} (3-4 μm) region has a strong resemblance to the emission profile of the proto-planetary nebula IRAS 05341 + 0852. Because UIR emission is likely to result from long-lived states of free molecules (Allamandola et al. 1989), the contribution of grains or grain coatings is not expected. A valid scenario is UIR emission from precursors of the molecular aggregate or from fragments ejected by a process such as photoerosion. The mass spectrum strongly indicates the presence of the hydrogenated PAH species acenaphthene (154) and hexahydropyrene (208), in equal or comparable abundances to the fully aromatic acenaphthalene (152) and pyrene (202). Production of hydrogenated PAHs is significant because these species and, in particular, hexahydropyrene have been proposed as the carrier of the satellite bands of the 3.3 μm UIR feature that are attributed to the C-H stretch vibration in the methylene ($-CH_2-$) functional group (Bernstein et al. 1996). Transformation of acenaphthalene or pyrene by hydrogenation to acenaphthene or hexahydropyrene results in the formation of a double-ring aromatic substructure which our experiments indicate is the chromophore giving rise to the 2175 Å feature. This establishes the existence of a connection between the carrier of the 2175 Å ultraviolet extinction feature and important aspects of the carrier of UIR emission.

3. A LABORATORY ANALOG FOR THE CARRIER OF THE 3 MICRON EMISSION OF THE PROTOPLANETARY NEBULA IRAS 05341+0852

3.1 IRAS 05341 + 0852

The object IRAS 05341 + 0852 (IRAS 05341) came to the attention of astronomers in the course of analysis of the results obtained with the Infrared Astronomy Satellite launched in 1983 and operated for approximately 1.5 yrs. until the liquid helium that cooled the telescope and instruments became exhausted. This star is considered to have left the asymptotic giant branch on the Hertzsprung-Russell diagram (Fig. 3.1) and is in the process of becoming a planetary nebula. As such, it is near or at the end of the triple alpha stage where $_2He^4$ nuclei are fused into $_6C^{12}$ via the process (Schwarzschild 1958)

$$_2He^4 + {}_2He^4 \rightarrow {}_2Be^8 + \gamma \qquad -95\ keV$$

$$_2Be^8 + {}_2He^4 \rightarrow {}_6C^{12} + \gamma \qquad +7.4\ Mev$$

It possesses a unique infrared spectrum in the 3 micron (3000 cm^{-1}) region that, while appearing to be related to what has been called the unidentified infrared (UIR) bands discovered by Gillett et al. (1973), shows a reversal of strengths of the features of the 3 micron region profile from the strengths usually observed for UIR sources (Geballe & van der Veen 1990; Joblin et al. 1996). Most 3 micron UIR emission profiles exhibit a dominant feature at about 3.3 micron (~3000 cm^{-1}) that is attributed to the C-H stretch vibration along the periphery of an aromatic structure, accompanied with weaker bands in the region between 3.3 and 3.6 microns. These weaker bands have been hypothesized as being due to C-H stretch vibrations of alkane components or harmonics of skeletal vibrations (de

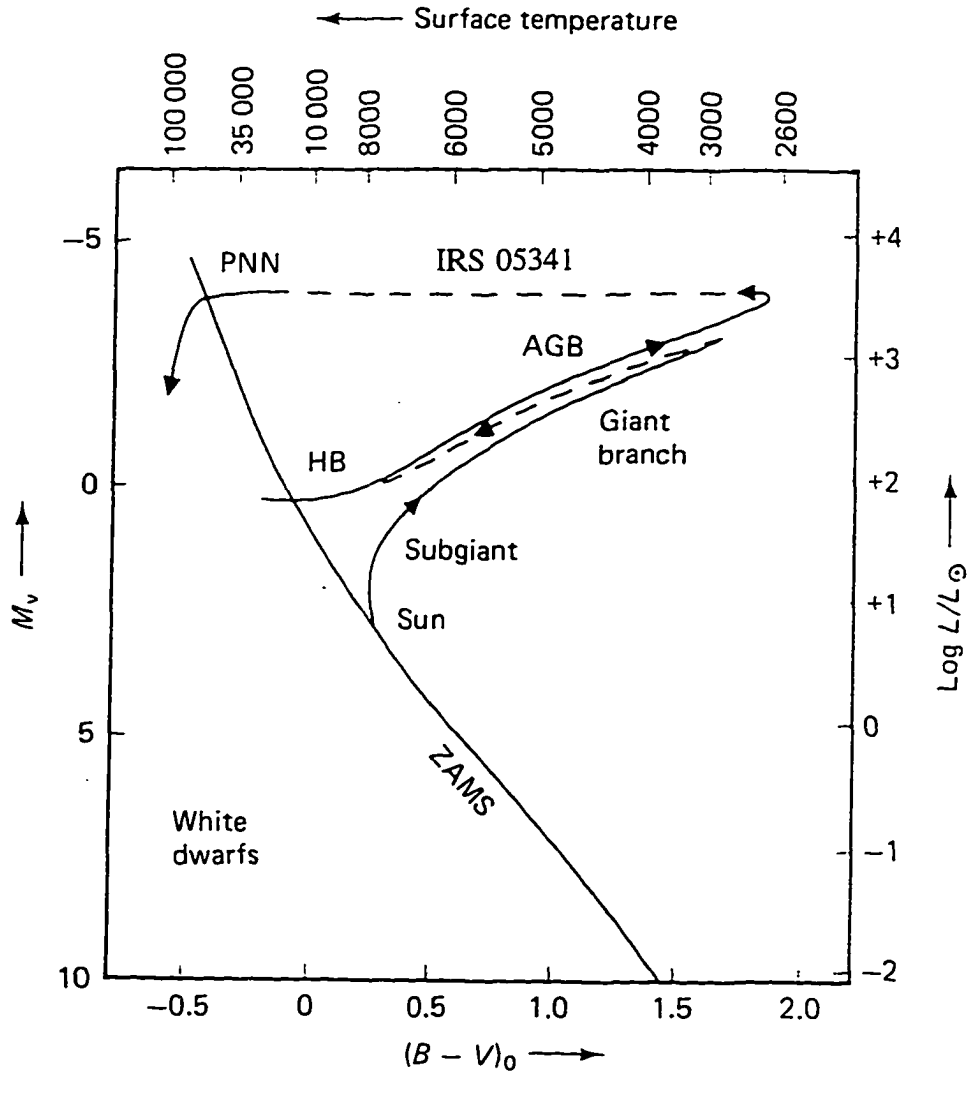

FIG. 3.1— Schematic tracks for the late stages of stellar evolution. Luminosities are given in terms of that of the sun and as absolute visual magnitudes M_V. The abscissa is the B - V color of the star corrected for interstellar extinction. The temperature scale at the top of the diagram corresponds to that valid for giants. ZAMS indicates the zero-age main sequence, HB the horizontal branch, and AGB the asymptotic giant branch. Dashed lines denote portions of evolutionary tracks where developments go very fast (as following the first ascent of the giant branch, or the development of the core to a planetary nebula nucleus (PNN), following the detachment of the circumstellar envelope). Artistic license is invoked at the top of the AGB, where the evolving star is hidden by a dust cloud, so neither B nor V magnitudes, are measurable; this stage occurs when a Mira or long-period variable evolves into an OH-IR star or a carbon-rich IR star, such as IRS 05341 (which has left the AGB), and the core starts on its way to becoming a white dwarf (Adapted from Aller 1991).

Muizon et al. 1986; Bernstein et al. 1996; Joblin et al. 1996). For IRAS 05341, while there is a band at 3.294 micron (3036 cm^{-1}) which is typical for a UIR source and that is likely due to aromatic C-H stretch, the 3.419 micron (2925 cm^{-1}) feature is stronger. Furthermore, this stronger feature, along with structure prominent in the 3.475 to 3.5 micron range, has a character best attributed to C-H stretch for the methylene ($-CH_2-$) functional group, which is an alkane (Colthup, Daly, & Wilberley 1990). There also appears to be a shoulder at about 3.38 micron (2959 cm^{-1}) in the observed spectrum presented by Joblin et al. (1996), which could be C-H stretch feature for the methyl ($-CH_3$) functional group (Colthup et al. 1990). It was recognized by Geballe and van der Veen (1990) that the spectral profile of the IRAS 05341 3 micron could bear on interpretations of the UIR bands. Experiments conducted in our laboratory have resulted in the synthesis of a material that may assist in that matter.

The processing of the polycyclic aromatic hydrocarbon (PAH) naphthalene ($C_{10}H_8$) in the energetic environment of a plasma, as described in Chapter 2, has yielded a material with ultraviolet spectral characteristics of interest in understanding the carrier of the 2175 Å interstellar extinction feature (Beegle et al. 1997). Infrared spectroscopy in the 3 micron region also revealed that the relative strengths of the bands due to the aromatic and aliphatic C-H stretch components were similar to that of IRAS 05341; however, profile of the aromatic feature of the synthesized material displayed some difference from that of the celestial band. Mass spectroscopy of that substance indicates that the precursor, naphthalene, was transformed into an aggregate of a multitude of larger PAH structures, some of which may be in the form of a polymer (Section 2.2.3). Of particular interest is the molecule acenaphthylene ($C_{12}H_8$) and its hydrogenated form acenaphthene ($C_{12}H_{10}$),

which have been suggested by Keller (1987), see Figure 3.2, to be next-step species after naphthalene, in his study of the condensation of carbon in stellar winds. Because our previous experiments resulted in the formation of these two species in comparable abundance, the use of them as precursor materials instead of naphthalene seemed to be of obvious interest, and such an experiment was performed. The molecular structures of naphthalene, acenaphthylene, and acenaphthene are represented by diagrams in Figure 3.3.

3.2 Experimental

The apparatus and protocols are the same as described in Section 2.1. For this experiment, approximately 800 mg of a PAH mixture (Aldrich Chemical Company product A80-5), having a composition of acenaphthylene (~ 75%), acenaphthene (~ 20%) and an uncharacterized component (~5%), was applied to the interior of a sapphire tube as in the previously described naphthalene precursor experiments. Hydrogen was employed as the gas to produce the plasma. It should be pointed out that acenaphthylene and acenaphthene are less volatile than naphthalene. For acenaphthylene, the melting point is 91°C, and the boiling point is 280°C, while that for acenaphthene is 94°C and 279°C. The melting and boiling points for naphthalene are 81°C and 218°C, respectively. Unlike naphthalene, the sample was excited to a yellow luminescence by the radiation from the plasma, which tended to remain quite steady in color through the first 40 min. of the experimental run. Then, the yellow luminescence changed to a deep green, and then went to a red color in the span of five min. The red luminescence was lighter in color than the final luminescence in a naphthalene precursor experiment. The final product harvested from the sapphire tube in reflectance exhibited a color of red.

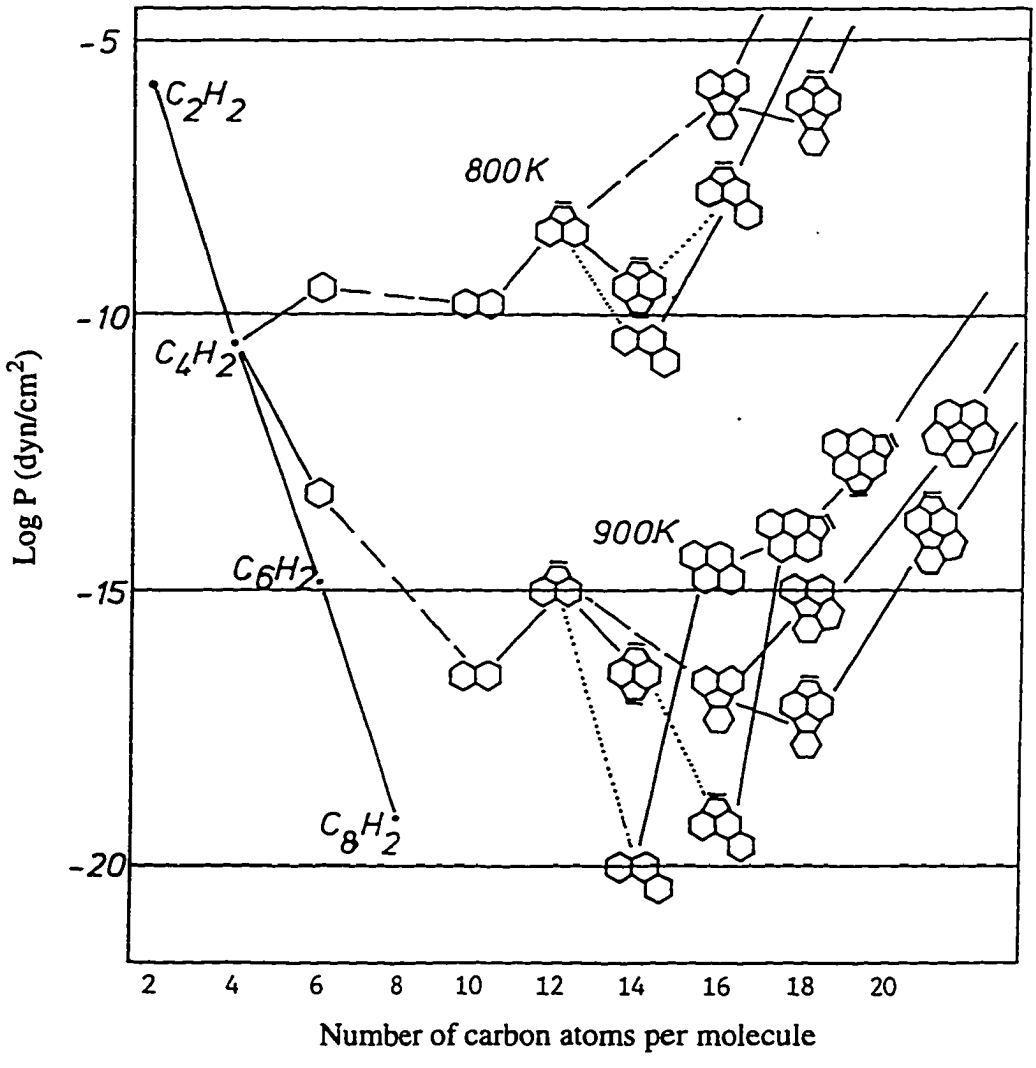

FIG. 3.2— Equilibrium densities of carbon molecules in a supercooled gas (stellar wind) as a function of their sizes considering only the most stable ones in each size class (Adapted from Keller 1987). The work presented in this dissertation suggests this scheme is essentially correct but must be extended to take into account hydrogenated PAH species.

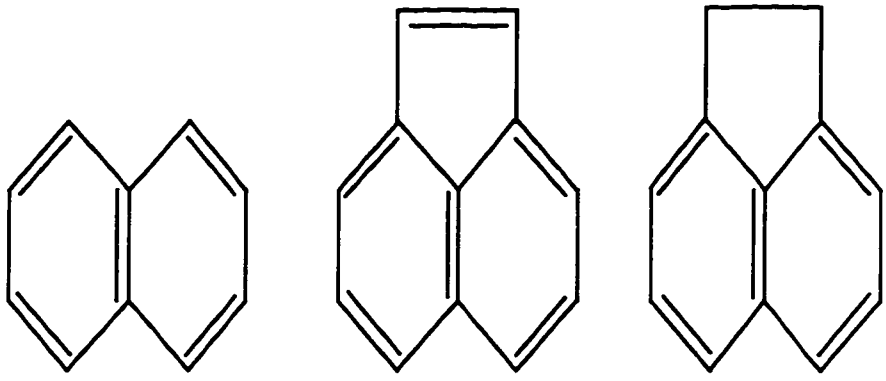

Naphthalene MW 128 | Acenaphthylene MW 152 | Acenaphthene MW 154

FIG. 3.3— Diagrams that represent the molecular structure of naphthalene, acenaphthylene, and acenaphthene along with the molecular weight (MW).

3.3 Comparison of Laboratory and IRAS 05341 Spectra

The spectrum of IRAS 05341 in the 3.2 micron to 3.65 micron region, along with an overlay (*solid line*) of the spectrum of the laboratory synthesized product, is shown in Figure 3.4. The IRAS 05341 spectrum has two aspects that need to be pointed out, namely that there is a contribution from the HII region of Pfund δ emission of hydrogen in the form of a spike atop the 3.294 micron feature, and enhanced error in the measurement at ~3.32 micron because of the presence of terrestrial atmospheric attenuation. Overall, there is a very good correlation between the profiles of the two spectra. The most striking aspects are the match in relative strengths of the 3.294 micron and 3.419 micron bands, and the long wavelength skew of the 3.294 micron band. The skew character of the band of the laboratory-synthesized material matches not only that of the 3.294 micron band for IRAS 05341, but also the profile of the 3.29 micron emission band of the Orion Bar (Sloan et al. 1997), although for that source, the longer wavelength components are at a fraction of the strength of the 3.29 micron features, unlike the case of IRAS 05341. What difference exists is in the 3.45 micron to 3.55 micron region, and perhaps the IRAS 05341 emission may have a component that could be attributed to methyl ($-CH_3$) vibrations in the form of a weak shoulder at ~3.4 micron, as noted before.

Geballe and van der Veen (1990) have commented on the similarity between the 3 micron region emission profile of IRAS 05341 and that of Nova Centauri 1986 (V842 Cen) some 300 days following the outburst and persisting for several months (Hyland & McGregor 1989). A 650 K dust shell appeared some 55 days after the outburst, but the 3 micron emission did not occur until later, with a shell temperature of 800 K. The 3.29 micron band of the shell is stronger than the band at 3.42 micron which is shifted redward

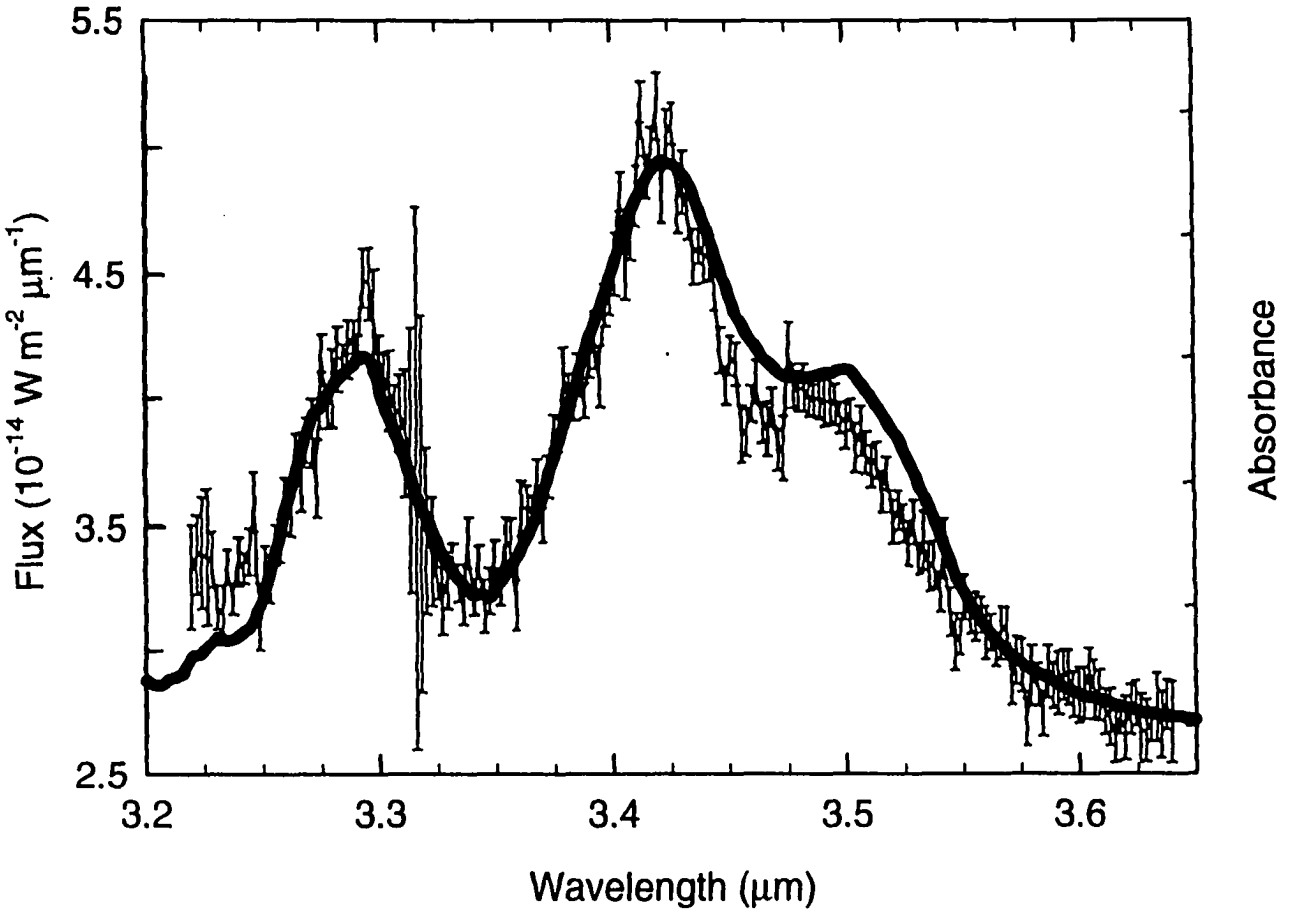

FIG. 3.4— The 3 micron region spectrum of material synthesized by subjecting a mixture of acenaphthylene and acenaphthene to the energetic hydrogen plasma environment (*solid line*) superimposed on the observed spectrum of IRAS 05341+0852 obtained using the UKIRT facility (Joblin et al. 1996).

compared to what is observed for the 3.4 micron emission feature for the Orion Bar (cf. Sloan et al. 1997), but coincident in wavelength with the strongest band of both IRAS 05341 and the laboratory synthesized material.

An ultraviolet/visible absorption spectrum of a film prepared by evaporating the red residue onto a quartz substrate in a vacuum shows a character similar to what has been obtained in experiments in which naphthalene is a precursor (Beegle et al. 1997). The absorption maxima is 2300 Å (4.35 μm^{-1}), which places it within the envelope of the 2175 Å (4.60 μm^{-1}) interstellar extinction feature which ranges between 2500 Å (4 μm^{-1}) and 2000 Å (5 μm^{-1}). This is consistent with the synthesized product being a candidate component of the carrier of the 2175 Å "bump."

3.4 Discussion and Conclusions

The molecule formation sequence worked out by Keller (1987) for carbon atoms condensing into PAH species could be a representation of what occurs in a stellar wind issuing from objects such as the proto-planetary nebula IRAS 05341 or Nova Cen 1986. We find it interesting that the 3 micron emission from Nova Cen 1986 appeared when the dust shell temperature was measured to be 800 K, because that temperature was utilized by Keller in his equilibrium densities determination in which acenaphthylene was the second PAH formed, after naphthalene, which was preceded by the single-ringed benzene.

The 3.419 micron (2925 cm^{-1}) band exhibited by the laboratory material and the emission band of IRAS 05341 at the same spectral position, by inference, are due to C-H stretch for the methylene ($-CH_2-$) functional groups. Acenaphthylene does not have this group, while acenaphthene does, because it is the hydrogenated form (Fig. 3.2). The methylene ($-CH_2-$) functional group must also be incorporated in other structures present in the

synthesized material, structures that have come about in the energetic environment of the plasma. This is the case for material synthesized from naphthalene as well. Our use of the acenaphthylene and acenaphthene mixture most likely resulted in a better spectral match to the IRAS 05341 spectrum than what was obtained when naphthalene was used, because while the plasma does possess some of the qualities probably present in the stellar wind situation, it can not be considered a simulation. Going a step beyond naphthalene appears to have made up for that deficiency, which is present in all laboratory experiments that attempt to mimic nature on the cosmic scale. In summary, the experiment has resulted in a very good match to the IRAS 05341 spectrum in the 3 micron range and appears to validate the modeling effort of Keller (1987). However, consideration must be given to extending that general scheme to take into account hydrogenated PAH species such as acenaphthene and hexahydropyrene, along with acenaphthylene and pyrene, as proposed in the original model.

4. THE NATURE OF THE POLYCYCLIC AROMATIC HYDROCARBON CARRIER FOR THE 6.2 MICRON INFRARED EMISSION BAND

4.1 The Issue of the UIR Band Strengths

The bands known as the unidentified infrared bands (UIR) at wavelengths at 3.3 μm (3040 cm^{-1}), 6.2 μm (1615 cm^{-1}), 7.7 μm (1310 cm^{-1}), 8.7 μm (1150 cm^{-1}), and 11.3 μm (885 cm^{-1}) were discovered by Gillett et al. (1973) and are associated with a large number of celestial objects. Duley & Williams (1981) attempted to identify the composition of the interstellar material and the mechanism of emission by using the hypothesis of radiative relaxation of vibrationally excited aromatic hydrocarbon material. Léger & Puget (1984) and Allamandola et al. (1985) proposed that the emissions might be due to the vibrations of individual molecules termed polycyclic aromatic hydrocarbons (PAHs). The attractiveness of the PAH model is that it accounts for both the relatively narrow UIR features, characteristic fluorescent emission of aromatic molecules, and the small ($r < 100$ nm) particle size dictated by the far-UV rise of the interstellar extinction curve. Problems with the hypothesis include an inability to match precisely all the wavelengths of the celestial infrared emissions with bands of specific molecules and a failure to adequately explain the broad UIR features (see Allamandola et al. 1989).

It is necessary to establish a detailed correlation between the spectroscopic character of the infrared emission of a variety of celestial objects, known as the unidentified infrared (UIR) bands, and that of specific molecules. Polycyclic aromatic hydrocarbon (PAH) molecules, because of general properties, including spectral, have been hypothe-

sized as the carrier of the UIR bands. On the basis of laboratory absorption and emission measurements, the correlation of C-H stretch vibration modes in PAH molecules with the observed profiles of 3.3 micron (3000 cm^{-1}) emission of a variety of sources is a good one. However, correlation of the strengths of the 6.2 micron (1600 cm^{-1}) UIR band and the C-C skeletal vibration modes of those PAH molecules studied is weak. Infrared absorption spectroscopy and *ab initio* molecular modeling of partially hydrogenated PAH molecules now indicates that the spectral feature at 1600 cm^{-1} for such molecules is enhanced relative to that of the fully aromatic form. This suggests that the 6.2 micron (1600 cm^{-1}) UIR band has as its carrier hydrogenated PAHs, which is consistent with conclusions recently reached regarding the structure in the 3.3 micron band profile and for the carrier of the 2175 Å interstellar extinction feature (Bernstein et al. 1996; Beegle et al. 1997a).

Infrared spectroscopy of acenaphthylene, acenaphthene, pyrene, and hexahydropyrene indicates that the skeletal (C-C) vibration of the normally planar aromatic ring structure may be enhanced in a hydrogenated PAH relative to a fully aromatic PAH. The 6.2 μm UIR band has been attributed to the skeletal vibration mode; however, its intensity in absorption for a PAH such as acenaphthene or pyrene is not great relative to other bands. Also, the absence of significant laser-excited emission in the mid-IR range from long-lived states of fully aromatic PAH molecules when 3.3 mm (3000 cm^{-1}) emission is present has been noted (Schlemmer et al. 1994). Experiments have been performed by a number of researchers (Cherchneff & Barker 1989; Brenner & Barker 1992; Schlemmer et al. 1994; Williams & Leone 1995; Cook et al. 1996) in which specific PAH species are put into the gas phase, subjected to a pulse of exciting ultraviolet radiation, and then the infrared radiation emitted during the experiment is examined by spectroscopy when sampling

over a sequence of very brief time intervals. This last aspect is of particular importance because it permits discrimination of fluorescent emission from thermal emission. The fluorescence occurs from long-lived states (Allamandola et al. 1989) which, at the gas densities that must be utilized in the laboratory, are for the most part collisionally de-excited before fluorescence can occur. This would not be the case in the interstellar medium, where densities are many magnitudes lower. In the experiment, the sampling procedure of measuring over a sequence of very brief time intervals allows the researcher to detect, early on, the photons emitted by fluorescence because, although the responsible states are long-lived, there is sufficient probability for some fluorescence to occur before extensive thermalization precludes it. By careful sampling, the fluorescent emission can be studied apart from the thermal emission which occurs later on. To do such experiments requires considerable skill on the part of the researcher and, of course, sophisticated instrumentation.

Such experiments, along with more conventional infrared absorption spectroscopy, have resulted in a good correlation of the character of the C-H stretch mode of vibration of various PAH molecules with that of the 3.3 micron (~3030 cm^{-1}) UIR emission of many sources in terms of wavelength profile. The first experiments were restricted to the ~3030 cm^{-1} spectral range because high speed detectors were available only for that range. The invention and availability of the blocked impurity band solid-state photomultiplier and the use of liquid helium cooled spectrometers now permit measurements in the range of the 6.2 micron (1600 cm^{-1}), 7.7 micron (1300 cm^{-1}), 8.6 micron (1163 cm^{-1}), and 11.3 micron (885 cm^{-1}) UIR emission bands (Schlemmer et al. 1994; Cook et al. 1996).

The more recent experiments, while confirming the earlier work in the 3.3 micron (3030 cm^{-1}) spectral range, indicate a lack of significant emission at longer wavelengths for most of the PAHs studied, which were phenanthrene, pyrene, perylene, coronene, methylnaphthalene, methylphenanthrene, phenanthridine, and dibenzofuran. Of these, only coronene exhibited strong peaks of emission longward of 3.3 micron, and these were at 7.6 micron (1315 cm^{-1}) and 11.9 micron (840 cm^{-1}) with 6.2 micron (1600 cm^{-1}) emission conspicuously absent (Cook et al. 1996).

The absence of 6.2 micron (1600 cm^{-1}) emission in the recent experiments is particularly disconcerting because it would be due to C-C skeletal modes of vibration that are common to all PAH structures and because it is a strong UIR band. The 6.2 micron (1600 cm^{-1}) band is also not very prominent in absorption relative to the 3030 cm^{-1} band for many PAHs, although it is comparable in strength for larger PAHs such as coronene (Léger & d'Hendecourt 1987) and hexabenzocoronene (Wdowiak 1991). The lack of 6.2 micron (1600 cm^{-1}) emission in the fluorescence experiments and its diminished intensities in the absorption spectra of many PAHs must be addressed because it is present in strength for the UIR.

4.2 Spectroscopy and Modeling of Hydrogenated PAHs

The series of experiments in which the simple PAH molecule naphthalene ($C_{10}H_8$) is subjected to the energetic environment of a plasma has resulted in the synthesis of a complex molecular aggregate, has components that may provide insight to the molecular structure of the carrier of the 6.2 micron UIR band. These experiments have been described in Chapter 2 and Chapter 3. Chemical analysis using the technique of time of flight (TOF) mass spectroscopy and gas chromatography mass spectroscopy (GCMS)

revealed the presence of hydrogenated PAH species as components of the synthesized material. These components included the molecules acenaphthene ($C_{12}H_{10}$) and hexahydropyrene ($C_{16}H_{16}$) which, because of spectral properties, are of interest in coming to an understanding of the nature of the chromophore giving rise to the 2175 Å interstellar extinction feature. In the course of the general investigation, it was noted that the C-C skeletal vibration band at 1600 cm^{-1} was enhanced in these hydrogenated PAHs relative to the non-hydrogenated forms of acenaphthylene ($C_{12}H_8$) and pyrene ($C_{16}H_{14}$).

Figure 4.1 and Figure 4.2 are a pairing of infrared spectra of acenaphthylene (bottom) and acenaphthene (top), and pyrene (bottom) and hexahydropyrene (top), where the 1600 cm^{-1} feature (it is marked with a star) is normalized in each pairing. This allows discernment of the strength of the 1600 cm^{-1} feature relative to the other bands for both the PAH and the hydrogenated PAH. Diagrams depicting the molecular structure for each species are also included with the spectra. In both pairings, it is readily seen that the 1600 cm^{-1} band for both (bottom spectra) acenaphthylene and pyrene is weak relative to most other bands, including the aromatic C-H feature at ~3030 cm^{-1}. It is particularly weak relative to the C-H out-of-plane wag bands in the 700 cm^{-1} to 800 cm^{-1} region which, because of their strength, exceed the scale used. Examination of the spectra of both (top spectra) acenaphthene and hexahydropyrene reveals a dramatic difference in that the 1600 cm^{-1} feature is stronger than the 3030 cm^{-1} bands of both the hydrogenated PAHs and is greatly enhanced in strength relative to the 700 cm^{-1} to 800 cm^{-1} C-H out-of-plane wag bands. The features that appear longward of the 3030 cm^{-1} band in both acenaphthene and hexahydropyrene are attributable to aliphatic C-H stretch.

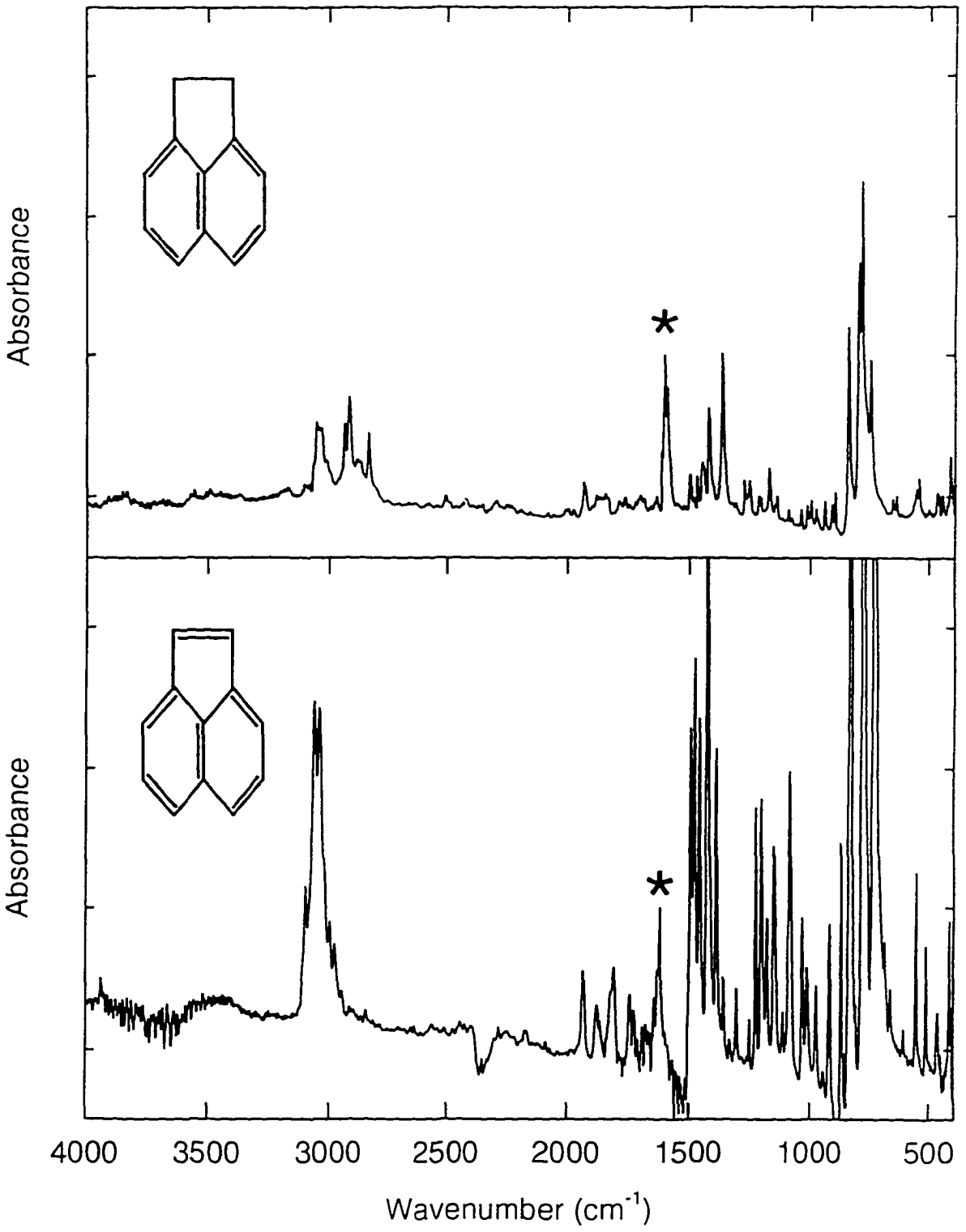

FIG. 4.1— Pairing of infrared spectra of acenaphthylene (bottom) and acenaphthene (top) where the 1600 cm^{-1} feature (marked with a star) is normalized. Note the enhancement of the 1600 cm^{-1} band relative to the other bands for acenaphthene.

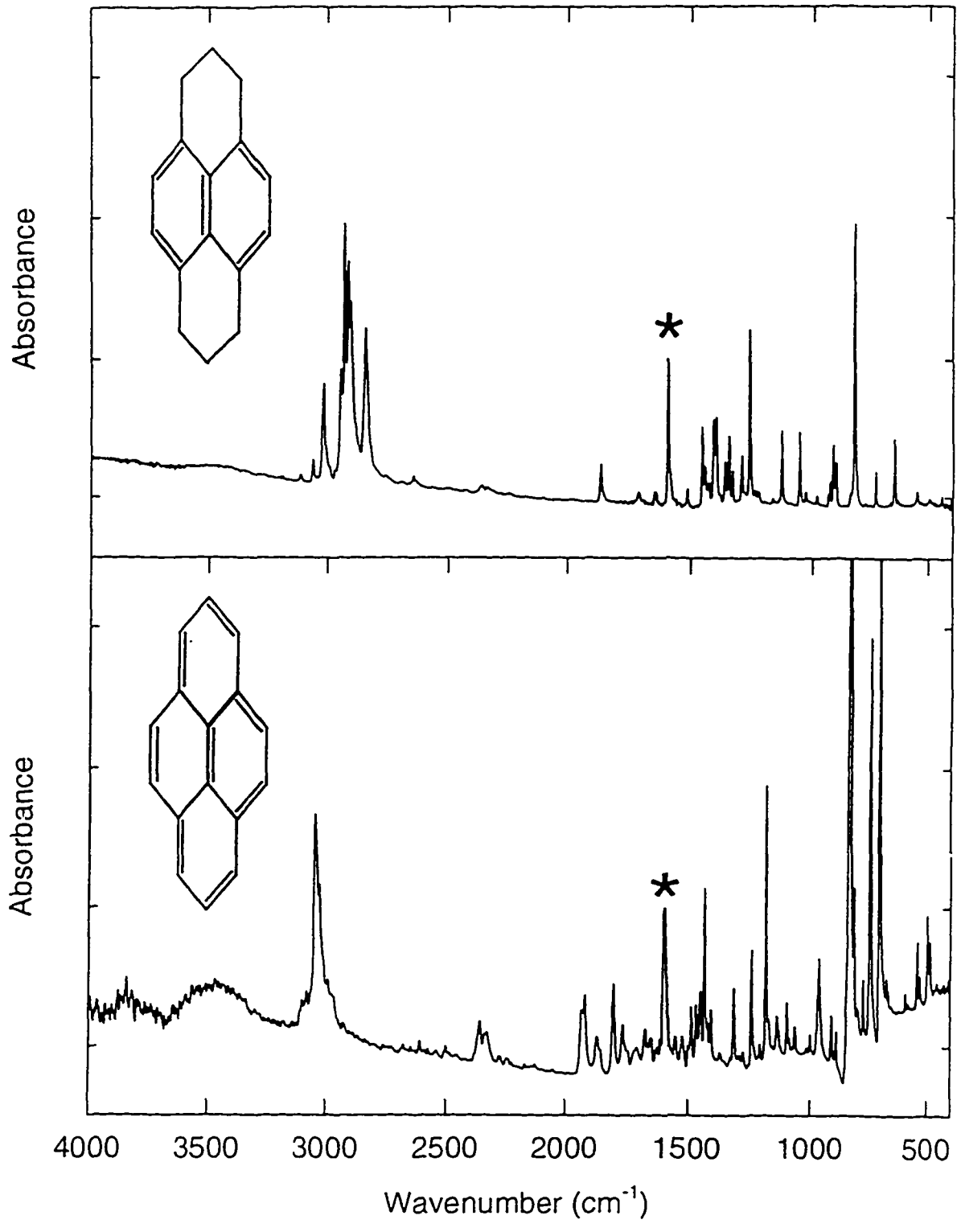

FIG. 4.2— Pairing of infrared spectra of pyrene (bottom) and hexahydropyrene (top) where the 1600 cm^{-1} feature (marked with a star) is normalized. Note the enhancement of the 1600 cm^{-1} band relative to the other bands for hexahydropyrene.

Bernstein et al. (1996) have proposed that the bands longward of the 3.3 micron emission peak from the Orion Bar can be attributed to the aliphatic C-H stretch vibrations of hexahydropyrene on the basis of correlation of the spectra. Our recent investigations (Beegle et al. 1997a, 1997b) indicate hexahydropyrene and other hydrogenated PAHs such as acenaphthene, because they incorporate an aromatic double-ring structure, may be components of a complex molecular aggregate which could be a grain mantle, a grain itself or as a mer in a polymer that gives rise to the 2175 Å interstellar extinction feature. Furthermore, we have found that a mixture of acenaphthylene and acenaphthene is a suitable precursor for synthesis in a plasma of a material having an excellent spectral match to the 3.3 micron emission of the proto-planetary nebula IRAS 05341 + 0852 (Beegle et al.1997b).

The enhancement of the C-C skeletal vibration feature at 1600 cm^{-1} for a hydrogenated PAH and the ramifications for the understanding of the nature of the carrier of the 6.2 UIR band were a sufficient prompt to initiate molecular modeling using Density Functional Theory (DFT) contained in the Gaussian 94 suite of programs (Frisch et al. 1995) implemented on a Cray computer. This was accomplished through the kind effort of Prof. Joseph G. Harrison. The results of modeling acenaphthylene (Fig 4.3, bottom) and acenaphthene (Fig 4.3, top) resulted in a very good match to the infrared spectra obtained by matrix isolation in a KBr pellet (Fig, 4.1). The results obtained for pyrene (Fig 4.4, bottom), and hexahydropyrene (Fig 4.4, top) are a close match when compared to the laboratory data. The Mulliken populations, which show the local charges on constituent atoms, for acenaphthylene (Fig. 4.5), acenaphthene (Fig. 4.6), pyrene (Fig. 4.7), and hexahydropyrene (Fig. 4.8), indicate that the most noticeable difference between the non-hydroge-

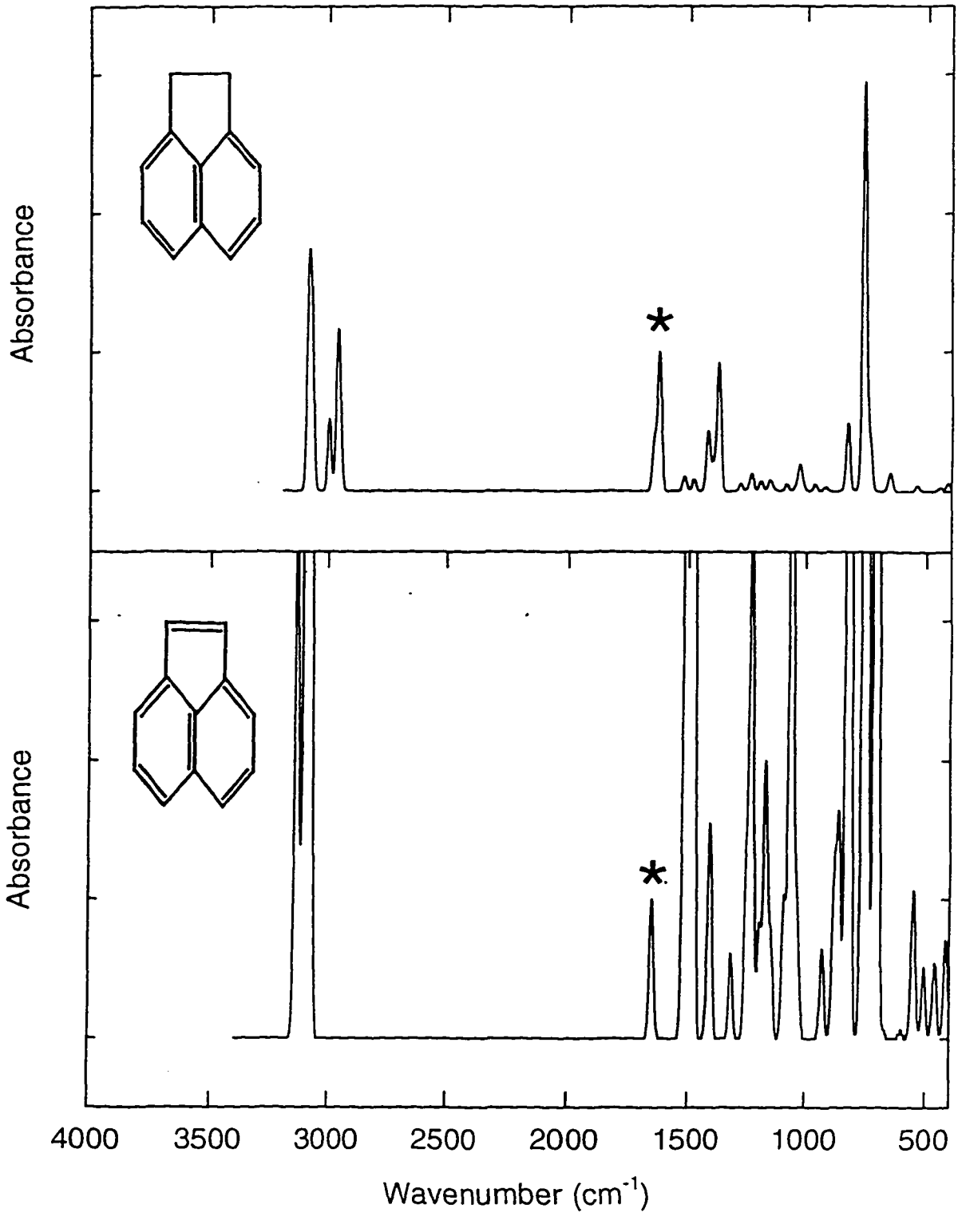

FIG. 4.3— DFT modeling of acenaphthylene (bottom) and acenaphthene (top) where the 1600 cm^{-1} feature (marked with a star) is normalized. The models essentially reproduce the spectra exhibited in Figure 4.1.

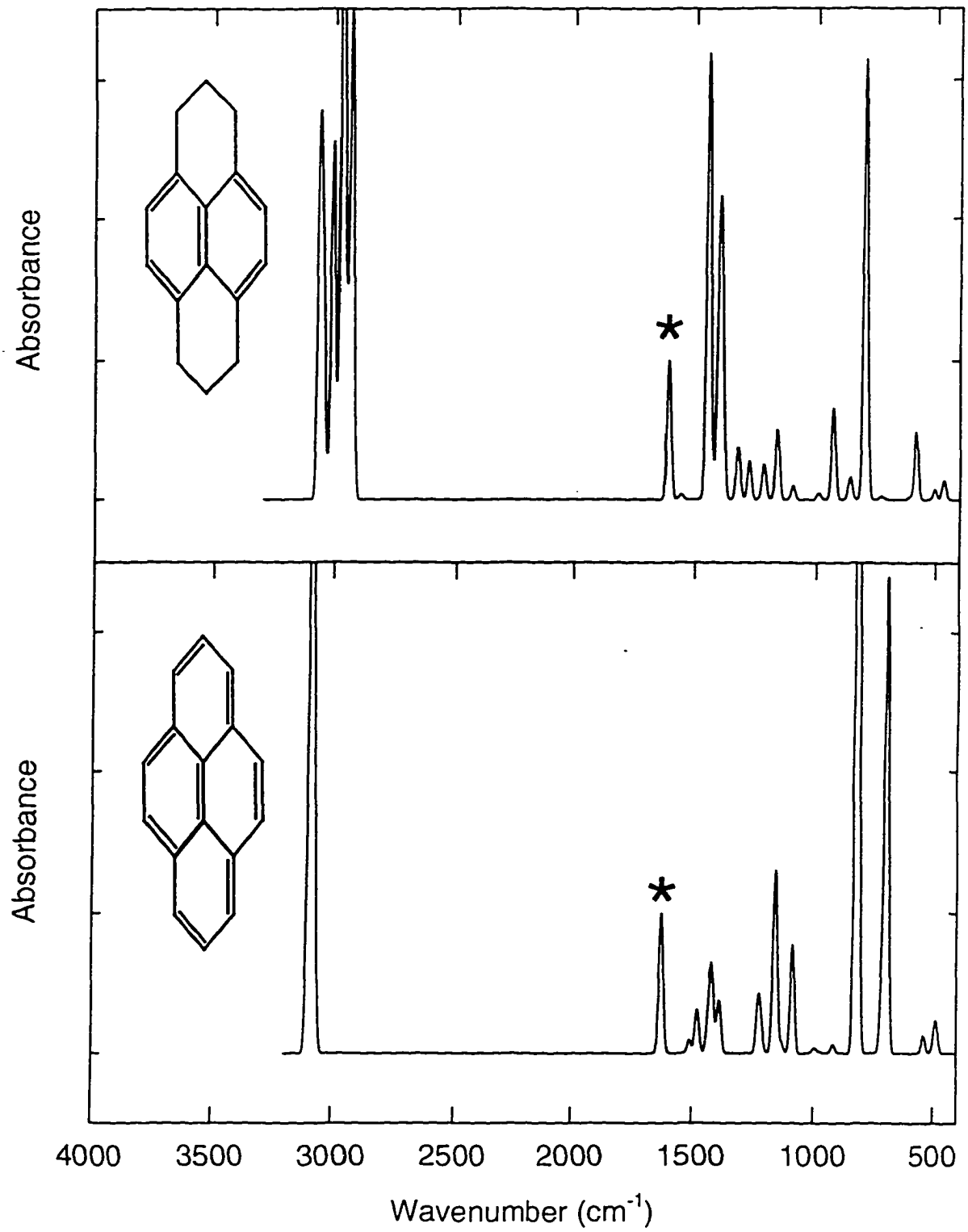

FIG. 4.4— DFT modeling of pyrene (bottom) and hexahydropyrene (top) where the 1600 cm^{-1} feature (marked with a star) is normalized. The models reproduce much of the character of the spectra exhibited in Figure 4.2.

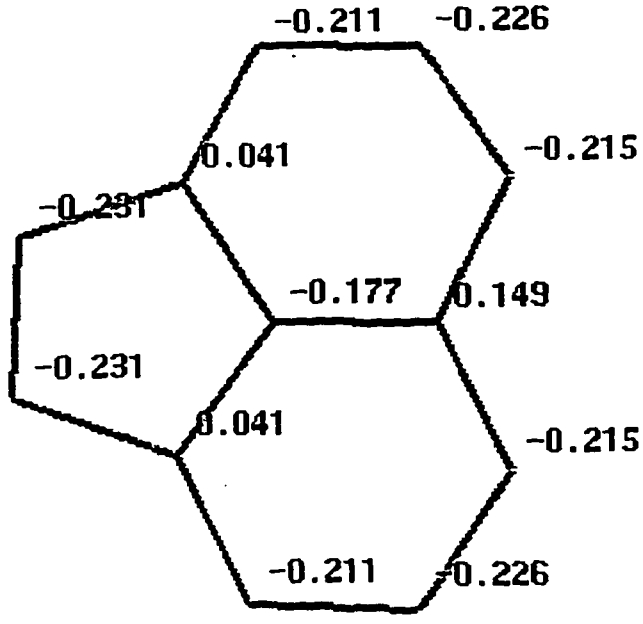

FIG. 4.5— Computed Mulliken populations for acenaphthene ($C_{12}H_8$), which shows the local charges on constituent atoms.

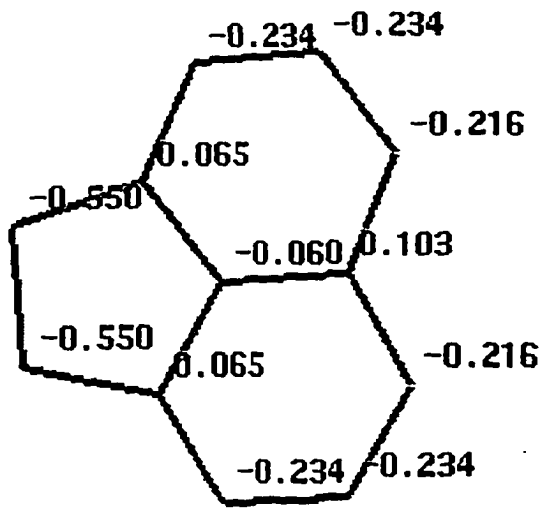

FIG. 4.6— Computed Mulliken populations for acenaphthylene ($C_{12}H_{10}$), which shows the local charges on constituent atoms.

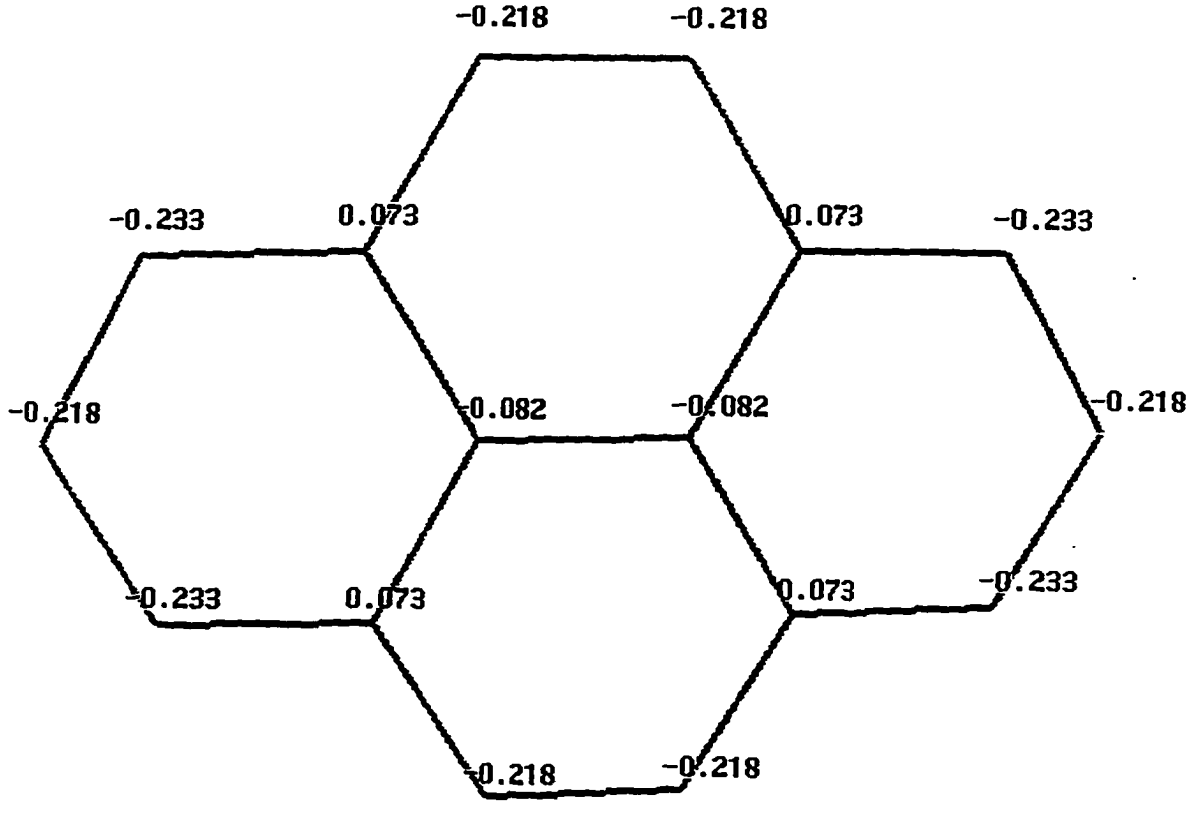

FIG. 4.7— Computed Mulliken populations for pyrene ($C_{16}H_{10}$), which shows the local charges on constituent atoms.

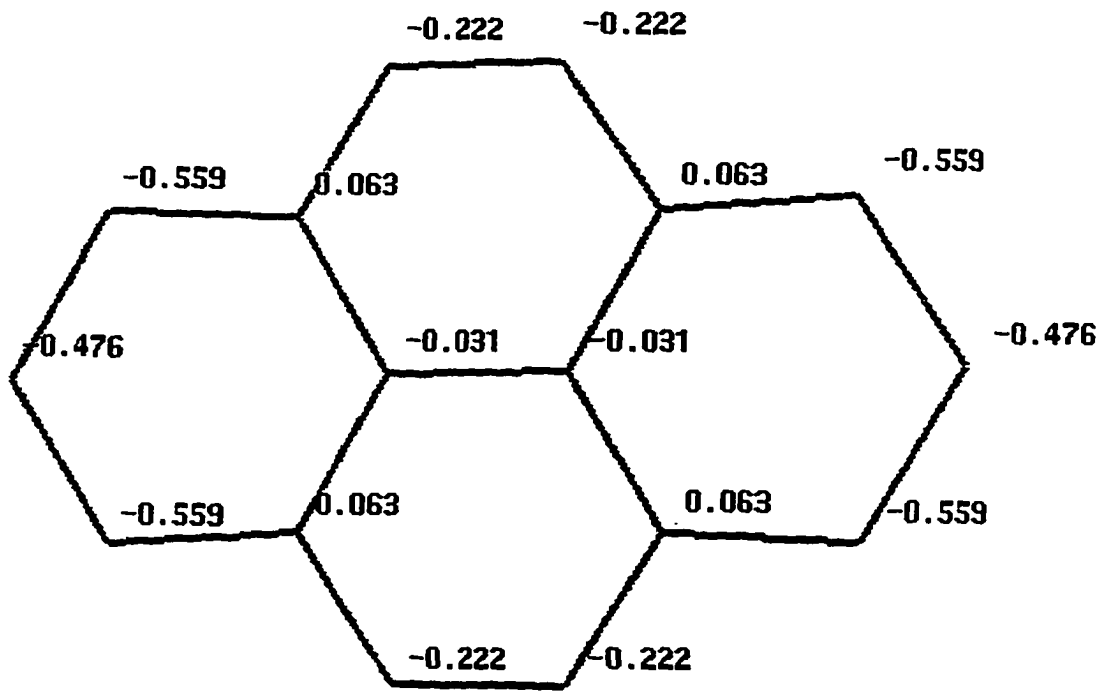

FIG. 4.8— Computed Mulliken populations for hexahydropyrene ($C_{16}H_{16}$), which shows the local charges on constituent atoms.

nated and the hydrogenated PAH is that the outer hydrogenated carbons have a charge that is 2x that of the same non-hydrogenated carbon. This would result in resistance to the carbon atoms coming closer together, thereby increasing the overall strain on the molecule with enhancement of the skeletal vibration that gives rise to the 6.2 μm band. To test whether hydrogenation does enhance the 6.2 mm (1600 cm^{-1}) emission, the laser-excited fluorescence experiments done with PAHs (Schlemmer et al. 1994; Cook et al. 1996) should be repeated with molecules such as acenaphthene and hexahydropyrene.

5. DISCUSSION AND CONCLUSIONS

5.1 Impact of the Research on the Five Spectroscopic Mysteries of the Interstellar Medium

5.1.1 The Diffuse Interstellar Bands

When embarking upon the experiments on which this dissertation is based, it was not expected that the experiments would yield spectral features that might be linked with the numerous interstellar absorption features, which range from wavelengths in the blue to the near infrared (see Fig. 1.1 and Table 1.1), because the DIBs are most likely arrived at by reactive radicals or ions. However, there is support for the hypothesis of Salama and Allamandola (1992a, 1992b), which proposed that there is a correlation between certain of the visible spectral absorption features of the naphthalene cation and the DIBs. The proposal of this dissertation regarding an aromatic double-ring naphthalene-like structure being the carrier of the 2175 Å interstellar extinction feature, which some have likened to a DIB, would appear to validate the interest of those researchers in naphthalene. Consideration of a family of molecules having a naphthalene-like chromophore should be given and experiments with the cations of those molecules performed. Chapter 2 of this dissertation provides a list with which to start. It is necessary to point out the possible connection between the multitude of PAHs that were identified in the time of flight mass spectroscopy data (Fig. 2.18) and the wide variety of DIBs categorized (Table 1.1). The wide variety of DIBs could arise from the various cations of the carrier of the 2175 Å feature.

5.1.2 The 2175 Å Extinction Feature

Chapter 2 of this dissertation speaks directly to this issue. The experiment-derived hypothesis is rich in implications not only for understanding the nature of the carbon containing component of interstellar dust and its formation, but also for panspectral observations. With a little artistic license and because the 2175 Å feature is ubiquitous not only in the Milky Way Galaxy but in many other galaxies as well, it can be proposed that the form of the aromatic double-ringed structure is the "fundamental chromophore of the universe."

5.1.3 The Unidentified Infrared Emission Bands

Chapters 3 and 4 exist to present what may be useful insight into certain of the characteristics of the UIR, namely the apparent aliphatic contributed emission features in the 3 micron wavelength region and the 6.2 micron feature. The research described in Chapter 3 along with the study of Bernstein et al. (1996) together, but independently, present the hypothesis that hydrogenated polycyclic aromatic hydrocarbons (PAH) must be considered along with neutral PAH and ionized PAH species in discussions of the carrier of the UIR. The dissertation presents an excellent spectral match from a synthesized material that is consistent with stellar wind considerations as in planetary nebula formation, with the spectral profile of 3 micron emission from the proto-planetary nebula object IRAS 05341 + 0852. Being able to do such a thing is not only a great joy as an experience, it also validates the insight of Keller (1987) into the formation of interstellar PAHs as a star dies.

5.1.4 The Galactic 3.4 Micron Absorption Band

What this research does, in this regard, is demonstrate how elusive the assignment for the 3.4 micron absorption feature observed against the infrared emission of sources in

the center of the Milky Way Galaxy really is. It was an objective at the initiation of the effort, but resolution of the question will have to remain for others. An excellent spectral match to the profile of the galactic feature was obtained, but it was from a commercial product, "Octoil," which is a pthalic ester utilized for diffusion pumping and hence difficult to explain in the astrophysical context. It is not discussed in this dissertation. A result was that it reinforced the notion that the methyl ($-CH_3$) to methylene ($-CH_2-$) ratio of the carrier of the galactic absorption feature is approximately 2:5.

5.1.5 The Extended Red Emission

In the discussion section 1.1.5, it was pointed out the ERE and UIR can be exhibited by the same cosmic source, and Figures 1.6 and 1.15 show the UIR and ERE spectra of HD44179 (the Red Rectangle). The broad laser-excited emission (Fig. 1.17) from a film prepared from naphthalene in earlier experiments (Wdowiak et al.1995b) is a good match to the 5500 Å to 7500 Å broad profile of the ERE of the Red Rectangle. It should be noted that superimposed on the broad band emission are structure emission features (Fig. 1.15). Spectrofluorometry of a film prepared from the red residue produced from acenaphthylene and acenaphthene on a KBr disk and having an infrared spectral match to the 3 micron emission of IRAS 05341 indicates relatively narrow emission peaked at 5800 Å. Unlike the Red Rectangle feature in that wavelength region which is distributed across six peaks, the Laboratory emission feature exhibits no structure; however, because vibrionic bands can be blended together ("smeared") in a solid, it would be interesting to explore the laboratory luminescence further in a manner that permits free molecules, as in an appropriate solvent or even in the gas phase.

REFERENCES

Allamandola, L. J., Tielens, A. G. G. M., & Barker, J. R. 1985, ApJ, 290, L25

Allamandola, L. J., Tielens, A. G. G. M., & Barker, J. R. 1989, ApJS, 71, 733

Aller, L. H. 1991, in Atoms, Stars, and Nebulae (Cambridge: Cambridge University Press), 176

Beegle, L. W., Wdowiak, T. J., & Arnoult, K. M. 1997b, ApJ, in press

Beegle, L. W., Wdowiak, T. J., Robinson, M. S., Cronin, J. R., McGehee, M. D., Clemett, S. J., & Gillette, S. 1997a, ApJ, in press

Bernstein, M. P., Sanford, S. A., & Allamandola, L. J. 1996, ApJ, 472, L127

Blanco, A., Bussoletti, E., & Colangeli, L. 1988, ApJ, 334, 875

Blanco, A., Fonti, S., Muci, A. M., & Orofino, V. 1996, ApJ, 472, 419

Bless, R. C. & Savage, B. D. 1972, ApJ, 171, 293

Borghesi, A., Bussoletti, E., & Colangeli, L. 1987, ApJ, 314, 422

Brenner, J. D., & Barker, J. R. 1992, ApJ, 388, L39

Cherchneff, I. & Barker, J. R. 1989, ApJ, 341, L21

Cohen, M., Allamandola, L. J., Tielens, A. G. G. M., Bregman, J., Simpson, J. P., Witteborn, F. C., Wooden, D., & Rank, D. 1986, ApJ, 302, 737

Cohen, M., Tielens, A. G. G. M., Bregman, J., Witteborn, F. C., Rank, D. M., Allamandola, L. J., Wooden, D., & de Muizon, M. 1989, ApJ, 341, 246

Colthup, N. B., Daly, L. H., & Wilberley, S. E. 1990, in Introduction to Infrared and Raman Spectroscopy (New York: Academic Press), 215

Cook, D. J., Schlemmer, S., Balucani, N., Wagner, D. R., Steiner, B., & Saykally, R. J. 1996, Nature, 380, 227

Crawford, M. K., Tielens, A. G. G. M., & Allamandola, L. J. 1985, ApJ, 293, L45

Cronin, J. R., & Pizzarello, S. 1990, Geochim. Cosmochim. Acta, 54, 2859

de Muizon, M., Geballe, T. R., d'Hendecourt, L. B., & Bass, F. 1986, ApJ, 306, L105

De Vries, M. S., Reihs, K., Wendt, H. R., Golden, W. G., Hunziker, H., Flemming, R., Peterson, E., & Chang, S. 1993, Geochim. Cosmochim. Acta, 57, 933

d'Hendecourt, L. B., Allamandola, L. J., & Greenberg, J. M. 1985, A&A, 152, 130

Donn, B. D., Allen, J. E., & Khanna, R. K. 1989, in Interstellar Dust, eds. L. J. Allamandola & A. G. G. M. Tielens (Dordrecht: Kluwer), 181

Douglas, A. E. 1977, Nature, 269, 130

Draine, B. T. 1989 in IAU Symp. 135, Interstellar Dust, ed. L. J. Allamandola & A. G. G. M. Tielens (Dordrecht: Kluwer), 313

Duley, W. W., & Williams, D. A. 1981, MNRAS, 196, 269

Fitzpatrick, E. L. & Messa, D. 1986, ApJ, 307, 286

Flickinger, G. C., & Wdowiak, T. J. 1990, ApJ, 362, L71

Flickinger, G. C., Wdowiak, T. J., & Gomez, P. E. 1991, ApJ, 380, L43

Frisch, M. J., Trucks, G. W., Schlegel, H. B., Gill, P. M. W. Johnson, B. G., Robb, M. A., Cheeseman, J. R., Keith, T., Petersson, G. A., Montgomery, J. A., Raghavachari, K. Al-Laham, M. A., Zakrzewski, V. G., Ortiz, J. V., Foresman, J. B., Cioslowski, J., Stefanov, B. B., Nanayakkara, A., Challacombe, M., Peng, C. Y., Ayala, P. Y., Chen, W., Wong, M. W., Andres, J. L., Replogle, E. S., Gomperts, R., Martin, R. L.,Fox, D. J., Binkley, J. S., Defrees, D. J., Baker, J., Stewart, J. P., Head-Gordon, M., Gonzalez, C., and Pople, J. A., computer code Gaussian 94 (Gaussian, Inc., Pittsburgh PA, 1995)

Geballe, T. R.1984, in 12 Proc. of Laboratory and Observatory IR Spectra of Interstellar Dust, eds. J. Greenberg and R. Wolstoncroft (Edinburg: Occasional Rept. Roy. Obs.), 94

Geballe, T. R. & van der Veen, W. E. C. J. 1990, A&A, 235, L9

Ghosh, S. K., & Drapatz, S. 1987, in Polycyclic Aromatic Hydrocarbons and Astrophysics, ed. A. Léger, L. d'Hendecourt, & N. Boccara (Dordrecht: Reidel), 317

Gillett, F. C., Forrest, W. J., & Merrill, K. M. 1973, ApJ, 183, 87

Greenberg, J. M. 1973, in IAU Symp. no. 52, Interstellar Dust and Related Topics, eds J. M. Greenberg & H. C. van de Hulst (Dordrecht: Reidel), 3

Greenberg, J. M. 1978, in Cosmic Dust, ed. J. A. M. McDonnell (New York: John Wiley), 187

Herbig, G. H. 1975, ApJ, 196, 129

Herbig, G. H., & Leka, K. D. 1991, ApJ, 382, 193

Hoyle, F., Wickramasinghe, N. C., Al-Mufti, S., Olauesen, A. H., & Wickramasinghe, D. T. 1982, A&SS, 83, 405

Huffman, D. R. 1989, in IAU Symp. 135, Interstellar Dust, eds. L. J. Allamandola & A. G. G. M. Tielens (Dordrecht: Kluwer), 329

Hyland, A. R., & McGregor, P. J. 1989, in Interstellar Dust: Contributed Papers, eds. A. G. G. M. Tielens and L. J. Allamandola (NASA Conf. Publ. 3036), 101

Jenniskens, P. M. M. 1992, Ph.D. dissertation, Leiden Univ., Netherlands

Jenniskens, P. M. M., & Desert, F. X. 1995, in The Diffuse Interstellar Bands, eds. A. G. G. M. Tielens, and T. P. Snow (Dordrecht: Kluwer), 39

Joblin, C., d'Hendecourt, L., Léger, A., & Defourneau, D. 1994, in The First Symposium on the Infrared Cirrus and Diffuse Interstellar Clouds, APS Conference Series, Vol.58, eds. R. M. Cutri & W. B. Latter (San Francisco: BookCrafters), 291

Joblin, C., Léger, A., & Martin, P. 1992, ApJ, 393, L79

Joblin, C., Tielens, A. G. G. M., Allamandola, L. J., & Geballe, T. R. 1996, ApJ, 458, 610

Jones, A. P., Duley, W. W., & Williams, D. A. 1987, MNRAS, 229, 213

Keller, R. 1987, in Polycyclic Aromatic Hydrocarbons and Astrophysics, eds. A. Léger, L. d'Hendecourt, & N. Boccara (Dordrecht: Reidel), 317

Khare, B. N., Thompson, W. R., Cheng, L., Chyba, C., Sagan, C., Arakawa, E. T., Meisse, C., & Tuminello, P. S. 1993, Icarus, 103, 290

Krätschmer, W., & Nachtigall, K. 1987, in Polycyclic Aromatic Hydrocarbons and Astrophysics, eds. A. Léger, L. d'Hendecourt, & N. Boccara (Dordrecht: Reidel), 75

Krelowski, J. 1988, PASA, 100, 896

Krelowski, J., Snow, T. P., Seab, C. G., & Papaj, J. 1992, MNRAS, 258, 693

Krelowski, J. & Walker, G. A. H. 1986, J. Roy. Astron. Soc. Can., 80, 274

Krelowski, J. & Walker, G. A. H. 1987, ApJ, 312, 860

Kroto, H. W., Heath, R. J., O'Brien, S. C., Curl, R. F., & Smalley, R. E. 1985, Nature, 318, 162

Leach, S. 1987, in Polycyclic Aromatic Hydrocarbons and Astrophysics, eds. A. Léger, L. d'Hendecourt, & N. Boccara (Dordrecht: Reidel), 99

Lee, W., & Wdowiak, T. J. 1993, ApJ, 410, L127

Lee, W., & Wdowiak, T. J. 1994, in Molecules and Grains in Space, ed. I. Nenner (New York: AIP), 675

Léger & d'Hendecourt 1987

Léger, A., & Puget, J. L. 1984, A&A, 137, L5

Mathis, J. S. 1990, Annu. Rev. Astron. Astrophys., 28, 37

Mathis, J. S. 1994, ApJ, 422, 176

Mennella, V., Colangeli, L., Palumbo, P., Rotundi, A., Schutte, W., & Bussoletti, E. 1996, ApJ, 464, L191

Merrill, P. W., & Wilson, O. C. 1938, ApJ, 87, 9

Meyer, D. M., & Savage, B. D. 1981, ApJ, 248, 545

Miles, J. R., & Sarre, P. J. 1992, J. Chem. Soc., Faraday Tans., 88, 1075

Miller, L. E., & Mann, D. J. 1951, JAC, 73, 45

Murrell, J. N. 1963, in The Theory of Electronic Spectra of Organic Molecules (New York: Wiley), 93

Nandy, K., Thompson, G. I., Jamar, C., Monfils, A., & Wilson, R. 1975, A&A, 44, 195

Nandy, K., Thompson, G. I., Jamar, C., Monfils, A., & Wilson, R. 1976, A&A, 51, 63

Pajot, F., Boisse, P., Gispert, R., Lamarre, J. M., Puget, J. L., & Serra, G. 1986, A&A, 157, 393

Pendleton, Y. J., Sanford, S. A., Allamandola, L. J., Tielens, A. G. G. M., & Sellgren, K. 1994, ApJ, 437, 683

Puget, J. L. 1987, in Polycyclic Aromatic Hydrocarbons and Astrophysics, eds. A. Léger, L. d'Hendecourt, & N. Boccara (Dordrecht: Reidel), 99

Robinson, M. S., Beegle, L. W. & Wdowiak, T. J. 1995, Planet. and Space Sci., 43, 1293

Robinson, M. S., Beegle, L. W. & Wdowiak, T. J. 1997, ApJ, 474, 474

Roche, P. F., Aitken, K. K., & Smith, C. H. 1989, MNRAS, 236, 485

Russell, R. W., Soifer, B. T., & Willner, S. P. 1977, ApJ, 217, L149

Sakata, A., Nakagawa, N., Iguchi, T., Isobe, S., Morimoto, M., Hoyle, F., & Wickramasinghe, N. C. 1977, Nature, 266, 241

Sakata, A., Wada, S., Okutsu, Y., Shintani, H., & Nakada, Y., 1983, Nature, 301 493

Sakata, A., Wada, S., Tokunaga, A. T., Narisawa, T., Nakagawa, H., & Ono, H. 1994, ApJ, 430, 311

Sakata, A., & Wada, S. 1989, in IAU Symp. 135, Interstellar Dust, eds. L. J. Allamandola & A. G. G. M. Tielens (Dordrecht: Kluwer), 191

Salama, F., & Allamandola, L. J. 1992a, ApJ, 394, 301

Salama, F., & Allamandola, L. J. 1992b, Nature, 358, 42

Sanford, S. A., Allamandola, L. J., Tielens, A. G. G. M., Sellgren, K., Tapia, M., & Pendleton, Y. 1991, ApJ, 371, 607

Savage, B. D. 1975, ApJ, 199, 92

Schlemmer, S., Cook, D. J., Harrison, J. A., Wurfel, B., Chapman, W., & Saykally, R. J. 1994, Science, 265, 1686

Schmidt, G. D., Cohen, M., & Margon, B. 1980, ApJ, 239, L133

Schutte, W. 1988, PhD. dissertation Univ. of Lieden

Schwarzschild, M. 1958. Structure and Evolution of the Stars (Princeton: Princeton Univ. Press)

Seab, C. G., Snow, T. P., & Joseph, C. L. 1981, ApJ, 246, 788

Seaton, M. J., 1979, MNRAS, 187

Sellgren, K., Brooke, T. Y., Smith, R. G., & Geballe, T. R. 1995,ApJ, 449, L69

Sloan, G. C., Bregman, J. D., Geballe, T. R., Allamandola, L. J., & Woodward, C. E. 1997, ApJ, 474, 735

Sneden, C., Woszczyk, A., & Krelowski, J. 1991, PASP, 103, 1005

Stanford, S. A., Allamandola, L. J., Tielens, A. G. G. M., Selgren, K., Tapia, M., & Pendleton, Y. J. 1991, ApJ, 371, 607

Stecher, T. P. 1965, ApJ, 142, 1683

Stecher, T. P., & Donn, B. 1965 ApJ, 142, 1681

Struve, F. G. W. 1847, Etudes d'Astronomie Stellaire

Trumpler, R. J. 1930a, Lick Obs. Bull., 14, 154

Trumpler, R. J. 1930b, Publ. Astron. Soc. Pacific, 42, 214

Trumpler, R. J. 1930c, Publ. Astron. Soc. Pacific, 42, 267

Van der Zwet, G. P., & Allamandola, L. J. 1985, A&A, 146, 76

Watanabe, I., Hasegawa, S., & Kurata, Y. 1982, Japanese J. Appl. Phys., 21, 856

Wdowiak, T. J. 1980, ApJ, 241, L55

Wdowiak, T. J. 1991, in Solid State Astrophysics eds. E. Bussoletti and G. Strazzulla (North Holland: Amsterdam), 279

Wdowiak, T. J., Beegle, L.W., Robinson, M. S., & Lee, W. 1995b, Planet. and Space Sci., 43, 1429

Wdowiak, T. J., Donn, B., Nuth, J. A., Chappelle, E., & Moore, M. N. 1989, ApJ, 336, 838

Wdowiak, T. J., Lee, W., & Beegle, L.W. 1994, in Molecules and Grains in Space, ed. I Neumer (New York: AIP Press), 687

Wdowiak, T. J., Lee, W., Cronin, J. R., Beegle, L.W., & Robinson, M. S. 1995a, Planet. and Space Sci., 43, 1175

Whittet, D. B. 1992, Dust in the Galactic Environment (Philadelphia: Bristol)

Williams, R. M., & Leone, S. R. 1995, ApJ, 443, 675

Witt, A. N., Bohlin, R. C., & Stecher, T. P. 1984, ApJ, 279, 698

Witt, A. N., & Schild, R. E. 1988, ApJ, 325, 837

Wu, C. G., Gilra, D. P. & van Duinen, R. J. 1980, ApJ, 241, 173

GRADUATE SCHOOL
UNIVERSITY OF ALABAMA AT BIRMINGHAM
DISSERTATION APPROVAL FORM

Name of Candidate Luther W. Beegle

Major Subject Physics

Title of Dissertation A Model of the Complex Hydrocarbon Component of the Interstellar Medium: Observational and Experimental Consideration

Dissertation Committee:

, Chairman

Director of Graduate Program

Dean, UAB Graduate School

Date 6/17/97

PS-1428